Republic of Iraq
Ministry of Higher Education
and Scientific Research
University of Babylon
College of Engineering
Mechanical Engineering Department

EXPERIMENTAL AND NUMERICAL INVESTIGATION OF THE EFFECT OF FUEL TYPE ON FLAME HEIGHT

A THESIS
Submitted to the College of Engineering / University of Babylon,
in Partial Fulfillment for the Degree of
Doctor of Philosophy in Engineering/ Mechanical Engineering/ (Power)

By
Mohammed Abd Al-Khaliq Hashim Abd Al-Rasool

Supervised By:

Prof. Dr.
Dhirgham A. Al-Khafaji

Prof. Dr.
Haroun A.K, Shahad

2022 A.D. **1444 A.H.**

بِسْمِ اللَّهِ الرَّحْمَٰنِ الرَّحِيمِ

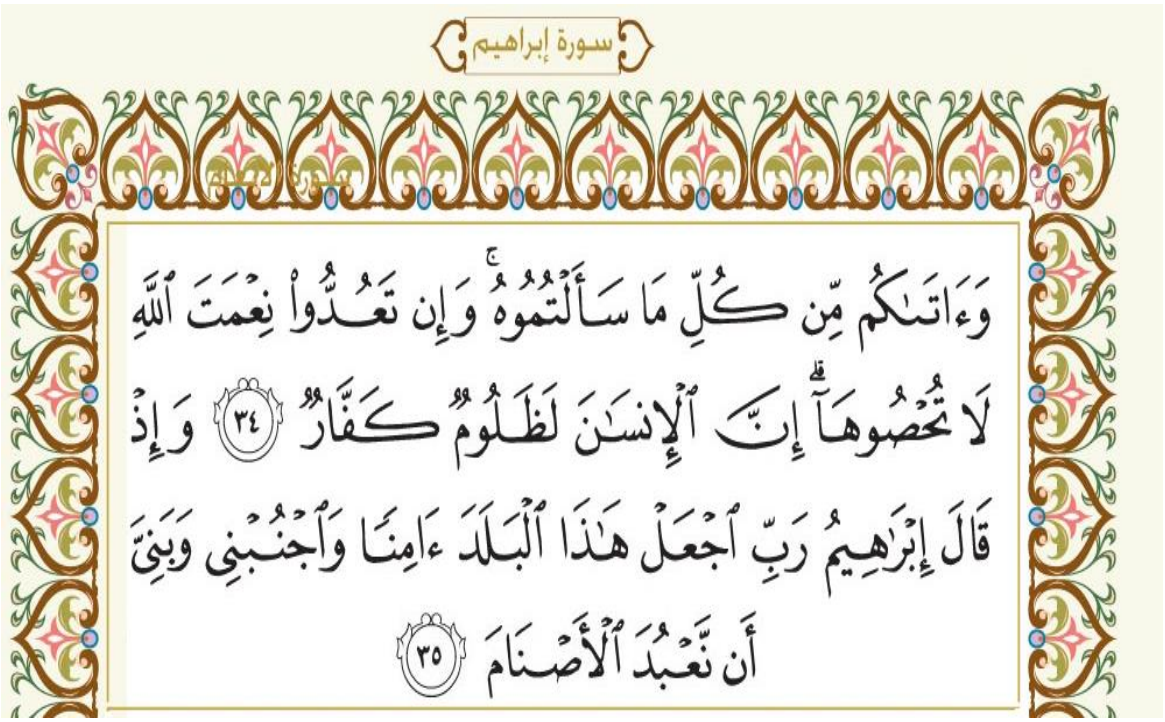

سورةُ إِبـراهِيـــم - الآيــات ﴿٣٤ و ٣٥﴾

Supervisor's Certification

This is to certify that the thesis entitled **"Experimental and Numerical Investigation of The Effect of Fuel Type on Flame Height"** has been carried out by **Mohammed Abd Al-Khaliq Hashim Al-Tayyar** under our supervision at the Department of Mechanical Engineering, University of Babylon/ Iraq, in partial fulfillments of the requirements for the degree of **Doctor of Philosophy in Mechanical Engineering / Power Engineering**.

Signature:

Prof. Dr. Dhirgham A. Al-Khafaji

Supervisor

Mechanical Engineering Dept.

College of Engineering

University of Babylon

Date: / / 2022

Signature:

Prof. Dr. Haroun A.K. Shahad

Supervisor

Mechanical Engineering Dept.

College of Engineering

University of Babylon

Date: / / 2022

Examination Committee Certification

We certify that we have read the thesis entitled "**Experimental and Numerical Investigation of The Effect of Fuel Type on Flame Height**" and examined the student **Mohammed Abd Al-Khaliq Hashim Al-Tayyar** in its content, and that in our opinion it is adequate for the debate the Partial Fulfilments of the Requirements for the Degree of Doctor of Philosophy in Mechanical Engineering / Power Engineering.

Signature:
Prof. Dr. Dhirgham A. Al-Khafaji
College of Engineering/Univ. of Babylon
(Member and Supervisor)
Date: / / 2022

Signature:
Prof. Dr. Haroun A.K. Shahad
College of Engineering/Univ. of Babylon
(Member and Supervisor)
Date: / / 2022

Signature:
Assist. Prof. Dr.Mahmoud A. Mashkour
Mech. Eng. Dept./ Univ. of Technology
(Member)
Date: 6 / 10 / 2022

Signature:
Assist. Prof. Dr. Samer M. Abdulhaleem
College of Engineering/Univ. of Babylon
(Member)
Date: / / 2022

Signature:
Assist. Prof. Dr. Adel M. Saleh
Mech. Eng. Dept./ Univ. of Technology
(Member)
Date: / / 2022

Signature:
Prof. Dr. Saba Y. Ahmed
College of Engineering/Univ. of Babylon
(Member)
Date: / / 2022

Signature:
Prof. Dr. Qasim Saleh Mahdi
College of Engineering/Univ. of Almustansiriyah
(Chairman)
Date: / / 2022

In view of the available recommendations, I forward this thesis for the debate by the examination committee.

Signature:
Assist. Prof. Dr. Samer M. Abdulhaleem
Chairman of Mechanical Engineering Department
College of Engineering, University of Babylon
Date: / / 2022

Approval of the Dean of collage of Engineering/ University of Babylon

Signature:
Prof. Dr. Hatem H. Obied
Dean of the College of Engineering
University of Babylon
Date: / / 2022

To the symbol of martyrdom and sacrifice "Imam Hussein & his brother Abbas",

To the cradle of science and civilization "wounded Iraq",

To my Compassionate mom and my late beloved father,

To the companion of my life, my lovely wife,

To my beloved daughter and dear son, whose their

childhood years accompanied my lengthy study,

and To my dear sister and brothers

I am pleased that you accept these Modest efforts of mine.

.....

Mohammed

ACKNOWLEDGEMENT

In the name of Allah, the first who deserves all thanks and gratitude for blessing all creatures and for providing the strength and willingness to establish this research.

I would like to express my deepest and sincere thanks to my supervisors Prof. Dr. Haroun A. K. Shahad & Prof. Dr. Dirgham A. Al-Khafaji for their advice, support, and ideas that were useful for completing this work.

Also, my sincere thanks to Asst. Prof. Dr. Samer M. AbdulHaleem the head of the Mechanical Engineering department at the University of Babylon and all the staff of the Department specifically Mr. Hussain Hamzah for his help and efforts, as well as all my colleagues.

Friends and people who have provided assistance and information are too numerous to list. Here, I take the opportunity to express my sincere thanks, love, and great appreciation for their efforts, opinions and observations. Here I wish to thank them especially my close friends Dr. Saif Wathiq from Mechanical Engineering Department at the University of Kufa, Dr. Mohammed Omar Ali from Al-Hussain University College, Asst. Prof. Ali J. Ramadhan, Dr. Naseer K. Bachache, and A. Lec. Kamal M. Raheem from University of Al-Kafeel and Mr. Haider Jabbar for their large favor in this work. Special thanks to my university, University of Al-Kafeel, for enduring my circumstances and supporting me during my studies.

Finally, I would like to thank my family, my wife, my daughter, my son, and my mother for their unconditional tolerance and support. During the years of this study, many friends and loved ones played an important role in encouraging to continue and complete the work, and I would like to express to all of them my sincere thanks and pride from my heart.

ABSTRACT

The current study investigates (both experimentally and numerically) how the type and composition of fuel affect flame height and characteristics as well as pollutant generation for the premixed liquified petroleum gas LPG via tube burner. The LPG was blended with hydrogen and the mixture was diluted with CO_2 at different equivalence ratios (ϕ), mixture flow rates, and burner's aspect ratios, using swirling/ non- swirling burners. Flame height has significant implications for the design of combustion systems, in addition to many economic and environmental considerations.

An experimental apparatus has been fabricated for the premixed combustion. A high-speed camera with a high resolution was used for flame capturing as well as recording the flame initiation history. Flame images were analysed by Matlab image processing and AutoCAD scaling. The practical examinations included testing five equivalence ratios (0.6, 0.8, 1, 1.2, & 1.4), five H_2 blending ratios (0%, 10%, 20%, 30%, & 40%,) four CO_2 dilution ratios (0%, 5%, 7.5%, & 10%,) with five burner's aspect ratios (2, 4, 6, 8, 10) for the non-swirling burner varying the mixture flow rate between flame flashback and blowoff limits. The effect of using a swirling burner was examined through the use of two swirler 0.78 & 0.48 swirl numbers respectively.

The numerical work comprises a 2D combustion modelling using OpenFOAM CFD code, XiFOAM solver, to predict flame height, location of preheating and reaction zones, and temperature distribution. Furthermore, the numerical study predicts qualitatively and quantitatively the formation of combustion products. The LPG/air combustion has been simulated for $\phi\ of$ (1, 1.2, 1.4, & 1.6) at 6 lpm. and also for (4, 5, 6, 7, & 8 lpm) at stoichiometric conditions. Besides, the effects of H_2 blending have been predicted for (0%, 5%, 20%, 40%, & 50%) ratios.

It has been noticed that ϕ dominants flame height and flame aspect ratio for all mixture types and composition at all operating conditions. Also, the predicted reaction zone thickness extends when ϕ increased. The measured inner zone and the visible flame of LPG elongate from 18.7 mm to 34.4 mm and from

35.8 mm to 56.5 mm respectively when increasing ϕ from 1 to 1.4. Mixture flow rate affects flame height and flame aspect ratio positively.

H_2 blending decreasing the flame aspect ratio while CO_2 dilution increasing it. Regarding to LPG-H_2-CO_2/air mixture, it was noticed that CO_2 prolonging the flame greater than the negative effect of H_2. The flame of LPG-5%CO_2-10%H_2 & LPG-10%CO_2-30%H_2 are taller by about 3% & 20% respectively than that of LPG at ϕ =1. When ϕ =1.2 the flame increase by about 12% & 30% for the aforementioned LPG-CO_2-H_2 mixtures.

Burner aspect ratio affects flame height insignificantly. The flame shortens clearly when using swirling burner for the stoichiometric and rich mixtures while there is not noticeably change in the lean side. Besides, increasing the swirl number increases flame height slightly.

Regarding to flame stability, it increases as ϕ increases and it enhances as a result of H_2 blending or CO_2 dilution. CO_2 enables the flame to overcome flashback while H_2 shifts flashback and blowoff limits towards higher flow rates. The use of a swirling burner enhancing flame stability dramatically when ϕ = 1 & 1.2 while the inverse observed when ϕ = 0.8.

The maximum predicted temperature of the flame decreases form 2383K to 1840K and then to 1608K when ϕ = 1, 1.4, & 1.6 respectively for LPG. A humble increase predicted in flame temperature due to H_2 blending. It increases 12K due to 50% H_2 blending with LPG when ϕ = 1. Temperature along the center line increases sharply & rapidly (about 2000K for LPG at ϕ = 1) throughout the reaction zone.

The numerical simulations indicate that the biggest quantity of fuel and oxidant are depleted within the reaction zone where the sharper increasing rate in the temperature and the progress variable shown along flame center line. Simultaneously, the higher increase in products mole fraction located in this tiny region. Regarding to pollutants formation, the maximum CO_2 mole fraction occurs at the stoichiometric condition and is less for lean side. The rich mixture producing lower fraction of CO_2. For the lean and stoichiometric mixtures, there are no CO production. For the rich mixtures, CO mole fraction increases

monotonically as ϕ increases. The blending of hydrogen at stoichiometric conditions decreasing O_2 & CO_2 mole fraction. The combustion of LPG-H_2 50% decreases O_2 & CO_2 mole fractions by about 3% and 9% respectively while the fuel mole fraction increases by about 78% as compared with LPG fuel.

The comparison of the present results shows a good coincides with about 2.8% & 1.8% error between the measured & predicted inner flame zone height for LPG & LPG-H_2 mixtures respectively. The maximum predicted flame temperature for LPG was compared with some previous works and the average difference is about 1.2%. The comparison of the predicted species mole fraction with previous works shows the same general trend for the curves.

LIST OF CONTENTS

CHAPTER FOUR: NUMERICAL STUDY

CHAPTER FIVE: RESULTS AND DISCUSSION

Nomenclatures

Symbol	Meaning	Unit
A	Area	m^2
b	Regress Variable	———
c	Progress Variable	———
$\mathbf{C_p}$	Specific heat at constant pressure	kJ/kg ^oC
d	CO_2 dilution ratio	%
h	Specific enthalpy	kJ/kg
k	Hydrogen blending ratio	%
n	Number of moles	Mole
P	Pressure	Pa
Pr	Prandtl number	———
Q	Volume Flow rate	lpm
Re	Reynolds number	———
Sc	Schmidt number	———
T	Temperature	K or ^oC
u	Velocity	m/s
V	Volume	Lt.

Greek Symbols

Symbol	Meaning	Unit
ρ	Density	kg/m^3
ϕ	Equivalence Ratio	———
λ	Thermal conductivity	W/m. K
μ	Dynamic Viscosity	Kg/m.s

SubScript

Symbol	Meaning
ad	Adiabatic
Air	Air flow
m	Average number of hydrogen atoms in LPG
n	Average number of carbon atoms in LPG
s	Specie
st.	*stoichiometric*
act.	Actual

Abbreviations

Symbol	Meaning	Unit
2D	Two Dimensional	———
CC	Combustion Chamber	———
CCD	Charge-coupled Device	———
CFD	Computational Fluid Dynamics	———
FOAM	Field Operation and Manipulation	———
fps	Frame per second	fps
GHG	Greenhouse Gases	———
I CCD	Intensified Charge-coupled Device	———
IDF	Inverse Diffusion Flame	———
LFG	Landfill Gas	
LPG	Liquified Petroleum Gas	———

PDF	probability density function	———
PLIF	Planner Laser-Induced Fluorescence	———
RGB	Red Green Blue	———

CHAPTER ONE

INTRODUCTION

1.1 Overview

The increase in the demand of energy has helped fossil-fuel combustion attract a great attention due to the rise in fuel consumptions and greenhouse gas emissions. Most of gas turbines, for example, burn fossil fuel air mixtures, which results in the emission of harmful greenhouse gases GHG including CO_2, NO_x, SO_x, soot, etc. The available techniques for exhaust gases capturing are still too complicated and costly if utilized in all gas-turbine industry [1].

The combustion investigations in every combustion system are a critical and complex problem. In general, the aim is to achieve a stable combustion appearing in industrial furnaces, combustors of gas turbines, diesel engines, spark ignition of engines and boiler furnaces etc. The research of describing and showcasing distinct forms of flame has become more vital than ever in order to boost combustion efficiency and minimize particle emissions [2]. Hydrocarbons combustion is still by far the most frequent source of energy in the world [3].

Laminar premixed flames, mostly combined with diffusion flames, are utilized in many residential, commercial, and industrial applications. These flames are by themselves significant; yet, possibly more significantly, understanding them is a necessary prerequisite for examining turbulent flames.

Flame height affects the design of combustion chamber and furnaces and the flame height is affected by the fuel type. The fuel type also affects the pollutants formation.

Validation of the models of flame structures and computing the residence time of the soot particle. The flame length is particularly significant since the flame should not strike the combustion chamber walls for safety and system integrity considerations. The spread of a flame over the surface of a combustible material is of importance to fire safety research because it has an effect on the early growth of the fire and the rate of heat release[4].

1.2 Modes of Combustion

There are three basic modes of combustion based on the method and nature of mixing the fuel and oxidant, namely premixed, diffusion or non-premixed, and partially premixed combustion. The present study is concerned with the study of flame height and pollutant formation in the premixed combustion of Iraqi LPG fuel that has been mixed with some blending.

1.2.1 Premixed Combustion

This mode is called the premixed mode, and it happens before combustion starts. The fuel is mixed at a molecular level with the oxidizer prior combustion chamber before the process starts. In this mode, there is a flame front that moves quickly into the unburned mixture with a certain rate of reaction and a certain speed. There are many practical combustion devices that have flames that have already been mixed together [5].

1.2. 2 Diffusion Combustion

In this type of combustion, the fuel and oxidizer move into the reaction zone mostly by diffusion as the reactants are separated at the beginning, mixing them happens at the reaction zone in which fuel mixes and burns [6]. Many combustors work in the diffusion mode for safety reasons. Fuel and oxidizers are not mixed together, which reduces the risk of an abrupt explosion. Also the diffusion flame is studied by many researchers worldwide such as [7] & [8].

1.2.3 Partial Premixed Combustion

Sometimes, both premixed and diffusion flames happen at the same time if the reactants are not in good mixture conditions. The diffusions are normally known as the chemical species diffusion from one side to another. This flames are known as partial premixed flame [9]. It occurs when part of the fuel is mixed with oxidant before burning while the other part is introduced to the CC during combustion process. This type of flame was studied by many research such as [10].

1.3 Flame and Flame Height

A flame is a localized combustion zone self-sustaining propagation at subsonic velocities. This definition has many keywords. First, flames are localized occupying only small portions of the combustible mixtures at any times. The second is subsonic. Discrete combustion waves traveling subsonically are called deflagrations [11]. The division of the flame into two zones is reasonable: the preheat zone, in which little heat is discharged. Then, the reaction zone which releases the bulk of the chemical energies. The flame was described as a narrow visible zone of highly exothermic chemical reaction where heat is significantly emitted [12].

Although the measurement of flame height has been defined in different ways, none is proved or preferred. So, comparing results of various studies must be taken care of and in applying correlation equations. Flame height is commonly defined as visual determinations by skilled observers, averaging some individual instantaneous seen flame lengths of photographic records that measure the axial locations of the mean peak center-line temperatures by thermocouples that calculate the axial locations in which the average mixture fractions on the flame axis is the stoichiometric values by gas sampling. Generally, these flame lengths seem to be bigger than those which are

according to the measurement of the temperature or concentrations [11] as shown in fig. (1.1).

The flame height has been defined as is the distances of the burner tips to the point where the fuel appears in a stoichiometric condition with the oxidizers over flame centerline. This definition is very common [13]. According to the National Wildfire Coordinating Group, the height of a flame is the average distance measured vertically, up and down, the flame height may be estimated by comparing the flame to a known dimension of an object. Newman and Wieczorek proposed a more accurate and more objective methodology according to the measurements of species along the flame axis [14] and are called chemical flame heights to be distinguished from luminous flame heights which is visually determined, see Fig. (1. 2).

1.3.1 Flame Height Measurement and Techniques

Hawthorne et al. [15] presented the idea of a chemical flame height, which they described as "the length to the point where 99% full combustion appears". The chemical flame height was specified as the axial point where the ratio of CO to CO2 was 0.15 [16]; however, no explanation was offered for this number. According to Wade and Gore [17], a chemical flame height may be defined as the point at which a flame's mole fraction decreases to less than 0.0005.

The flame reaction zone is described via the Planar Laser-induced fluorescence spectroscopy (PLIF) by the detection of the spatial distribution of OH, CH, and C_2 species, see Fig. (1. 3). PLIF is costly (of about 500,000 $) for the most university laboratory for using [13]. Yet, measuring OH PLIF shows that the maximum OH concentration is only in lean sides of the stoichiometric mixtures in laminar nonpremixed flames.

The most frequent method to measure flame height is visual inspection of the flame for determining the heights of the blue reaction zones. A more

consistent measuring flame height is through the measurement of the peak blue intensities on flame axis which the colour charge- coupled device (CCD) cameras record.

As the flame peak temperature reaches near stoichiometric circumstances, some researchers used the height of the flame by the measurement of highest centerline temperatures by using thermocouples [18].

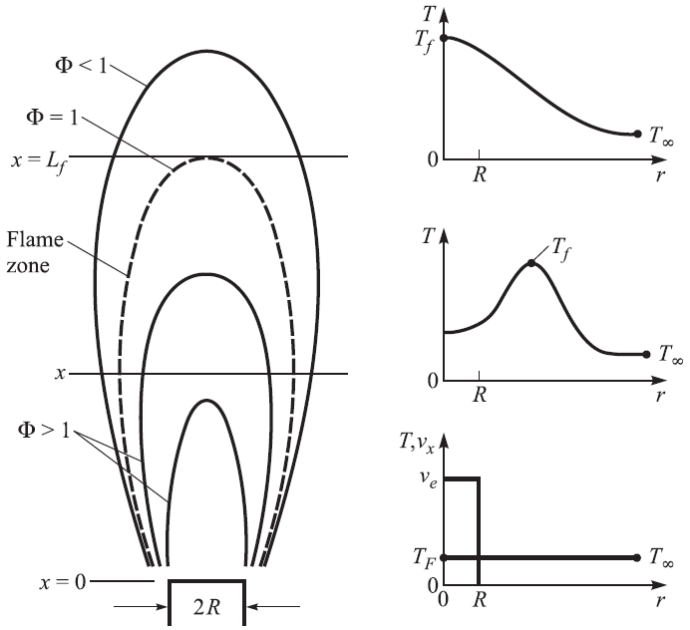

Fig. (1. 1) Laminar diffusion flame structure [11]

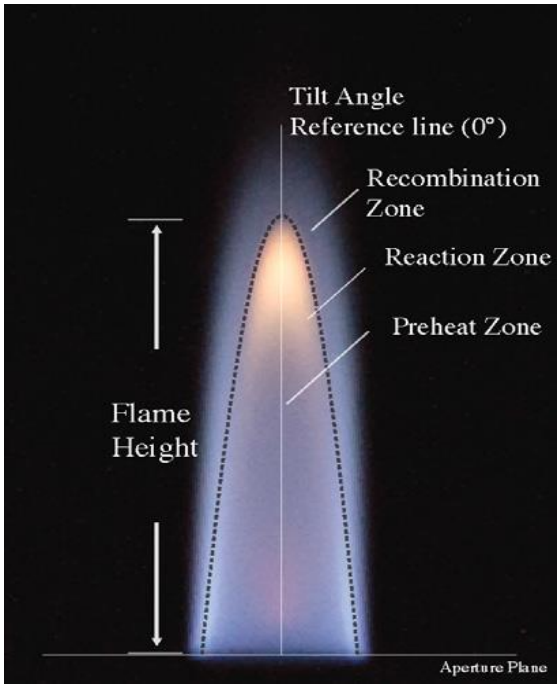

Fig. (1. 2) Schematic of a Typical Bunsen-type Flame [19]

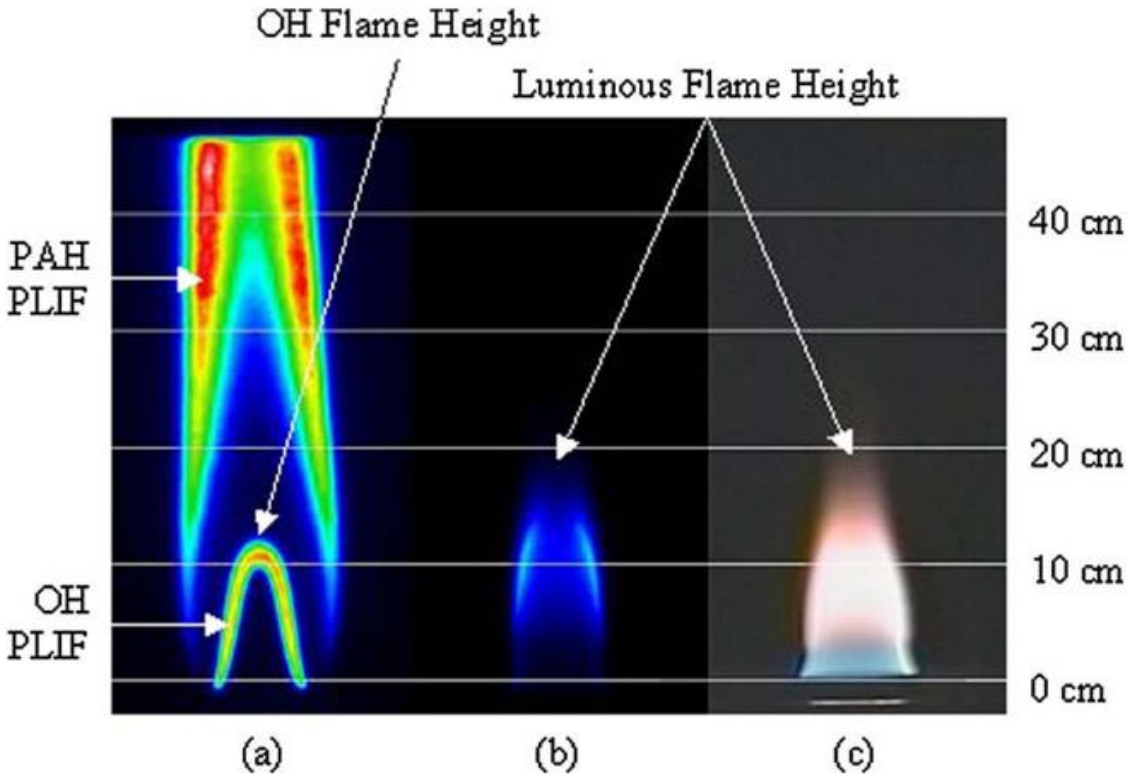

Fig. (1. 3) Image of inverse diffusion flame by [20]*: (a) OH PLIF, (b) luminous flame (absolute intensity) from the ICCD, and (c) visible flame recorded with a CCD camera*

1.3.2 Factors Influencing the Height of the Flame

Fuel or mixture jet issue into a quiescent environment creates a vertical flame, with four primary factors influencing the flame height [11]. These factors are: "the relative significance of preliminary jet momentum fluxes and buoyancy forces which acts on flames, stoichiometry conditions, the density ratios of nozzle fluid to ambient gas, the initial jet diameters".

In addition, flame height is influenced by some other factors such as:

1. Fuel type and blending ratio.
2. Laminar or turbulent.
3. Supply (inlet) velocity.
4. Nozzle configuration
5. Burner and combustion chamber design.

1.4 Liquefied petroleum gas (LPG)

Consuming more energy means that fossil fuels are depleting faster, which means that pollution from burning them is growing in the atmosphere, as are emissions of greenhouse gases and other pollutants that contribute to global warming. There is a growing emphasis on energy and environmental concerns nowadays, and the biggest obstacle for enhanced combustion of fossil fuels is environment, efficiency, and economical considerations [21].

LPG is extensively used in household, commercial, and industrial settings since it is one of the cleanest gaseous fuels. Its high volumetric heating value makes LPG a distinctive commodity in energy supply chains. Comparing hydrogen fuel to LPG in terms of availability and pollution emissions, hydrogen offers significant benefits. H_2 has the fastest flame speed of any chemical due to its tiniest molecule. The flame performance and stability range for the fuel mixture are likely to be severely affected by a low concentration of H_2 addition to the fuel.

For cooking and transportation, LPG is extensively utilized across the world. It consists mostly of propane and butane hydrocarbons and it is almost entirely derived from fossil fuel sources. LPG flames have been the subject of several experiments in the past. Flame length, lift-off height, blow-off velocity, and pollutant emissions were measured by [22] & [23] from pure LPG jet diffusion flames and LPG-H_2 flames. Preheated LPG-H_2 mixes also had an influence on visual flame characteristics [24]. LPG partly premixed flame soot generation and temperature dispersion were studied in Ref.[25].

Currently, the hydrocarbon fuels that blended with hydrogen have gained a lot of interest since of the opportunity to enhance the stability of the flame for fuel-lean combustion, boost heating performance, and minimize CO_2 and other pollutant emissions associated to burning carbon, such as CO, HC, and soot formation.

1.5 Aims of the Current Study

The main goals of the current research are to investigate the effects of different fuel mixtures, LPG/air mixture blended with hydrogen and diluted with CO_2, on the premixed stationary flame structure and flame height since it is a major parameter that affect combustion system design. Five equivalence ratios (0.6, 0.8, 1, 1.2, & 1.4) with five hydrogen blending ratios (0%, 10%, 20%, 30%, & 40%,) and four CO_2 dilution ratios (0%, 5%, 7.5%, & 10%,) have been tested experimentally. These effects will be investigated also with diverse sets of influencing factors. In order to achieve this study, experimental work & numerical analysis have been implemented.

The details of the experimental & numerical program are summarized as:

1) An experimental apparatus has constructed in order to visualize the height and the structure of the flame with the use of a high-speed camera.

2) Different experimental tests conducted comprise numerous compositions of LPG fuel / air mixture varying the equivalence ratio, hydrogen blending percentage, and CO_2 dilution percentage.

3) The experimental work also investigates the effect of burner geometry & configuration by testing different burner aspect ratios (length to diameter ratio) and by testing swirling & non-swirling burners.

4) In addition, the effect of flow rate of fuel/ air mixture on flame has been investigated experimentally.

5) This work also includes a numerical study through implementing a 2-D simulation for the combustion model using OpenFOAM CFD code and XiFOAM solver.

CHAPTER TWO

LITERATURE REVIEW

2.1 Introduction

One of the most significant and difficult challenges in combustion science is understanding how fuels burn. Improved efficiency in industrial furnaces, gas turbine combustors, and boiler furnaces, for example, necessitates a greater focus on identifying and showing different kinds of flames in order to minimize emissions of particulate matter and other air pollutants. Because of the low achievable level of NO_X emissions by limiting the peak combustion temperature by the quantity of excess air, the gas turbine industry, for example, is moving toward lean premixed combustion. Premixed combustion of hydrogen-rich gases, on the other hand, remains a difficult task [25]. Many households, commercial, and industrial equipment and processes use laminar premixed flames, which are typically used in combination with diffusion flames [26].

Measurements of flame height have been used to verify flame structure models and to calculate the residence times of soot particles. In industry, the flame height is particularly important since, for safety reasons and system integrity, the flame should not contact the combustion chamber walls in many applications. The flame length, also known as luminous flame height, is the distance between the burner outlet and the point at which the flame is no longer visible to the naked eye [27]. The flame height is known to influence the design of combustion chambers and furnaces, and the flame height is influenced by the fuel type. Pollution formation is also influenced by the type of fuel used.

This survey is devoted to a comprehensive review of the research literature available on experimental and / or theoretical studies, related to the

subject of flame structure and its propagation and pollution with respect to numerous considerations such fuel chemistry and composition, type of flame, design and fabrication of burners and their accessories

The following sections presents a review for the available literature which related to the subject of the current study. This review is divided into three parts: experimental studies, theoretical and/ or numerical studies, and the studies that involves both experimental with theoretical or numerical investigations.

2.2 Experimental Studies

According to Mikofski et al. 2006 [20], the flame heights is measured with methane-air laminar inverse diffusion flames IDF and co-flowing cylindrical ethylene-air. The height of luminous flames were longer than the heights of the reaction zones which the planar laser-induced fluorescence (PLIF) of hydroxyl radicals (OH) determine due to the luminous soot above the reaction zones. Yet, the locations of the peak luminous signals with the centerline matches the OH flame heights which is predicted by Roper's analyses for circular port burners confirming the calculated reaction zone heights by the value use for the features of diffusion coefficient and/or diffusion temperatures different from which Roper [28] recommends.

Shet et al. (2009) [29], investigated the effect of steam addition on flame luminosity, flame height and yellow-tipping zone by employing digital image processing technique for the flame captures. Piloted partially premixed laminar flames which a tubular burner was tested & flame images issue which a digital camera capture was processed by a MATLAB code. The flame height is calculated by noting the maximum luminosity point in the axial plot with reference to the burner rim. Axial pixel intensity plots of stoichiometric and two fuel-rich flames with (no) steam in the main fuel-air mixture stream were

examined. With increase in steam flow rate added the flame luminosity is decreased while flame height increased. The yellow-tipping flame zone appears brighter than the upstream flame zone. Further, its luminosity is seen to decrease and finally vanish when steam flow rate rises. The digital flame analysis is useful to quantify accurately the extent of yellow-tipping flame zone. Axial pixel intensity plotting is an easy and remarkable to determine the height of burner flames.

The turbulent LPG-IDF that is stable in a backstep burner was considered via **Mahesh and Mishra (2010)** [30] according to its visible length of flames, twin flame structures, centerline temperature distributions, and O_2 concentrations. Global Momentum Ratio (GMR) was utilized to show how air and fuel jet velocities affect the length of the visible flame. Air jet velocity has been found to make visible flame length shorter for fixed fuel jet velocities. The centreline temperature and oxygen concentration measurements confirm the dual flame structure of IDF and by the analysis of CH-chemiluminescence pattern.

Dong, Cheung et al. (2011) [31], examined an IDF which central air jet characterizes with arrays of fuel jets in experiments. The effects of ports diameter ratios of air to fuel (d_{air}/d_{fuel}) on the IDF structures in particular on its thermal and emission features have been also studied. The study investigated the small, moderate and large d_{air}/d_{fuel}. For example, the former had a blue flame with a superior thermal profile, with higher maximum temperatures of flame (Tf_{max}), larger ranges of air jet Reynolds number (Re_{air}) of flame stabilities, and larger operating ranges of the same rates in general. More CO and HC and less NOx were found in the exhaust of smaller d_{air} as a result of their smaller volumes and shorter flame residence durations.

Zheng et al. (2011) [13], employed the image processing method for the measurement of the the flame height by the common-used digital camera for the pulverized coal jet flame at high temperature air combustion situation.

Then, processed the jet flame image by ROI (region of interest), gray, binarizing, and edge detecting processing. By this processing, the pixels contain at the roots of the flame and the tips of flames are calculated. The flame region which is in pixels could be easily gotten through the variation of the flame root from the flame tip. The flame height is measured through the multiplication of the differences in pixels along side the pixel resolution(in millimeters per pixel).

Miao et al. (2013) [27], studied the flame structure and flame length of LPG-air and 50% H_2-LPG-air flames for circumferential-fuel-jets inverse diffusion flame burner. Reynolds number (1500 & 3000), equivalence ratio and fuel jet velocity of the two models flames (LPG and the 50% H_2-LPG mixed fuel) was identified. Small percentage addition of hydrogen could give significantly enlargement on LPG flame stable range. Lengths of the two model flames were obtained under a fixed Reynolds number were gradually increased with equivalence ratio. Lengths of both flames could be correlated well with Global Momentum Ratio (GMR) at Re=1500 and Re = 3000. LPG flame were seen to be longer than H_2-LPG flames in fuel rich situations.

Hu et al. (2013) [32], studied the reduced atmosphere for turbulent buoyant jet diffusion flames and global correlations. They found a reduced atmospheric pressure. The experiments were compared for measuring the mean flame height and lift-off behaviors. The study showed that the normalized mean heights of flame increased in the lower pressure atmospheres.

A methodology given by **Trindade et al. (2014)** [33], includes a mechanism that converts one RGB picture data, produced by standard CCD cameras, into dependable sensing on local combustion condition for practical use of premixed methane and propane gases. At a high rate for images resolution of 0.6 Mpixel/s, the improved image processing method can process high-resolution photos on a typical desktop computer. A broad range of

application for air/fuel ratio sensing, running approximately between 0.8 and 1, was discovered experimentally by observing how camera "blue and green" channels imitate flame CH and C emissions.

Tamadonfar & Gülder (2014) [34], examined the features of the flame brush of premixed turbulent methane/air flame for Bunsen-type burner. Particle image velocimetry and Rayleigh scattering techniques were used for measuring the temperature fields and the instantaneous velocity. They conducted the experiments in different equivalence ratios and bulk flow velocities. Normalized flame height and centerline flame brush thickness correlate negatively with ϕ, longitudinal integral length scales, & total turbulence intensities, but positively with bulk flow velocity. Half-burning surface turbulent burning velocity adjusted by bulk flow velocity decreased as flame height climbed. A time-averaged view of a laminar premixed flame showed an extremely complex response front, with the most folds towards the flame's peak. A turbulent flame brush is a term used to describe this dense response zone, but the immediate view clearly displays the real reaction front to be quite narrow. Laminar flamelets are another name for these reaction fronts, which are caused by fast chemical reactions and change locations fast in space [11] as shown in Fig. (2. 1).

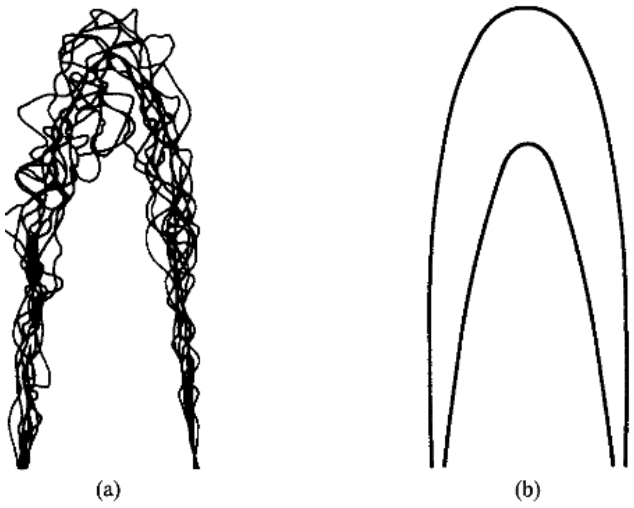

Fig. (2. 1): a superposition of instantaneous reaction fronts recorded at various intervals, b) turbulent flame "brush" coupled with a time-averaged image of the same flame [11].

In **2014 Hu et al** [35] experimentally studied the calculations for the premixed laminar flames for the mixtures of CH_4/air and CH_4/air with hydrogen additions. They used roaming approaches thermocouple for measuring the profiles of axial flame temperature in a range of ϕ and H_2 enrichments rates. The calculated temperatures were examined through estimating the rates of flame heat releases. Many significant flames characteristics, like the temperature at the peak and average values, reaction zone and combustion efficiency thickness. The heat release profile analysis showed that adding hydrogen significantly influence the early parts of flame heat discharge profiles. The promoted H formation makes the flame burning velocity quicker.

A number of distinct LPG/air mixes with various compositions, temperatures, and pressures were subjected to a numerical simulation by **Kishore et. al. (2015)** [36] using the USC Mech II reaction mechanism to determine the effects of H_2 blending. The LPG was considered to be composed of 50% C_3H_8 and 50% C_4H_{10}. The simulation comprised varying the volumetric H_2 addition between 0-50% testing different values for ϕ while temperature of the mixture was up to 450 K varying the pressure between 1 & 10 bar. Results marked that flame speed effected linearly regarding to the amount of H2 addition and in a parabolic way with ϕ, with a maximum value for a somewhat rich mixture. The speed of a laminar flame changes with both temperature and pressure. A good agreement was observed between the predicted results and the experimental data of Tang et. al. [37]

To better understand the impact of preheating and dilution on the flame properties of Bunsen-type premixed flames, **Zhen et al. (2016)** [21] conducted an experimental investigation. CH_4-H_2/air mixture with $\phi = 1$ was diluted with CO_2 or N_2, while the temperature of the initial reactants was incremented at 5 levels between 20 ^oC - 100 ^oC. The flame of CH_4-H_2-CO_2 mixture has a faster burning rate and a higher flame temperature than the N_2 flame. The

conical flame height drops monotonically as the preheating temperature rises. Shortening the height of the flame indicates a greater rate of laminar burning vs a higher temperature of preheating. The N_2 flame's height is less than the CO_2 flames. The temperature of the flame's centerline decreases monotonically as the axial distance above the burner increases. N_2 has a greater centerline temperature than CO_2 in a flame. In the absence of dilution, the concentrations of NO_x and CO rise in lockstep with the rise in preheating temperature. only slightly greater NO_x concentration in N_2 diluted flames than CO_2 In the same vein, CO_2 diluted flames have the greatest CO concentration, whilst a CH_4-H_2 diluted flame has the lowest.

Najafian and Ashjaee (2016) [38], worked on laminar premixed LFG fuel to study the influence of Re and ϕ on flame temperature fields and thermal flame heights. A slot burner with 6 mm width and 60 mm length was used with three cases of fuel: pure CH_4, LFG_{70}, and LFG_{30} while Re and ϕ were varying between 100-600 and 0.7-1.3, respectively. Mach-Zehnder interferometry technique is utilized for obtaining perspicuity into the overall temperature fields. LFG flames compared has lower flame temperature than that of CH_4 flame. As CO_2 volume fraction increased the thermal flame height was augmented at the lean mixture and it then reduced for stoichiometric and rich flames. With Re increase, thermal flame height augments linearly, while for lean mixtures Re effects is insignificant.

Zheng et al. (2017) [39], investigated the effect of hydrogen addition on flame propagation of premixed hydrogen/methane/air. Various lengths and widths of Plexiglas conduit were used to construct six horizontal ducts. All mixtures were stoichiometric while hydrogen fractions varied (0-100%) with a 25% increment. A high-speed camera, 4000 fps with 1024 * 1024 pixels, was used for monitored the detailed flame evolution process. Flame shape is affected by both aspect ratio and hydrogen percentage. An indented "tulip" flame with tulip lips was seen for pure hydrogen. Lower hydrogen percentages

resulted in an asymmetric flame front. A cellular flame emerged in the duct before to the conclusion of propagation of the flame, which continued to propagate while keeping its tulip shape.

In 2017 **Chang Fa Tao et al** [40] studied temperature distribution as well as the air entrainments of buoyancy-controlled jet flames experimentally from inclined nozzles surrounded by the walls. These experiments include the square nozzles, the wall thermocouples. Also, the flow meter is controlled and the fuel was Methane. Increased inclination angles result in a rise in the parameter constant for jet flames' intermittent and plume regions. Air entrainment reduces as the inclination angle rises. When incorporating air entrainment in buoyancy-controlled jet flames from the nozzles on the inclined wall, an improved temperature profile model has been discovered.

Wang et al. (2018) [41], implemented sets of experiments on rectangular nozzles to investigate the mean flame heights and the air entrainment rates of double buoyancy-controlled methane fires jets using CCD camera. The rectangular nozzles were with various geometric shapes of 36mm^2 sectional areas. They considered two identical nozzles alongside a similar heat release rates at all tests and changing the distances between the two nozzles from 1 to 12 cm. The flame height expands when the heat release rate increase, while it shrinks against distances between the two nozzles at first, and then flame height remains unchanged with wide distance. A new correlation was suggested among the flame height, spacing between the two nozzles, and the heat release rate taking into account effect of the air entrainment rate.

Kumaran et al. (2018) [42]**,** studied experimentally LPG flames in different configurations for a *lab-scale co-flow burner* using shadowgraph with a parabolic mirror and direct images. The images were processed using an image processing software ImageJ. The plume width is obtained by the shadowgraph

grayscale intensity plots. Jet diffusion flames, partially premixed flames, jet diffusion flames in co-flow and partially premixed flames in co-flow. The visible flame extents were measured by flame direct photographs.

Patel & Shah (2018) [43]**,** tested the flame and emissions of LPG-IDF practically. Flame height, the emissions of CO and NO_x were tested for different values of ϕ and vane angles of the swirler. For the non-swirling IDFs the flame lengths lengthened with fuel jet velocity and shortens with air jet velocity.The soot free length fraction correlates with air jet velocities as effective entrainments of the fuel enhancing the fuel premixing with air and generating extended blue zones of the IDF with swirl being larger, shorter, and stable than IDFs with no swirl. Flame of a swirler with 30° emitted CO and NO_x similarly to non-swirling IDFs. The flame neck, which is yellow, indicates the presence of soot (soot ring). The flame torch comprises the inner blue zone and external luminous zone as shown in Fig. (2. 2).

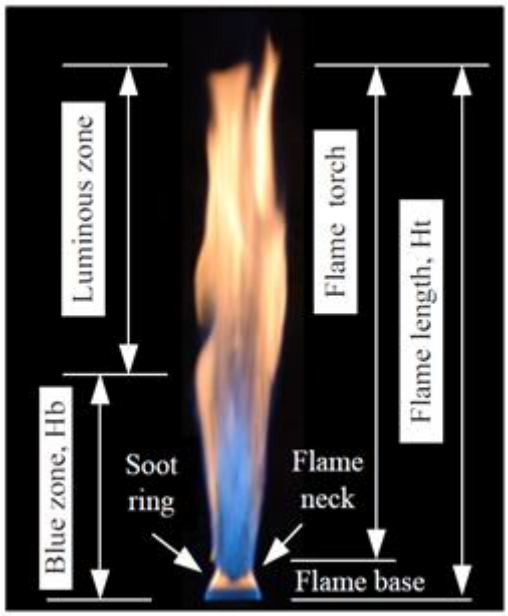

Fig. (2. 2) Inverse diffusion flame structure [43]

Verdier et al. (2018) [44], performed experiments on n-heptane spray flames to examine their structure, local extinction processesm & flow topology. A Planar Laser Induced Fluorescence PLIF of high-speed intended

for use with OH radicals as well as a Phase Doppler Anemometry PDA are used to quantify droplet size and velocity. Investigated flame structure, flow topology and local extinction mechanisms of n -heptane spray flames experimentally. The experiments include measurements of droplet size and velocity by Phase Doppler Anemometry (PDA), flame structure by High-Speed Planar Laser Induced Fluorescence of OH radical (HS-OH-PLIF).

There are extensive studies of the air entrainment rates and flame heights of the ring pool fire **Tao et al. (2018)** [45]. Ring pool fires exterior diameters were 15 cm, 20 cm, 25 cm, 35 cm, 45 cm, and 55 cm, respectively. For each pool, the variation between the internal and external diameters is 10 cm. The flame height of ethanol varies somewhat as the comparable pool diameter rises, but the flame height of *n*-heptane rises meaningfully. For both fuels, a unified correlation based on air entrainment was constructed, and the calculations collapsed well with the physical models.

The burner geometry impact on operation windows of small commercial LPG burner was examined in Ref. [46]–[50]. Three ratios (1, 2, and 3) for the burner rim length to diameter were examined. The burner has been provided with a swirl vane guide to improve the stability of combustion and flame structure. Results exhibited that the swirl coherent structure decrease as length of burner neck increase and thus the flow will have turned to diffusion flows cauding the abilities of having boundary layer flashbacks. Yet, with the limits of burners, the length of burner neck increase produces good results in blow off sides. In term of the burner powers, when LPG mixed with swirl flow raises the burner powers. However, the enhancement is because of the fuel types yet the flow structures have important impacts on flame stabilities.

Zhang et al. (2019) [51], analyzed turbulent flame topology features of the model syngas for two distinct hydrogen ratios analytically, CO/H2 ratios of 80/20 and 65/35 , at $\phi = 0.7$. Syngas flames exhibit a lesser scale of flame inherent instability than CH_4/air flames, which is likely to be the primary cause

of this. CO2 was diluted with the model syngas by a mole fraction of 0.3 wih to imitate turbulent combustion flue, gas recycling. Image analysis yielded flame front parameters, which were then used to deduce information about the flame's morphology.

The low-turbulence CH_4/air and C_3H_8/air premixed Bunsen flames were studied by **Nie et al. (2019)** [52] for their flame height and brush thickness. A hot wire anemometry was used to measure the perforated plates and outlet velocity to produce and regulate the turbulence flow field. The OH-PLIF method was used to identify the turbulence of the flame fronts. The typical length of turbulent Bunsen flame as well as the flame brush thickness at the centerline are decrease due to the increas in the values of ϕ, whereas they expand as the outlet velocity increases.

He et al. (2019) [53], investigated the flame binary rectangular pool fire height with various aspect ratios and lengths in the environment experimentally. Four gas burners were utilized, each with the similar surface areas and different aspect ratios. The distance between two gas burners was studied. The speed of air from the ambient region to the additional and flame zones is unaffected by variations in heat release rates or distance. Twin rectangular flames of varied aspect ratios and distance may be predicted using a non-dimensional correlation model. The dimensionless heights of flames are thus power functions of the rates of dimensionless heat release.

The effect of adding H_2 to CH_4 on the development of swirling and non-swirling inverse diffusion flames (IDF) and their emissions properties was studied experimentally by **Patel and Shah (2019)** [54]. Flame length, axial and radial temperature variation, and other combustion parameters were investigated. For a constant energy input and a constant volumetric fuel flow rate, hydrogen was added to methane on a mass and volume basis. Hydrogen blending reduced the entrainment area, mixing area, reaction zone, and post-

combustion area, resulting in a shorter flame. Methane mass enrichment with hydrogen reduces CO emissions by up to 6% while increasing NOx emissions moderately. The impact of hydrogen on combustion and emission parameters is greater in non-swirling IDF.

Tao et al. (2021) [55], tested the mixture of C_3H_8-CO_2 under identical heat release rate to investigate the flame length and lift-off height while varying CO_2 concentrations with various nozzle diameters. Raised CO_2 level in the gas mixture lowered the flame height initially, then increased it again, for similar heat release rate. When the heat release rate was adequately high, the height of flame reduced as CO_2 concentration increased. The lift-off height of the gas mixture expanded as the CO_2 level in the gas mixture raised for the same heat release rate and nozzle diameter.

2.3 Numerical and Theoretical Studies

Roper (1977) [56]**,** developed and confirmed through experiment expressions the prediction of the laminar jet flame lengths to several burner geometries (circulars, squares, slots, and curved slots) and flow regimes (buoyancy-controlled, momentum-controlled, and transitional). To the circular burner ports, the next estimates were suggested for flame lengths [11],

$$L_{f,thy} = \frac{Q_F \left(\frac{T_\infty}{T_F}\right)}{4\pi D_\infty \ln\left(1+\frac{1}{S}\right)} \left(\frac{T_\infty}{T_f}\right)^{0.67} \quad (2.1)$$

$$L_{\mathrm{f,exp}} = 1330 \frac{Q_F \left(\frac{T_\infty}{T_F}\right)}{\ln\left(1+\frac{1}{S}\right)} \quad (2.2)$$

Here S is the molar stoichiometric oxidizer–fuel ratios and D_∞ refers to the the oxidizer's mean diffusion coefficient at the oxidizer stream temperatures, T_∞. T_F & T_f represent the fuel stream temperature and mean flame temperature, respectively. All quantities are evaluated in SI units. Note that the burner diameter does not explicitly appear in either of these expressions.

In **1998 Plessing et al** [57] investigated the velocity fields, OH-LIPF , and C_2Hx-LIF imaging practically for key concentrations of the species, with a Rayleigh techniques for temperatures. Numerical simulations for solving axisymmetric two-dimensional Navier-Stokes equations at zero Mach number, incorporating temperature and species balance equations. All methods of molecular transport have constant and non-unity Lewis numbers. Chemistry's ten-step methane oxidation process. Heat exchanges between branches and heat loss at bent flame fronts at triple points influenced the construction greatly.

A two-dimensional propagation of an argon-diluted hydrogen-oxygen detonation under low pressure was estimated by **Oran et al in 1998** [58] utilizing a comprehensive chemical reaction mechanism. A one-dimensional solution was developed into a two-dimensional grid. After the first burst behind the Mach stem, a second burst occurs halfway through the detonation cell, which is seen in the pattern of energy release in a detonation cell. When transverse waves contact and ignite, an explosion occurs, releasing a large quantity of energy and covering a large area. To increase the speed and efficiency of the integrations, new methodologies were devised for massively parallel Connection Mechanisms.

Using a lean premixed H2/air flame as a starting point, **Cabra et. al. in 2005** [59] created a coaxial flow of hot combustion materials in which a fuel jet was introduced from the middle nozzles. A mixture of CH_4 and air is used to power the engine. For the single base case, they produced multiscalar point computations from the combined Raman–Rayleigh–LIF models. They presented and contrasted the experimental results and computed PDF findings integrating several models for mixing. Reactive scalar distributions in the flame stabilization areas were found to have extended bimodal distributions. PDF measurements employing the corrected Curl model for mixing reveal many elements of the multiscale experiments, but not the instantaneous

distributions of temperature and composition, the time averaged scalar profiles, or the conditional statistics. According to PDF model estimations corresponding circumsntance, the height of flame liftoff sensitivity to the jet velocities and co-flow temperatures of the sensitivities for the co-flow velocities is under-predicted.

Knudsen et al. (2006) [60]**,** presented transport equation for the flame brush thickness and new modeling approaches to the unclosed production and dissipation terms were suggested. To validate and test these approaches, a series of direct numerical simulations (DNS) of turbulent level set propagation were performed. The resulting transport equation for the flame brush thickness accurately describes transient cases and thus offers an improved means of predicting flame properties in non-equilibrium regions, e.g., near burner nozzles or flame stabilizers.

A flame length approach that uses a CFD framework to calculate the flame structure simulates the human eye or camera was presented by **Cumber and Spearpoint (2006)** [61]**,** The assumption that a temperature value delineates the visible area of the flame is a frequent technique. A 200 K shift in axial temperature results in a 20–25 percent variance in flame length. The following stages make up the flame length methodology: firstly using a CFD model to figure out the jet flame structure, then define the camera's position and angle, next calculate the camera lens's intensity field, later reflect the intensity field of the incident back onto a plane perpendicular to the camera through the fire, and finaly from the projected intensity field, calculate the flame length.

Smith et al. (2007) [62], showed that the CFD analyses of the gas flares and illustrated the CFD tools are able to simulate soot formations, radiant fluxes, flame shapes, and flame heights for industrial scale low-profile flare fields. Test findings calibrate the combustion models and validate CFD predictions of flame height and air demand. For the facilitation of the efficient

and practical CFD calculations, minimum numbers of chemical reactions was used fulfilling the requirements of total energy yields and species consumptions and productions.

CFD simulations were used by **Dabade et al. (2012)** [3] to model the flame structure for diffusion combustion. The flame properties of an enclosed cylinder were predicted using ANSYS Fluent 13.0. This is done by inserting a micro jet into the burner's core. Flow rates of the micro jet, fuel jet, and co-flow jet were tested for their influence on flame properties. It demonstrated that numerical modeling may be used to build new approaches for precise control of various kinds of flames.

Li (2016) [63], investigated the effects of pressure on flame structure and soot formation based on the simulation of the simple laminar co-flow diffusion flame of *n*-heptane/air by the developed skeletal reaction mechanism. According to the results, the flame height keeps constant at a pressure range of 0.7~3.0 MPa. The maximum carbon conversion to soot is in proportion to pressure range 0.1~2.0 MPa; the same is true with maximum soot volume concentration and pressure as p^{2}.

Essa Salem (2018) [9]**,** achieved a several simulations with reduced mechanisms for the combustion of hydrocarbons diluted with hydrogen, syngas, and bi-product fuel in a 2D cylindrical tube combustor to visualize the flame characteristics. The simulations were carried out using the ANSYS Fluent 19.1. The equivalence ratios were changed from "lean" to "rich". Small amounts of hydrogen were also added to the fuel blends. Changes in temperature, formation of radicals, the speed at which they burned, and the decrease in NOx and CO2 emissions were observed. The results compared to experimental data to study the changes. It was determined that the reduced mechanisms provided results within an acceptable range.

Xie et al. (2019) [64]**,** proposed a novel burner capable of keeping efficiency high while reducing the amount of NO_x that was released. An inert

gas stream was used for separating the fuel and oxidant. This is speculated to delay the fuel and oxidant reaction and to speed up the formation of "moderate or intense low-oxygen dilution" (MILD) regime. CFD simulations were done for O_2 concentrations ranging from 19.5% to 26.5% to look into how the new burner worked after a lot of testing. Comparison the temperature, species, and NO_x emission of the O_2 levels to see which one is best for your health. Using the novel burner, the maximum temperature of the original burner can be reduced by a range of 58 to 106 K for the O_2 concentrations that were used. The novel burners have been evaluated to lower NO_x emissions by as much as 1/8-1/2 of the original quantity when they are utilized at the O_2 concentrations measured according to the MILD combustion status.

Zhong (2020) [65]**,** presented LES n-heptane/air turbulent premixed combustion simulation in a slot burner in various preheating conditions. The low temperature chemistry influence was studied on turbulent burning velocities for different flame regimes, such as chemically frozen regime in which there is low temperature ignition (LTI) regimes with the mixture in the burner undergoing LTI reactions, and transition regimes from CF to LTI. The findings indicate flames in the LTI regimes exhibit the highest turbulent burning velocities. For the study of the influence of LTI flame reactions, series of two-dimensional laminar flames was stimulated eliminating turbulence on the flames. The laminar burning velocities in the LTI improved greatly the heat release zones expand. So, as the reactants initial temperatures rise, the heights of the flame reduce & flame cone angles rise improving burning velocities. When the three cases are compared, the flame wrinkling drops from CF toward LTI regimes, with a decrease in flame heights, enhancing burning velocities but a reducing the impact of turbulent flame wrinkling. These cases are examined according to the experiment of the burners of Won et al. [66].

Kutkan and Guerrero (2021) [67], performed a simulations for the turbulent premixed Bunsen flame using OpenFOAM and Ansys Fluent for the

Algebraic Flame Surface Wrinkling AFSW model. The results of both solvers were compared to the results from the experiments. Each simulation involved a 2D axisymmetric model with the standard $k-\epsilon$ model with wall functions for all of the simulations. fuel/air mixtures were tested by varying the volumetric ratio. 100% CH_4 and 60% CH_4 -40% H_2 were tested. The open-source library Cantera concurrently with the GRI Mech 3.0 chemical mechanism were used to predict the mixture's thermophysical and transport properties as the temperature changed. The AFSW model that was used in both solvers was found to be work well with the experimental results, both quantitatively and qualitatively. From another side chemical reactions, the turbulence model and turbulent boundary/initial conditions have a big impact on the shape and height of the flames.

A numerical study on a methane-air micro-burner was performed by **Zarvandi et al. (2022)** [68]**,** to investigate the effects of the location and diameter of an inserted wire on flame characteristics. Flame position and distribution of temperature, H and OH species were observed as a result of these characteristics. While changing the location and diameter of the wire, it turns out that the location of flame in the burner was affected. The peak values of the hot-flame crucial OH and H chemical species changed, although the maximum temperature of the burner's auxiliary axis or the exterior wall remained unaffected. It was also found that temperature distribution on the burner's exterior was impacted by the wire's position in relation to its diameter more than by its diameter.

Afonso et. al. (2022) [69]**,** reported the influence of flame and flame stability by the design of the burner through a numerical simulation for the combustion of premixed hydrogen and air in an undulate microchannel. As flow dynamics and combustion behavior are so complicated, only the effect of the fuel inlet rate on the flame characteristics have been taken into account, keeping other variables the same. The flame would be stretched along the

microchannel. For faster speeds, flame separation was seen, with two different areas of combustion, and the temperature profiles along the burner centerline changed in a non-monotonic way because of the dynamics of the vortices seen in the convex areas of the undulated geometry walls.

2.4 Experimental with Numerical/ Theoretical Investigations

Samantaray & Mohanta (2015) [2], in a 500 kW PF pilot swirl burner, used digital image processing to identify various types of combustion flames. Under co-firing circumstances, a natural gas flame and several pulverized fuel flames of coal and biomass were compared to each other. Two-dimensional distributions of the flame's statistical and spectral properties have been derived via digital image processing and visually shown. Co-firing of coal and biomass in pulverized fuel fires has been studied and compared by both groups, although the results are divergent.

Xu et al. (2017) [70], examined the effect of replacing N_2 in the air by H_2O and CO_2 up to 30% on the structure and shape of flames in laminar coflow syngas nonpremixed combustion while keeping the oxygen content at 21% both experimentally and numerically. Two cameras were used, ICCD & CCD camera, for capturing OH-chemiluminescence and flame luminance in respect camera for identifying the flame heights and radii. The numerical work involves the chemical, thermal, radiative, transport, and adding H_2O and CO_2 influence. The results indited that the addition of CO_2 and H_2O and as a diluent gas reduces the peak flame temperatures, while their impact on the flame distributions of centerline temperatures were disparate. Flame temperatures decrease as a result of the thermal and radiative effects of the dilution of both H_2O and CO_2, whereas they were affected differently concerning the chemical

and transport effects. With more H_2O increment, OH concentration boost leading to more combustion intensity which makes flame height and radius reduce. On the other hand, OH concentration was decreased with CO_2 addition and the overall combustion process was quelled, resulting in increased flame height and radius.

Weiguo Cao et. al (2018) [71], studied flame propagation tendency and the mechanism of premixed methane-hydrogen/air mixtures , a pressure recording device was utilized for measuring explosion pressure with varying volume fractions of methane-hydrogen in a closed duct. In the meantime, a high-speed video camera was employed for evaluating flame propagation behaviour with the optimal fraction. A 2-D simulation was conducted using CFD software ANSYS Fluent 17.0 for predicting the flame propagation behaviour. Comparison of the numerical and experimental data indicated acceptable qualitative and quantitative agreement. Additionally, the numerical simulation was employed for resolving technical issues of understanding the process of flame propagation.

To forecast flame height intermittency using image processing and dimensional analysis, **Maynard & Butta (2018)** [72] developed a physical model. The height & intermittency of flame as a function of the pulsation to burnout timings were shown. The flame was sequestered from its backgrounds via an image segmentation tool coupled with MATLAB. This is repeated for a series of images. CH_4 burners with equivalent diameters of 23, 34, 47, and 81 cm were used to test the physical model and measurement procedures where maximum heat release rates were 50, 550, 550, and 1500 kW, respectively. When the ratio of burnout to fire pulsation timeframes is more than one, the flame intermittency increases to one-fifth power. Because there is just one pulse of flame in the plume, the relative flame intermittency quickly reaches unity when this ratio is smaller than one.

With the use of three high-definition cameras, **Cruz-Ávila et al. (2020)** [73] created a flame-height correlation for the nonpremixed flames in laminar to turbulent regimes in the form of computational and experimental research. The height of the flame was determined using an image processing method. The unsteady Reynolds-Averaged Navier-Stokes' method was used to find the total chemical-flame-length in simulations. A 16.9 percent adjustment variance in luminous flame-height for the laminar regime suggests that this suggested correlation best characterizes the flame-height in this regime without the usage of the intermittent buoyant flame-height correlation. According to well-known flame-height correlations, the adjustment variations for the laminar and transition-to-turbulence regimes are 5.54 percent, indicating an acceptable match. In comparison to the experimental flame pictures, the numerical findings reveal that the recommended range for the chemical-flame-length is between the luminous and flickering flame regions.

Abdulameer (2020) [74], [75], investigated experimentally and theoretically the stability zone of laminar premixed Iraqi LPG/H2-air flames at Non-swirled burners. Pyrex tubes (10, 12.5, and 17 mm) in diameters were used as burners and the flames were captured using high-speed camera and a concave mirror. Different H2 blends (0%-50%) at equivalence ratios (0.6-1.4) were examined. At equivalence ratios somewhat greater than unity, maximum flashback limits were reached. The stability zone was found to be narrow on the lean combustion side and enhanced with increasing diameter and hydrogen addition. With increased burner diameter, the flashback limits were shown to decrease. The blow-off limit rose with rising fuel concentration, but its limit increased when increasing blended hydrogen.

A 3D computational investigation with LES model in ANSYS Fluent 19R3 was performed by **Nemitallah et al. (2021)** [1], to predict the combustion, exhaust-gas concentrations, and stability characteristics. The numerical results were validated against some previous experimental results.

The simulations comprised lean premixed oxy-propane diluted with CO_2 ($C_3H_8/O_2/CO_2$) flames with equivalence ratio of 0.26 – 0.8 while O_2 fraction (OF: 35-60 percentage) considering a swirl-stabilized model gas turbine combustor. In terms of macro- and flowfield structures, results reveal that flames of equal adiabatic flame temperatures have comparable flame shapes, flow circulation, and temperature distributions, as well as species concentrations. As the T_{ad} rises, the flames of oxy-propane become more compact, with a thinner flame and a higher Damkohler number. CO concentration at the combustor outlet is influenced by the composition of the mixture and the combustion temperature. The flame with the highest Φ and Tad emitted the most CO (0.17 ppm), whereas flames with high OF and low Φ emitted no CO.

H. M. Mjbel et al. (2021) [76]**,** presented a numerical and an experiential study for the combustion Iraqi LPG-air mixture in a horizontal cylindrical Pyrex combustion chamber for Φ ranging from 0.6- 1.4. The flame propagation through the combustion chamber was recorded using A high-speed camera. The laminar flame propagation speed was attained from these videos using Tracker program. The numerical prediction of flame speed was carried out by Chemkin USC mech 2.0. The flame speed was found to be increased, both experimentally and numerically, with equivalence ratio and reaches its maximum value at stoichiometry and then declines as the mixture grows richer. The numerical analysis exhibited that high propane ratio enhances flame speed.

2.5 Motivations of the Present Work

It is obvious from the previously cited survey that the study of flame and flame structure is complex, thorny, and varied where each work investigated some points of the inclusive different considerations related to the combustion. The previous literature indicates the deficient for a comprehensive study comprises an experimental & numerical investigation about premixed LPG-

fuel flames, which deals with the influence of fuel mixture composition and its influence on the flame structure and pollution formation.

In the present work, the premixed flame height & flame structure, as well as pollution emission of the Iraqi LPG-fuel blended with hydrogen will be investigated experimentally & numerically concerning the following parameters:

- Equivalent ratio.
- H_2 blending ratio.
- Dilution with CO_2 with different ratios.
- Supply (inlet) velocity of the premixing mixture.
- Burner aspect ratios.
- Swirl & non- Swirl burners.

An experimental rig was fabricated for studying premixed flame structure regarding the parameters illustrated above with various burner configurations and to study the initial stage of the flame formation using high-speed photography besides. A two-dimensional simulation was performed for the combustion model with OpenFoam and to predict the maximum and instantaneous flame heights for different fuels and fuel mixtures. The program shall also predict qualitatively and quantitatively the formation of different combustion products.

CHAPTER THREE

EXPERIMENTAL WORK

3.1 Introduction

An experimental study has been conducted to investigate the flame characterization of premixed LPG fuel, LPG-H_2, and LPG-H_2 diluted with CO_2 for both the swirling and non-swirling burners regarding the effects of a wide range of operating conditions and design considerations.

The experimental study deals with the flame height and flame structure of stationary premixed continuous combustion for LPG fuel blended with hydrogen and diluted with CO_2, i.e., premixed (LPG/H_2/CO_2-air) combustion in a tube burner. Numerous cases of fuel-air mixture composition are tested for equivalent ratio with the range of (0.6-1.4), the H_2 blending ratio of (0-40%), and CO_2 dilution ratio of (0 - 10%). Each case is carried out with different flow rates of the fuel-air mixture that passed through the burner. Five non-swirling copper tube burners with aspect ratios of (2, 4, 6, 8, and 10) and two swirler burners are fabricated and tested.

This chapter is devoted to clarifying the experimental apparatus, experimental procedures, and a series of mathematical calculations, regarding the preparation of the premixed fuel/air mixture, related to it. These calculations are essential for implementing the experimental tests and preparing a wide range of fuel/air mixtures.

Details of the experimental test rig and its units and components, types of fuel, studied parameters, and burners configurations are illustrated throughout this chapter. All the experimental tests have been carried out at the mechanical engineering department / postgraduate laboratory at the University of Babylon – Iraq.

3.2 General Description of the Experimental Apparatus

A special combustion system is fabricated to work with the premixed fuel-air mixtures for multiple types of fuel. Fig. 3.1 and Fig. 3.2 show photography and schematic layout of the experimental test rig, respectively, which consists of the following main units & components:

1. fuel-air mixture preparation unit.
2. Burner unit.
3. Flame photography unit.
4. measurement instruments and control of mixture flow.
5. Safety components.

A precise description of each unit, comprising its role in experimental tests, its devices and/or components, as well as their specifications, will be illustrated in the following sections of this chapter consecutively.

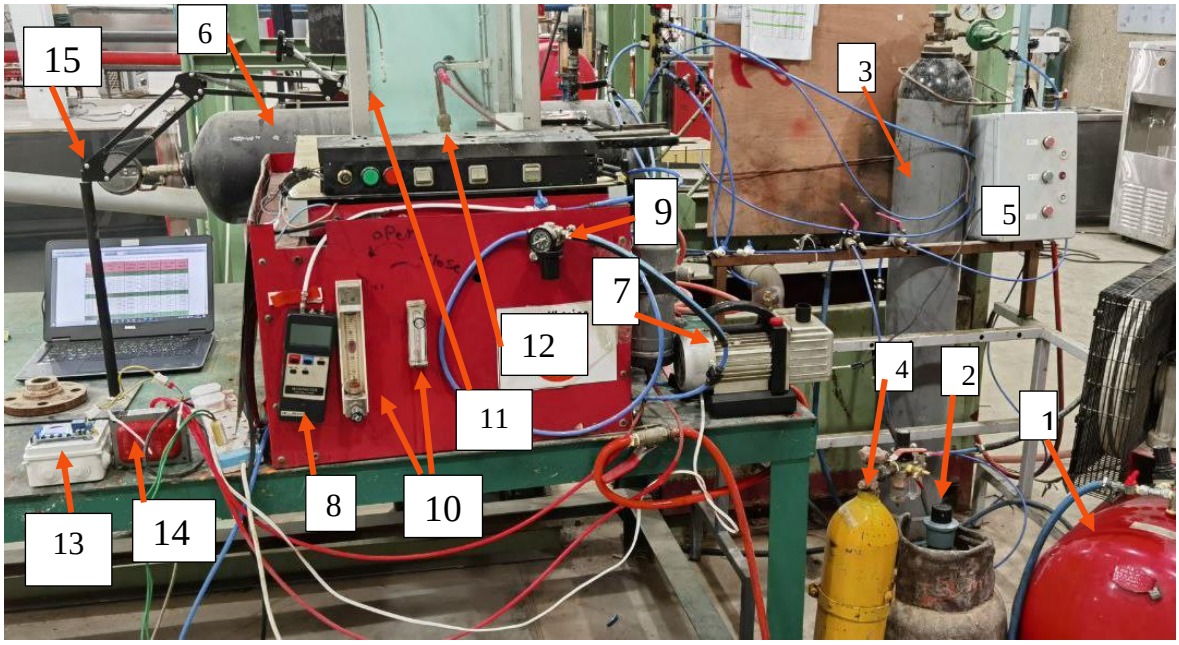

1	Air Compressor		**9**	Pressure Regulator
2	LPG fuel cylinder		**10**	Flowmeters
3	H_2 fuel cylinder		**11**	Combustion chamber
4	CO_2 cylinder		**12**	Burner
5	Mixture Preparation Control Unit		**13**	Ignitor Control Circuit
6	Mixer		**14**	Ignitor Transformer
7	Vacuum Pump		**15**	Stand for the Camera
8	Digital Pressure Manometer			

Fig. (3. 1) Photo of the experimental rig

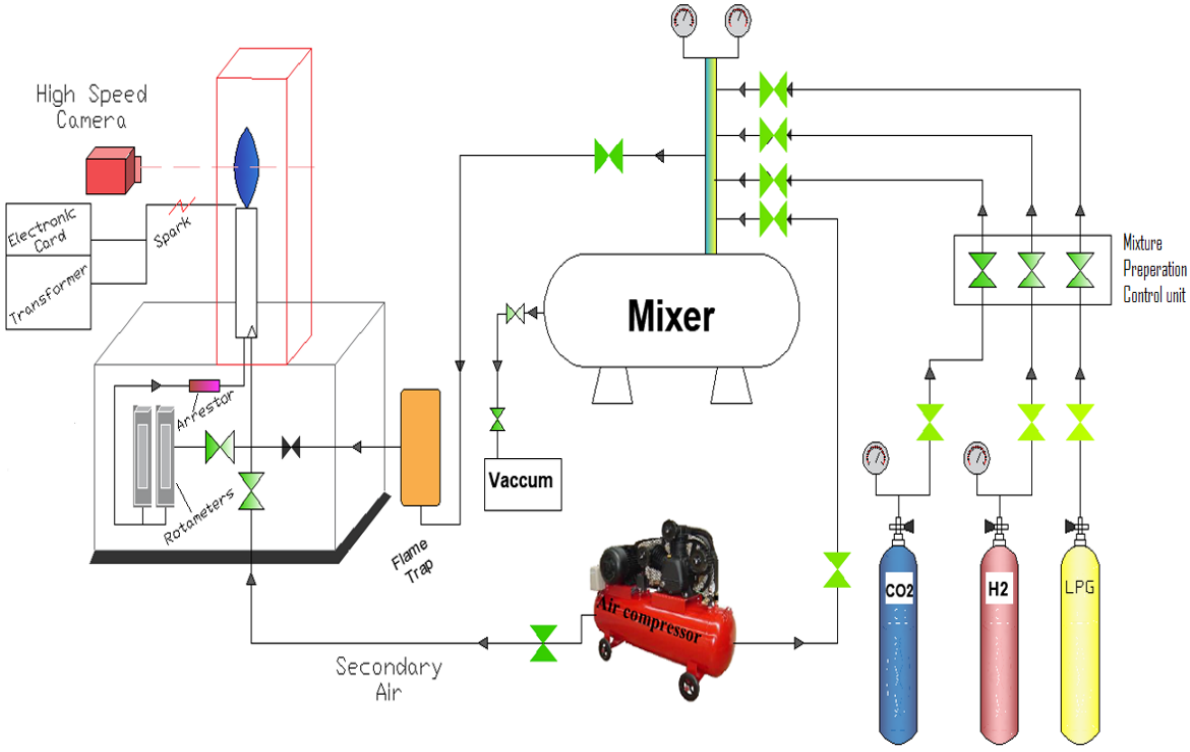

Fig. (3. 2) Schematic layout of the experimental test rig

3.3 Fuel-Air Mixture Preparation Unit

This unit consists of air compressor, fuel cylinders, mixer, vacuum pump, solenoid valves, pressure gauges, and some tubes and flow valves according to the following details. The experimental procedure for fuel-air mixture preparation is illustrated in section 3.8.

Dalton's law for partial pressures is used to prepare different fuel/air mixtures using this unit. To confirm the proper amount of each component of the mixture as well as to obtain a homogenous mixture, the experimental rig is provided with a mixing cylinder (mixer). An absolute pressure of 6 bar for the mixture, inside the mixer, has been considered to calculate the partial pressure of each constituent. This value for the total pressure is considered to increase the partial pressure of each componentof the mixture, especially H_2, maximizing the accuracy of the readings.

3.3.1 Air compressor & Fuel Cylinders

Three cylinders for LPG fuel, H_2, and CO_2 in addition to an air compressor are used to obtain the required fuel/air mixture according to the partial pressure of each component. These cylinders and the air compressor have been connected to the mixer header. The LPG pipe is provided with two valves (one ball valve and one fine valve) and a pressure regulator as well, while the H_2 as well as the CO_2 pipes are provided with three valves (two ball valves and one fine valve) and a pressure regulator for each one. These valves and pressure regulators are requisite for safety considerations and to adjust the flow to get a correct proportion for each component in the premixed mixture. The air is furnished to the mixer by a compressor.

3.3.2 Mixing Cylinder: (The Mixer)

An iron cylindrical shape tank is used as a mixer with dimensions of 1020 mm in length, 220 mm in diameter, and 2 mm in thickness. The mixer has two openings of 12.7mm in diameter, one is used for scavenging while the

other is connected to the header where the air, LPG fuel, H_2, and CO_2 are supplied as shown in fig. (3. 3). The homogeneous mixture is flowing to the burner unit through a valve fixed at the mixer header. The mixer and all its valves and connecting pipes have been pre-tested by increasing the inner pressure up to 7 bar to ensure there is no any leakage.

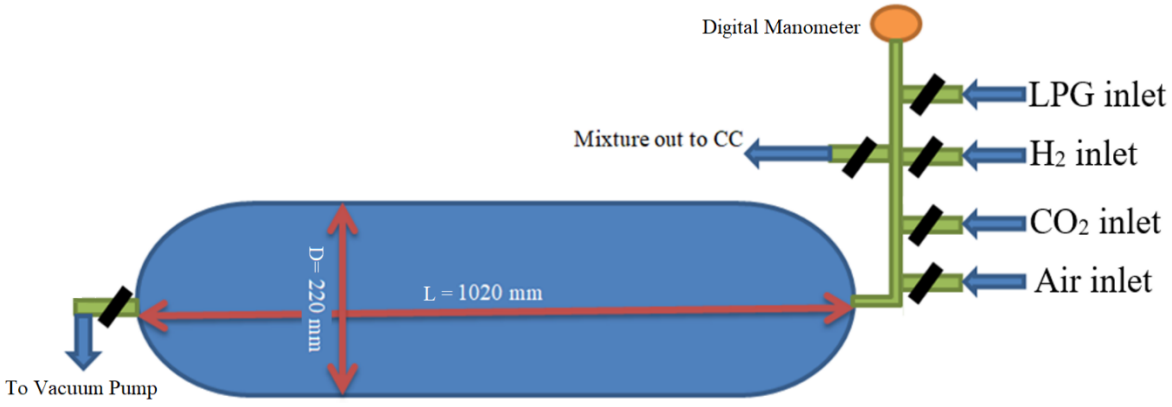

Fig. (3. 3) Schematic diagram of the mixer

3.3.3 The Vacuum Pump

In order to scavenge the remaining previous mixtures, a vacuum pump is linked to the mixer as shown in fig. (3. 2) & fig. (3. 3). This process is carried out by closing all the valves except the valves of the vacuum pump and the pump stay running until the pressure inside the mixer reaches approximately (- 0.95 bar) according to the digital manometer reading.

3.3.4 Solenoid control unit & Pressure Gauges

In order to control the flow and to provide a specific mixture composition with an accurate equivalence ratio, three solenoid valves working on 24V DC are installed on the pipes that conveying the LPG, H_2, and CO_2 towards the mixer. The solenoid box involves the solenoid valves, DC power supply, three push buttons, on/ off switch, and some electrical connectors as shown in fig. (3.4).

The mixture has been prepared inside the mixer using a digital manometer to measure the pressure inside the mixer as shown in fig. (3.5).

This digital manometer is Lutron PM-9107 operates for pressure range of ∓ 7000 mbar. The manometer has an accuracy of ∓ 2% and the resolution is 5mbar with 2.75" LCD that displays 8 kinds of measuring units.

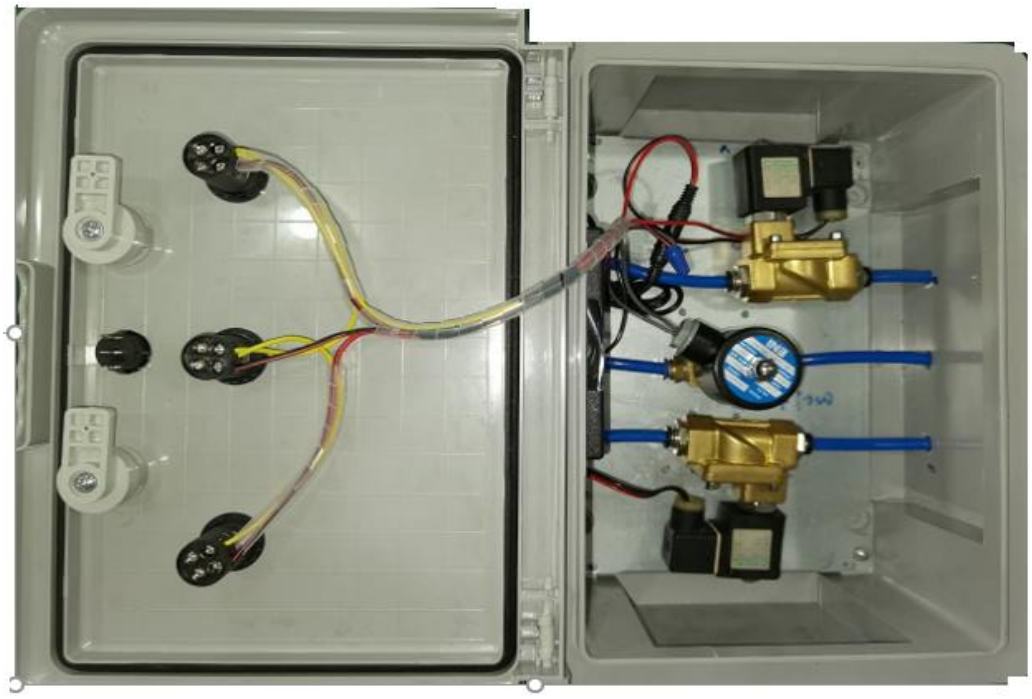

Fig. (3. 4) Mixing flow control by solenoid valves

Fig. (3. 5) Pressure gauges used for mixture preparation

3.4 Measurement & Control of Mixture Flow

3.4.1 Flowmeters

Two glass tube (Rotameter) flowmeters are used to monitor the volumetric flow rate of the fuel/air mixture which passes through the burner tube portion as shown in fig. (3.6). One rotameter has a volume flow rate range of (0.5-6) lpm, while the other has a volume flow rate range of (6 - 50) lpm. The values of mixture flow rate, throughout experimental tests, are sometimes within the first flowmeter range and sometimes within that of the second flowmeter. These flowmeters are intended for measuring the volume flow rate of air. The values of flow rate measured by the flowmeters have been readjusted to be used to measure the fuel/air mixture flow rate with a correction factor. The standard pressure and temperature for designing the flowmeter are (1 bar) and (298 K) [77]. The procedure and calculations of the correction of the measured flowrate of mixture are shown in appendix C-1. The details of the calibration of the flowmeters are shown in appendix C-2 using the orifice meter procedure [78].

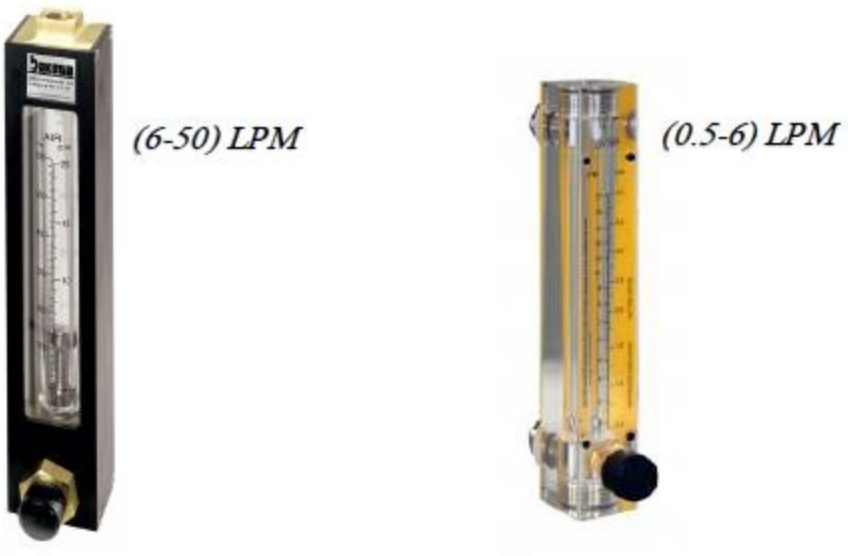

Fig. (3. 6) Rotameters used in present work

3.4.2 Pressure regulator

In addition to the pressure regulators which installed on the H_2 & CO_2 cylinders, another pressure regulator, as shown in fig. (3.7), (Startz Electric RA2000) with a range of (0 – 10 bar) has been installed on the pipe that conveys the fuel/air mixture from the mixer to the burner tube. This pressure regulator is used to control the pressure of the mixture before it passed through the rotameters. The pressue of the fuel/air mixture passing through the burner is kept constant at 1 bar for all tests.

Fig. (3. 7) Pressure regulator of the mixture

3.4.3 Mixture flow valves

Three valves have been used for controlling the flow of mixture from the mixer to the burner and for safety insurances. the first is a ball valve at the mixer outlet, the second is a ball valve put before the pressure regulator and the flame trap.

The third one is a special valve, intended for use in pneumatic and hydraulic systems, is installed after the pressure regulators and before the rotameters to regulate the mixture flow going to the burner. The valve's opening may be fine-tuned easily by fingers using the shaft's rotation to get a required accurate flow rate. Due to the steel ring within which squeezes tightly

on the pipe, it can sustain pressures of up to 16 bar without leaking, making it an excellent choice for low-flow increment applications as shown in fig. (3.8).

Fig. (3. 8) Fine valve used to adjust the mixture flowrate and mixture preparation

3.5 Safety Precautions

To avoid any damage or danger resulting from flame flashback phenomena inside the burner tube and to prevent any explosion in the mixer, fuel cylinders, or pipelines, some safety devices have been installed on the experimental setup.

3.5.1 Flashback Arrestor

One way to restrict the reverse flame or flow of gas back into an equipment or supply line that has already been used is to use a flashback arrestor. Both the user and the equipment are safeguarded against danger or explosions as a result of this. When a flame flashback is formed, this device is mainly used to prevent flame propagation towards the preparation unit. Installed in the flashback arrestor is a gas non-return valve. The spring-loaded non-return valve engages and stops the return flow immediately, preventing the production of the explosive gas mixture as shown in fig. (3.9).

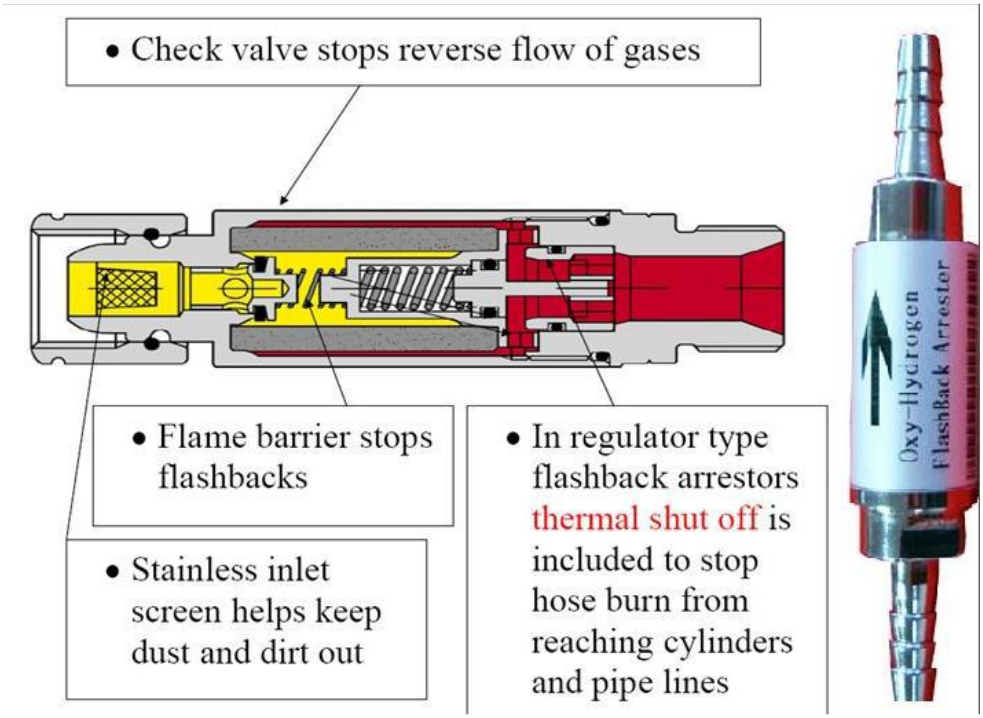

Fig. (3. 9) Schematic of flame flashback arrestor [79]

3.5.2 Flame Trap

Flame trap is a safety device that prevents a fire from spreading to a fuel mixer. This decreases the possibility of an explosion or fire, making the system safer to use. Flame traps are utilized in a broad range of systems in a variety of circumstances. It is critical to keep them clean and clear so that they can continue to perform effectively. Fig. (3.10) shows the photography and the schematic of the flame trap.

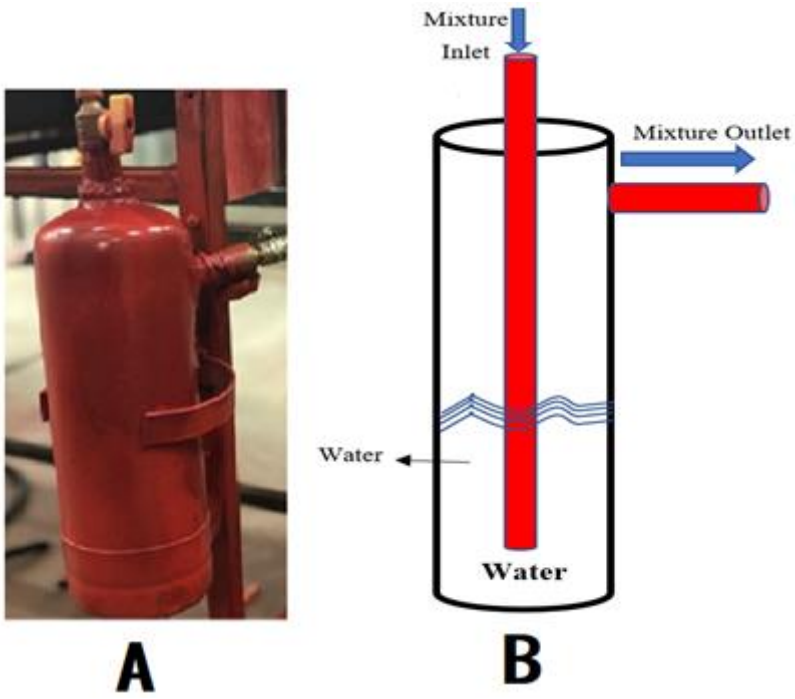

Fig. (3. 10) A: flame trap, B: flame trap Schematic

3.5.3 Secondary Air Pipe

The experimental rig has been provided with a secondary air pipe from the air compressor to the burner inlet directly. This pipe is very useful when the flame is flowing backward into the burner in the case of flame flashback. In this instance, the flame is expelled outside the burner by opening the valve of this pipe with an extreme flow rate and then cut-off the combustion. Another benefit is to cool the burner as the temperature of the air coming from this pipe will be much lower than the temperature of the burner. The use of this air stream is useful to dismiss the combustion products away from the combustion chamber after any experiment.

3.6 Burning unit

The main unit of the experimental rig is the burning unit which is shown in fig. (3.11). This unit comprises the burner and the burner frame, the combustion chamber, the spark ignition combination as well as the spark control. Other parts related to measurements and the safe operation are linked

to the burning unit and connected with it, these parts are discussed and illustrated later.

Fig. (3. 11) The Burning unit

3.6.1 The Burners

The burners are constructed from a copper tube of inside and outside diameters of 10mm & 12mm respectively. The burner's body is constructed from two parts of the same material and diameter to make switching the different burners easier. The first part is a fixed part while the second part could be exchangeable as they are joined by union nuts of copper pipe connectors as shown in fig. (3.12 A). Five pieces for the second part are manufactured with length to diameter ratio, aspect ratio, of 2, 4, 6, 8, and 10.

In addition to the five non-swirling burners mentioned above, two swirling burners are manufactured with the same diameter and material of the non-swirling burners to investigate the impact of the swirling flow. The first swirl burner contains a swirled shaft with 5 blades at 30° (swirl number is 0.78),

while the second contains a swirled shaft with 9 blades at 45° (swirl number is 0.48), as shown in fig. (3.12 B). Both burners are of a length to the diameter ratio of 8, and the swirl shafts have been fitted inside the burner at the burner tip before the flame region. Swirl numbers is calculated according to eq. (3.1) where r_h & r_o represent hub radius & swirler tip radius respectively and θ is the angle vanes slope [80] as shown in fig. (3.13).

The above-mentioned burners have been considered after many other burners have been tried. 15 mm as well as 19 mm diameter burners with different aspect ratios are examined. Besides, some burners with other configurations are examined as shown in fig. (3.14). All these burners are not considered in the experiments because they all caused problems such as flame flashback, short length of flame, instability of flame and others as these burners are not compatible with other parts of the experimental apparatus.

$$S_n = \frac{2}{3}\left[\frac{1-\left(\frac{r_h}{r_o}\right)^3}{1-\left(\frac{r_h}{r_o}\right)^2}\right]\tan(\theta) \qquad (3.1)$$

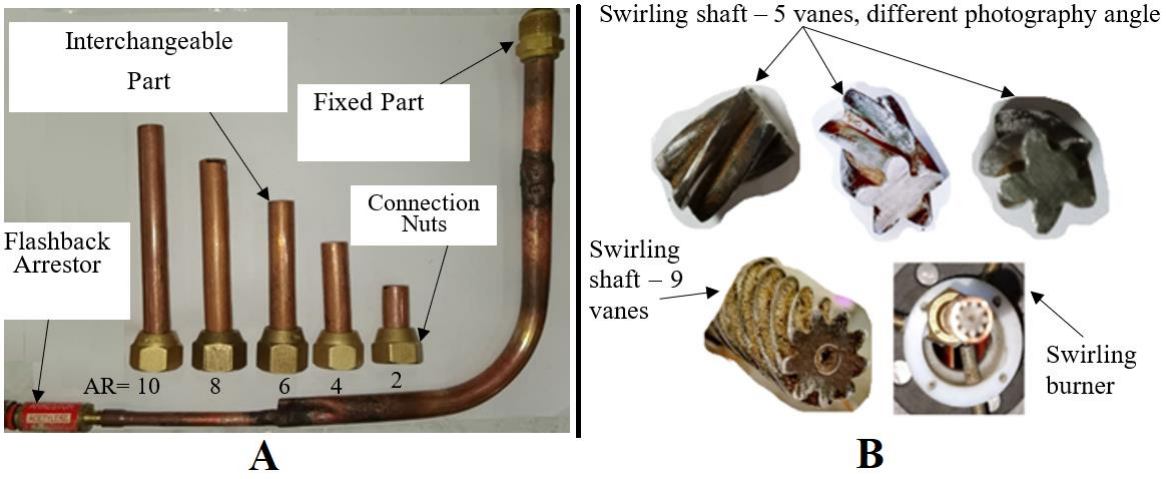

Fig. (3. 12) The used burners: A) Non-swirling Burners with AR=2,4,6,8, and 10 and B) Swirling burners of the present study

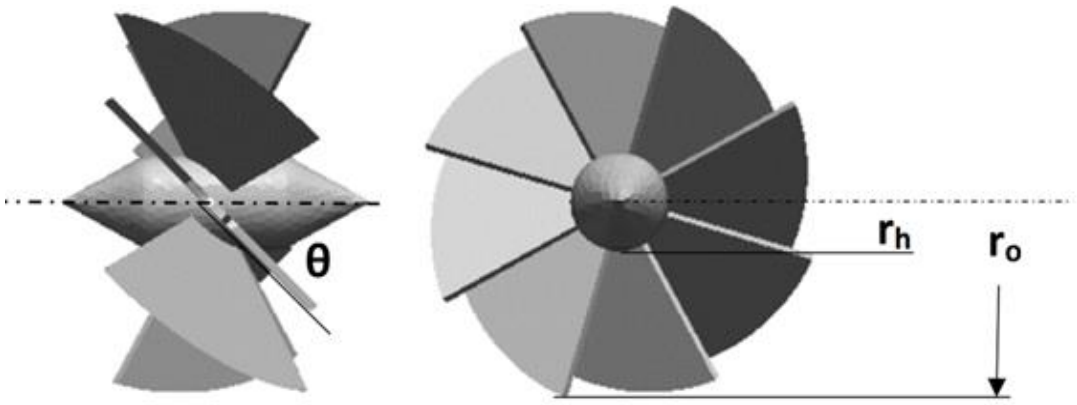

Fig. (3. 13) Dimensions used in eq. (3.1) for calculating swirl number

Fig. (3. 14) Other different burners which not considered

3.6.2 Combustion Chamber & Burner Frame

An iron frame with a suitable size has been made of to include gas pipes, flashback arrestor and flowmeters, as well as the vertical combustion chamber, installed at the top of the frame, made of heat resistant glass for easy capturing and pursue of the flame, and also an electric control panel. The burner holder is placed inside the combustion chamber. Burner holder is made of a Teflon material as a cylindrical ring. It is possible through this holder to install the burner and control the length of the burner to reach the position of igniter and possible to change to another burner as shown in fig. (3.15).

Fig. (3. 15) Burner holder

3.6.3 Spark Ignition Combination

3.6.3.1 Electric & Electronic Circuit

To produce a powerful spark, an electronic circuit is used to supply the power needed for the electrodes as shown in fig. (3.16). A DC power supply is produced from a transformer connected to AC power line (220 V AC). The transformer (2*7.5 kV HOSEL) output is 14 kV at the peak. An electronic circuit has been fabricated to control the duration of the triggering with an electronic push button. It is placed on the transformer to produce an on-off signal to initiate the spark at the burner tip.

Two opposed, co-linear electrodes that form a spark gap, with 1 mm distance, at the burner tip to ignite the fuel/ air mixture. The waste oil burner's electrodes are used with some modification and adjustment to make them in parallel axis and the tip of the rod is then machined to minimize the diameter of electrodes. As shown in fig. (3.17). These electrodes have been fixed at the burner circumference near the burner tip in order to avoid the distortion that they may cause to the flow of the mixture and the flame.

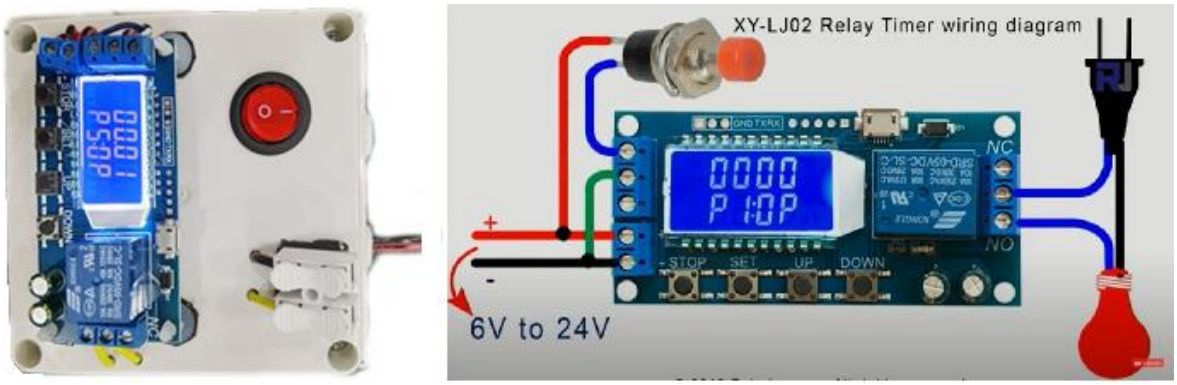

Fig. (3. 16) Electronic circuit to control the spark ignition

Fig. (3. 17) The electrodes used for mixture ignition

3.6.3.2 Electrodes Frame

A frame has been assembled to carry the electrodes and to fixed their horizontal & vertical locations at the burner circumference near its tip. Different burners with different lengths are tested. This frame also used to adjust the electrodes elevation corresponding to the tested burner. The frame comprises a spring linked with a pin that fixed the electrodes at the required location. Half second after pressing the push button of the electronic circuit that controlling the spark, the circuit beeps. At this instant, the spring pull out the frame away from the burner to avoid the disturbance and distortion created by the electrodes to the flame.

3.7 Flame Imaging Unit

An optical system is used to visualize and record the flame and flame propagation process with a high-speed camera. The flame imaging unit comprises the high-speed camera, camera stand, and a light source.

3.7.1 The High-Speed Camera

An ultra-slow-motion with high-resolution camera of Huawei-P 40 pro, fig. (3.18), has been used for capturing and recording the flame propagation and its instantaneous initiation. The device has four cameras:

- 50 MP ultra-vision camera,
- 40 MP ultra-wide cine-camera,
- 12 MP optical supersensing telephoto camera support autofocus mode,
- Time of Flight (TOF) camera.

The image resolution supports up to 8192 x 6144 pixels. The video resolution supports 720p@7680fps ultra slow-motion video. It can slow down the motion by 256 times. The camera has been installed on a photo frame and is provided with a bluetooth remote control to start/ stop the capturing or video.

Fig. (3. 18) High-Speed Camera: Huawei - P 40 with 7860 FPS

3.7.2 Light Source

A lamp type neon (12V DC) is placed in a closed box with one small hole to focus light on burner's body. It is used to assemble the light and then scatter it to the camera. Consequently, this lamp contributes to get an accurate photography of flame. All light in the lab are switched off during recording.

3.8 Test Procedure

To prepare a specific composition of fuel/air mixture with an exact equivalence ratio, Gibbs-Dalton's Law of the partial pressure has been applied

for each mixture component during the mixing process. The pressure of the mixer is set to be 6 bar (absolute pressure) for all cases of the prepared mixtures. The fuel/air mixture preparation process has been done using the pressure regulators, the fine valves, the solenoid valves control unit, and the digital manometer which has a high accuracy with very low resolution (5mbar).

The mixture preparation process comprises the following steps:

1: Scavenging process

This process is done by emptying the mixer of all the remaining mixtures inside it from previous experiments by operating the vacuum pump. Then air is pumping to the mixer for several minutes. This process is repeated three times to ensure that the mixer is completely flushed from previous contents.

2: Vacuum process

The vacuum process takes place by closing all the valves except the valves of the vacuum pump and the vacuum gauge so that the pump can sufficiently evacuate the mixer from any previous air until its pressure reaches approximately (- 0.95 bar).

3: Mixing process

The mixing process is included the following steps:

a) Vacuum gauge valve is closed.

b) The (LPG, H_2, or CO_2) with the lowest partial pressure is admitted firstly to the mixer then the next substance and so on.

c) Air will be admitted until utotal pressure, inside the mixer, reaches (6 bar).

d) Repeating the above steps for the other mixtures.

3.9 Mathematical Calculations

3.9.1 Mixing Ratio and Combustion Process

3.9.1.1 Calculation of Average Chemical Formula for LPG

Liquefied petroleum gas LPG does not have a unique chemical formula, so an average chemical formula (C_nH_m) is required for LPG which involves a mixture of some hydrocarbons (Ethane, Propane, Butane, and Pentane). The volumetric analysis of LPG chemical component is supplied by Al-Hillah gas factory at Iraq as shown in Table (3.1):

Table (3. 1) Volumetric Percent of LPG Fuel Component

Partial Component of LPG	C_2H_6	C_3H_8	C_4H_{10}	C_5H_{12}
	Ethane	Propane	Butane	n- Pentane
Volumetric Percent %	**0.7**	**55.8**	**41.5**	**2**

To calculate the average chemical formula of LPG **(C_nH_m)**, the following mathematical formula is used:

$$C_n = \sum X_i C_i \quad (3.1)$$

$$H_m = \sum X_i H_i \quad (3.2)$$

Where:

C_nH_m: The average chemical formula of LPG, ***i :*** Component number, X_i **:** Mole fraction for component (i), C_i & H_i: Number of carbon & hydrogen atoms respectively for component (i**),** C_n & H_m: Average number of carbon & hydrogen atoms respectively in LPG.

LPG fuel is a mixture of several components, and equations (3.1 and 3.2) are used for calculating its average chemical formula according to the percentage of each component as shown in Table (3.1). It is found that the average chemical formula of LPG which is used in all tests through the present work found is $C_{3.448}H_{8.896}$ with molecular weight MW_{LPG} = 50.272 kg/kmol.

3.9.1.2 Mixture Preparation and Combustion Equations

In the combustion chamber, commensurate masses of air and fuel enter where the chemical reaction takes place and the combustion products are expelled to the exhaust. The chemical reaction equation is obligated for knowing: (i) the reactants and the products of combustion as a qualitative analysis, (ii) the reactants and products as a quantitative analysis. The combustion equation should be consistent on both sides, with the same number of atoms of each element involved on each side.

The oxygen for the mixture is supplied by atmospheric air, so an accurate and consistent analysis of air by volume is required. In combustion calculations, air is typically assumed to be 21% O_2 with 79% N_2 by volume. The general combustion equation used in this work is:

$$[k\ H_2 + (1-k)LPG] + \left[d\ CO_2 + (1-d)\left(\frac{x}{\phi}\right)Air\right] \rightarrow Products \quad (3.3)$$

Where:

LPG is $C_{3.448}H_{8.896}$ and air is 21% O_2 with 79% N_2 by volume.

k: Hydrogen blending volume fraction.

d: CO_2 dilution volume fraction.

$\emptyset$: Equivalence ratio.

$$k = \frac{V_{H_2}}{V_{H_2} + V_{LPG}} \quad (3.4)$$

$$d = \frac{V_{CO_2}}{V_{CO_2} + V_{air}} \quad (3.5)$$

$$x = \frac{k}{2} + (1-k) * 5.672 \quad (3.6)$$

$$\phi = \frac{(\frac{F}{A})_{act.}}{(\frac{F}{A})_{stoichiometric}} \quad (3.7)$$

Where $V_{H_2}, V_{LPG}, V_{CO_2}$, and V_{air} represent the volume of H_2, LPG, CO_2, and air respectively. The coefficient 5.672 in eq. (3.6) equals the number of carbon atoms added to a quarter of the number of hydrogen atoms of LPG composition $\mathbf{C_{3.448}H_{8.896}}$, i.e., **3.448 + 0.25* 8.896 = 5.672** and it represents the required moles of oxygen for one mole of LPG without hydrogen belnding.

For the combustion without dilution, i.e. (H_2 - LPG / air mixture), the coefficient ***(d)*** in eq. 3.3 equals zero. Thus eq. 3.3 reduced to:

$$[k\ H_2 + (1-k)LPG] + \left[\left(\frac{x}{\phi}\right) Air\right] \rightarrow Products \qquad (3.8)$$

As well as, for LPG alone combustion, i.e. (LPG – air mixture) both coefficients (***k*** and ***d)*** in eq. 3.3 equals zero. Thus eq. 3.3 reduced to:

$$[LPG] + \left[\left(\frac{x}{\phi}\right) Air\right] \rightarrow Products \qquad (3.9)$$

According to equations (3.3, 3.8 & 3.9), the reaction equations of combustion is obtained for a wide range of tests cover numerous varieties of the mixture (LPG alone, LPG-H_2, LPG-H_2-CO_2) with different equivalence ratios, H_2 blending ratios, and CO_2 dilution with different burner configuration.

Table (3.2) shows the total number of moles of air required for the combustion of 1 mole of fuel after setting the equivalence ratio. These calculations are carried out using equation (3.8).

It is necessary to calculate the actual total number of moles of reactants supplied to the mixer. This could be done using the equation of state, knowing the mixer volume, required total pressure, and initial temperature:

$$p\ V = n\ R_o T \qquad (3.10)$$

For the experimental conditions of (6 bar total pressure inside the mixer, 298 K initial temperature, 37.5 litre mixer volume, and 8314.3 J/mol. K for the universal molar gas constant (R_o), then the actual total number of moles of all reactants in the mixer is:

$$n_T = \frac{6 * 10^5 \ * 37.5 * 10^{-3}}{8314.3 * 298} = \mathbf{0.00908\ mole} \quad (3.11)$$

The actual mole of each reactant supplied to the mixer is calculated for each experimental test using eq. 3.12, and the results are shown in Table (3.3) where the equivalent ratio is varied through the range (0.6- 1.4) with increment (0.2) for LPG fuel with (10% - 40%) H_2 blending ratio with increment (10%) as well as (2.5%, 5%, and 10%) CO_2 dilution ratio. Eq. 3.13 is Dalton's law of partial pressures which indicates that the ratio of the partial pressures of the fuel and air is equal to their molar ratio.

$$(n_i)_{mixer} = x_{i\ per\ 1\ mole\ of\ fuel} * n_{\text{actual mole in mixer}} \quad (3.12)$$

$$(P_i)_{mixer} = x_i * P_T \quad (3.13)$$

$$(x_i) = \left(\frac{n_i}{n_T}\right) \quad (3.14)$$

Where:

$\boldsymbol{P_i}$: partial pressure of component $\boldsymbol{i}$, $\boldsymbol{P_T}$: Total pressure of mixer (6 bar abs.),

$\boldsymbol{x_i}$: Mole fraction for component $\boldsymbol{i}$, $\boldsymbol{n_T}$: Total mole in mixer (0.00908 moles),

$\boldsymbol{n_i}$: Number of moles for component (hydrogen, LPG, CO_2, and air)

The partial pressures for the premixed combustion of H_2, LPG, and air for all fuel tests are shown in Table (3.4), while the partial pressures of reactants inside the mixer for tests with CO_2 added as a diluent gas are shown in Table (3.5).

Fig. (3.19) presents a summary for the procedure and calculations required for the preparation of the fuel/ air mixture for each experimental test using the abovementioned equations. The results of these calculations are presented in tables (3.2, 3.3, 3.4, & 3.5).

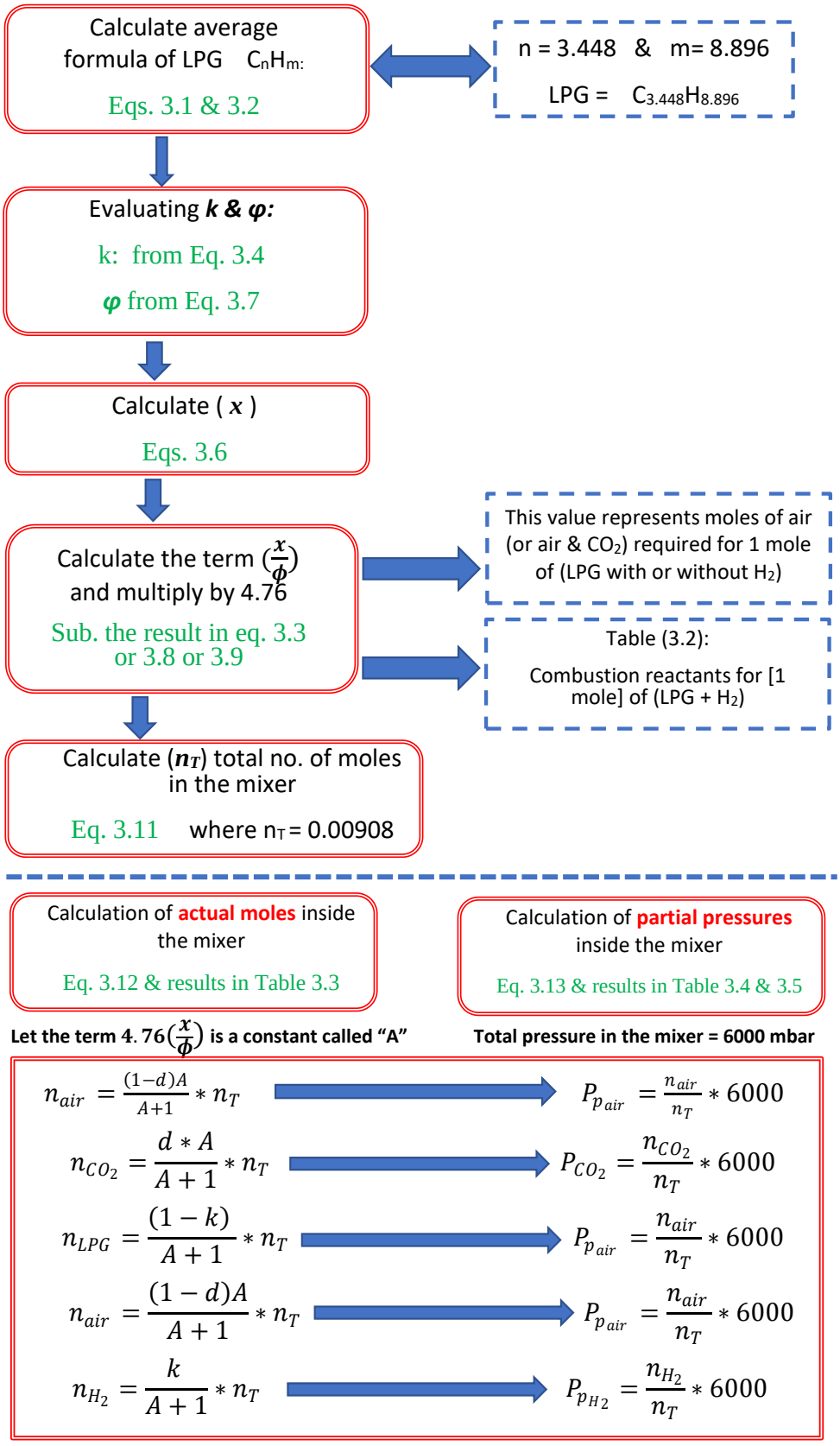

Fig. (3. 19) Flowchart for the calculations of moles & partial pressure throughout mixing process

Table (3. 2) Combustion reaction equation: Number of moles for 1 moles of (LPG + H2)

Test No.	H2 Blending (k)	LPG (1-k)	φ	Stoichiometric air/fuel ratio	Actual air/fuel ratio	Total moles for Reactants
1	**0**	**1**	**0.6**	26.99872	44.9978667	45.9978667
2	0.1	0.9	0.6	24.536848	40.894747	41.894747
3	0.2	0.8	0.6	22.074976	36.791627	37.791627
4	0.3	0.7	0.6	19.613104	32.688507	33.688507
5	0.4	0.6	0.6	17.151232	28.585387	29.585387
6	**0**	**1**	**0.8**	26.99872	33.7484	34.7484
7	0.1	0.9	0.8	24.536848	30.67106	31.67106
8	0.2	0.8	0.8	22.074976	27.59372	28.59372
9	0.3	0.7	0.8	19.613104	24.51638	25.51638
10	0.4	0.6	0.8	17.151232	21.43904	22.43904
11	**0**	**1**	**1**	26.99872	26.99872	27.99872
12	0.1	0.9	1	24.536848	24.536848	25.536848
13	0.2	0.8	1	22.074976	22.074976	23.074976
14	0.3	0.7	1	19.613104	19.613104	20.613104
15	0.4	0.6	1	17.151232	17.151232	18.151232
16	**0**	**1**	**1.2**	26.99872	22.4989333	23.4989333
17	0.1	0.9	1.2	24.536848	20.447373	21.447373
18	0.2	0.8	1.2	22.074976	18.395813	19.395813
19	0.3	0.7	1.2	19.613104	16.344253	17.344253
20	0.4	0.6	1.2	17.151232	14.292693	15.292693
21	**0**	**1**	**1.4**	26.99872	19.2848	20.2848
22	0.1	0.9	1.4	24.536848	17.52632	18.52632
23	0.2	0.8	1.4	22.074976	15.76784	16.76784
24	0.3	0.7	1.4	19.613104	14.00936	15.00936

Table (3. 3) Actual moles supplied to the mixer for reactants

Test No.	H_2 (k)	LPG (1-k)	φ	Mole of air for 1 mole of (LPG + H_2)	n_T for 1 mole of (LPG + H_2)	Overall moles inside the mixer	moles of air inside the mixer	moles of LPG inside the mixer	moles of H_2 inside the mixer
1	0	1	0.6	45.00	46.00	0.00908	0.00888	0.000197	0.000000
2	0.1	0.9	0.6	40.89	41.89	0.00908	0.00886	0.000195	0.000022
3	0.2	0.8	0.6	36.79	37.79	0.00908	0.00884	0.000192	0.000048
4	0.3	0.7	0.6	32.69	33.69	0.00908	0.00881	0.000189	0.000081
5	0.4	0.6	0.6	28.59	29.59	0.00908	0.00877	0.000184	0.000123
6	0	1	0.8	33.75	34.75	0.00908	0.00882	0.000261	0.000000
7	0.1	0.9	0.8	30.67	31.67	0.00908	0.00879	0.000258	0.000029
8	0.2	0.8	0.8	27.59	28.59	0.00908	0.00876	0.000254	0.000064
9	0.3	0.7	0.8	24.52	25.52	0.00908	0.00872	0.000249	0.000107
10	0.4	0.6	0.8	21.44	22.44	0.00908	0.00868	0.000243	0.000162
11	0	1	1	27.00	28.00	0.00908	0.00876	0.000324	0.000000
12	0.1	0.9	1	24.54	25.54	0.00908	0.00872	0.000320	0.000036
13	0.2	0.8	1	22.07	23.07	0.00908	0.00869	0.000315	0.000079
14	0.3	0.7	1	19.61	20.61	0.00908	0.00864	0.000308	0.000132
15	0.4	0.6	1	17.15	18.15	0.00908	0.00858	0.000300	0.000200
16	0	1	1.2	22.50	23.50	0.00908	0.00869	0.000386	0.000000
17	0.1	0.9	1.2	20.45	21.45	0.00908	0.00866	0.000381	0.000042
18	0.2	0.8	1.2	18.40	19.40	0.00908	0.00861	0.000375	0.000094
19	0.3	0.7	1.2	16.34	17.34	0.00908	0.00856	0.000366	0.000157
20	0.4	0.6	1.2	14.29	15.29	0.00908	0.00849	0.000356	0.000237
21	0	1	1.4	19.28	20.28	0.00908	0.00863	0.000448	0.000000
22	0.1	0.9	1.4	17.53	18.53	0.00908	0.00859	0.000441	0.000049
23	0.2	0.8	1.4	15.77	16.77	0.00908	0.00854	0.000433	0.000108
24	0.3	0.7	1.4	14.01	15.01	0.00908	0.00848	0.000423	0.000181
25	0.4	0.6	1.4	12.25	13.25	0.00908	0.00839	0.000411	0.000274

Table (3. 4) Partial pressures of reactants inside the mixer: without dilution

Test No.	H2 Blending (k)	LPG (1-k)	φ	P Total (mbar)	P H2 (mbar)	P LPG (mbar)	P H2+LPG (mbar)	P Air (mbar)
1	**0**	**1**	**0.6**	6000	0	130.44	130.44	5869.6
2	0.1	0.9	0.6	6000	14.322	128.89	143.22	5856.8
3	0.2	0.8	0.6	6000	31.753	127.01	158.77	5841.2
4	0.3	0.7	0.6	6000	53.431	124.67	178.1	5821.9
5	0.4	0.6	0.6	6000	81.121	121.68	202.8	5797.2
6	**0**	**1**	**0.8**	6000	0	172.67	172.67	5827.3
7	0.1	0.9	0.8	6000	18.945	170.5	189.45	5810.6
8	0.2	0.8	0.8	6000	41.967	167.87	209.84	5790.2
9	0.3	0.7	0.8	6000	70.543	164.6	235.14	5764.9
10	0.4	0.6	0.8	6000	106.96	160.43	267.39	5732.6
11	**0**	**1**	**1**	6000	0	214.3	214.3	5785.7
12	0.1	0.9	1	6000	23.495	211.46	234.95	5765
13	0.2	0.8	1	6000	52.004	208.02	260.02	5740
14	0.3	0.7	1	6000	87.323	203.75	291.08	5708.9
15	0.4	0.6	1	6000	132.22	198.33	330.56	5669.4
16	**0**	**1**	**1.2**	6000	0	255.33	255.33	5744.7
17	0.1	0.9	1.2	6000	27.975	251.78	279.75	5720.2
18	0.2	0.8	1.2	6000	61.869	247.48	309.35	5690.7
19	0.3	0.7	1.2	6000	103.78	242.16	345.94	5654.1
20	0.4	0.6	1.2	6000	156.94	235.41	392.34	5607.7
21	**0**	**1**	**1.4**	6000	0	295.79	295.79	5704.2
22	0.1	0.9	1.4	6000	32.386	291.48	323.86	5676.1
23	0.2	0.8	1.4	6000	71.566	286.26	357.83	5642.2
24	0.3	0.7	1.4	6000	119.93	279.83	399.75	5600.2
25	0.4	0.6	1.4	6000	181.12	271.68	452.8	5547.2

Table (3. 5) Partial pressures of reactants inside the mixer for dilution tests

								5 % Dilution			7.5 % Dilution			10 % Dilution		
Test No.	H2 Blending (k)	LPG (1-k)	φ	P H2 (mbar)	P LPG (mbar)	P H2+ LPG (mbar)	P (Air+ CO2) (mbar)	P CO2	P (H2+ LPG+ CO2) (mbar)	P AIR (mbar)	P CO2 (mbar)	P (H2+ LPG+ CO2) (mbar)	P AIR (mbar)	P CO2 (mbar)	P (H2+ LPG+ CO2) (mbar)	P AIR (mbar)
26	0	1	0.8	0	172.7	172.7	5827	291	464	5536	437	609.7	5390	582.7	6410	5244.6
27	0.1	0.9	0.8	18.94	170.5	189.4	5811	291	480	5520	436	625.2	5375	581.1	6392	5229.5
28	0.3	0.7	0.8	70.54	164.6	235.1	5765	288	523.4	5477	432	667.5	5332	576.5	6341	5188.4
29	0	1	1	0	214.3	214.3	5786	289	503.6	5496	434	648.2	5352	578.6	6364	5207.1
30	0.1	0.9	1	23.5	211.5	235	5765	288	523.2	5477	432	667.3	5333	576.5	6342	5188.5
31	0.3	0.7	1	87.32	203.8	291.1	5709	285	576.5	5423	428	719.2	5281	570.9	6280	5138
32	0	1	1.2	0	255.3	255.3	5745	287	542.6	5457	431	686.2	5314	574.5	6319	5170.2
33	0.1	0.9	1.2	27.98	251.8	279.8	5720	286	565.8	5434	429	708.8	5291	572	6292	5148.2
34	0.3	0.7	1.2	103.8	242.2	345.9	5654	283	628.6	5371	424	770	5230	565.4	6219	5088.7

CHAPTER FOUR

NUMERICAL STUDY

4.1 General

As the Computational Fluid Dynamics (CFD) techniques evolves, research methods keep changing to meet the requirements of research experiments and labs. However, experiments implementation in labs requires additional costs. Because it's hard to control all the conditions in a lab so that healthy experiments could be accomplished, comparing between cases also requires the installation of enough test rigs to meet the number of cases needed for a proper comparison. Using CFD tools eliminates all of these obstacles because researchers can simulate the research virtually on a PC and solve all the equations numerically using a model. However, these techniques are so complicated, so the model solver needs a lot of computing power. This is especially true if chemical reactions and/or turbulent models are included.

In the present work, a CFD model has been developed and used for studying flame propagation and characteristics for different LPG/ air mixtures with different blending conditions. Chemical reactions and turbulent models would be used and requiring a highly computing resourcing. This chapter is devoted to clarify the numerical works of the present investigation. The simulation of the combustion process of these mixtures has been implemented by a complex chemical reactions and turbulent models solved using OpenFOAM code.

4.2 Numerical Modeling and Methodology

There are number of commercial and non-commercial solvers used for solving the numerical models in which, chemical reactions and combustion are implemented such as ANSYS CHEMKIN, CFX, FDS, and SMAFS [81].

OpenFOAM code (Field Operation and Manipulation [2] has been selected for solving the present numerical problems because it involves several solvers that investigate and cover different combustion situations including the numerous effects nested in action with combustion details such as turbulence, and radiation. Another distinctive in selecting OpenFOAM is an open GL (General License) code.

4.2.1 OpenFOAM Methodology

As has been mentioned previously, OpenFOAM code (Open Source of Field Operation and Manipulation) is used in the present numerical simulation to solve the combustion computational domain. OpenFOAM code is written by C++ language. Regarding the combustion model, it can be solved using different solvers; rho-Reacting-Foam, rho-Reacting-Buoyant-Foam, reactingFoam, FireFoam, and XiFoam [82]. In the present numerical simulation, XiFoam solver is used to solve all the relevant governing equations. XiFoam is a transient solver for compressible combustion in premixed and partially premixed with turbulence modeling. This solver uses finite volume method (FVM) to discretize the PDE (partial differential equations) [67] & [83].

4.2.2 Cases Assumptions

The present study has been implemented using the XiFoam solver by considering the following assumptions for the current work: -

1- The flow is unsteady, and the solver ceases at time when the residuals are converged.
2- (2-D) numerical simulation would be considered where the flow is considered in x and y coordinates while it would be neglected in z-direction.
3- The flow is compressible.
4- The thermophysical properties for all the components are not constants.

5- All the reactants and the products of the combustion reactions are implemented in the multi-species solver.

4.2.3 CFD Models

As mentioned previously, XiFoam solver is used in the current simulation to solve the present combustion model. In this solver, finite volume method is used to discretize the PDE. XiFoam solver is unsteady solver in which the run time and time step must be set in such a way that Courant No. does not pass the maximum set value. Courant number is a dimensionless value representing the time that a particle stays in one cell of the mesh [84], [85]. In the current simulation, maximum Courant number is set as (0.5), thus: -

Co. No. = $\frac{u\,\Delta t}{\Delta x} \leq 0.5$.

However, in the current set up, adjustable time step is turned on to avoid any divergence in the solution through the simulation. PIMPLE algorithm is used to solve the pressure-velocity coupling which represents a combination between PISO (Pressure-Implicit-Split-Operator) algorithm and SIMPLE (Semi-Implicit-Method- of -Pressure-Linked-Equation) algorithm [86]. Second order scheme discretization (LUST) is used to discretize the momentum equation while (Gauss limited linear) is used for the other equations; Energy equation, turbulence model equation (the *standard k- ϵ* model is utilized in the current work as would be discussed in the next sections), and species conservation equations. Combustion model is enabled in the case file, and the reactions were set properly where there are different reactions according to different cases investigated in the present study as being shown in the next section.

4.3. Model Governing Equations

In the current numerical study, the combustion inside a chamber would be modeled using OpenFOAM code. XiFoam solver will be used to solve the

relevant governing equations using FVM (Finite Volume Method) with different discretization methods. The combustion numerical model is very complex due to including Multiphysics problems in the simulation modeling. Moreover, modeling the reactions involving multispecies in the problem causes an increase in the relevant equations which should be solved. Furthermore, turbulence model adds more complexity to the modeled problem.

In the fluid flow problems, there are basic governing equations that should be implemented in the model first. Any other specifications for the model can be added as a source or sink to the main governing equations such as the combustion and/or radiation sources. On the other hand, if there are scalars transport additives, these scalars can be added as a separate governing equation such as the energy equation, multispecies equation, and turbulence model. In the present section, all governing equations related to numerical modeling are described in detail.

4.3.1 Mass Conservation Equation (Continuity Equation)

The mass conservation equation or what is called by *Continuity Equation*. The basic well-known form of continuity equation from which mass conservation equation is derived can be written as [81], [82], [87]:

$$\frac{\partial \rho}{\partial t} + \frac{\partial (\rho u_j)}{\partial x_j} = 0 \tag{4.1}$$

4.3.2 Momentum Equation

The momentum equation or what is called by Navier-Stock's Equation is defined as the equation that describes the flow characteristics (velocity and pressure) in all flow directions. In general, the final form of the Navier-Stock's equation in *x & y* direction is:

$$\frac{\partial (\rho u_i)}{\partial t} + \frac{\partial (\rho u_i u_j)}{\partial x_j} = \frac{\partial P}{\partial x_i} + \frac{\partial}{\partial x_j} \left\{ \mu \left(\frac{\partial u_i}{\partial x_j} + \frac{\partial u_j}{\partial x_i} - \left(\frac{2}{3} \delta_{ij} \frac{\partial u_k}{\partial x_k} \right) \right) \right\} \tag{4.2}$$

Where u_i and ∂x_i are the velocity component and spatial distance in the flow direction while u_j and ∂x_j represent the velocity components and spatial distances in the other directions, P is the pressure, and δ_{ij} is the kronecher Delta. ρ is the mixture density which can be calculated from ideal gas law:

$$PV = mRT \longrightarrow \rho_{mixture} = \frac{P}{RT} \quad (4.3)$$

$$R = \frac{R_o}{M_{ave}}$$

$$M_{ave} = \frac{1}{\sum_s \frac{Y_S}{M_S}}$$

Where R_o is the universal gas constant. M_{ave} is the average molar mass of the mixture [86] where Y_s and M_s are the mass fraction and the molar mass for each one of the chemical species respectively, where the subscription s refer to the species, and *T* is the gas temperature.

The Sutherland's law is used for calculating the gas dynamic viscosity μ in the present transport model as a function of temperature T [88]:

$$\mu = A_s \frac{\sqrt{T}}{T + T_s}$$

where A_s is Sutherland coefficient and T_s is Sutherland temperature and they are constants of the specie.

4.3.3 Energy Transport Equation

Temperature is the most important property which affects the reactions for the combustion model. Thus, the energy transport equation or what is called by energy conservation equation must be implemented in the computational model to calculate the temperature. However, the combustion and radiation sources must be added to the energy transport equation to include their effects in the final calculations. Energy conservation equation with including the effect of combustion and radiation can be written as below [86], [87]:

$$\frac{\partial(\rho h)}{\partial t} + \frac{\partial(\rho h u_j)}{\partial x_j} = \frac{\partial}{\partial x_j}\left\{\frac{\mu}{Pr_h}\frac{\partial h}{\partial x_j} + \mu\left(\frac{1}{Sc_s} - \frac{1}{Pr_h}\right)\sum_s h_s \frac{\partial Y_s}{\partial x_j}\right\} + \frac{\partial P}{\partial t} + S_{rad.} + S_{comb.} \quad (4.4)$$

Pr_h and Sc_s are the mixture Prandtl Number and the specie Schmidt number, respectively and $S_{comb.}$ & $S_{rad.}$ are source terms added to the energy equation in order to consider the combustion and radiation effects, where:

$Pr_h = \frac{\mu c_p}{\lambda}$, while $Sc_s = \frac{\mu}{\rho D_s}$

Where λ and D_s are the mixture thermal conductivity and the specie's diffusion coefficient respectively.

The field mixture's temperature is calculated at each updated enthalpy value as below:

$$T = \frac{h - Y_{fuel}\, h_{fuel}}{\overline{cp}} \quad (4.5)$$

$Y_{fuel}\ and\ h_{fuel}$ are the mole fraction and the enthalpy of the fuel, respectively. JANAF model is the most widely used thermo-physical model to calculate the enthalpy of the mixture. JANAFcalculates c_p as a function of temperature from a set of coefficients taken from JANAF tables of thermodynamics. Two sets of coefficients are specified, the first set for temperatures above a common temperature T_c, the second for temperatures below T_c [89].

The function relating c_p to temperature is:

$$c_p = R\left(\left(\left(\left(a_4 T + a_3\right)T + a_2\right)T + a_1\right)T + a_o\right)$$

In addition, there are constants of integration, a_5 and a_6, both at high and low temperature, used to evaluating h.

$$h = \sum_s Y_s h_s$$

$$h_s = h_s^o + \int_{T_o}^{T} C_{p,s}\,(T)dT$$

Where $C_{p,s}$ is the specific heat of the specie (s) at constant pressure while h_s is the enthalpy of specie (s).

4.3.4 Species Transport Equation

Each chemical component in flame combustion reaction is treated as a single specie in the present computational model where each specie's equation is included in the computation model as scalar transport equation or scalar conservation equation.

Under the assumption of simple one-step chemistry, the species transport equations can be reduced to a single combustion progress variable equation, as follows [67]:

$$\frac{\partial (\bar{\rho}\,\tilde{c})}{\partial t} + \frac{\partial (\bar{\rho}\,\tilde{u}_i\,\tilde{c})}{\partial x_i} = \frac{\partial}{\partial x_i}\left(\rho^{-}\alpha + \frac{\mu_t}{Sc_t}\frac{\partial\,\tilde{c}}{\partial\,x_i}\right) + \dot{\omega_c} \qquad (4.6)$$

where the subscription (t) refers to turbulent property and the overbar ¯ and the tilde ˜ refer to the Reynolds and Favre averaging, respectively. The transported quantity c refers to the normalized mass fraction of the products, which is called as the progress variable. The combustion progress variable describes the thermochemical state of the mixture at any point in space and time (products and reactants). A progress variable can be set with the help of any quantity, like temperature, reactant mass fraction, provided it is bounded by a single value in the reactants and another one in the product [90]:

$$c = \frac{T - T_r}{T_p - T_r}$$

where r stands for unburned reactants gas, and p stands for product gas.

The combustion process is characterized by a progress variable (c = 1 in the burned product gas and c = 0 in the reactant gas). None of the existing solvers in OpenFOAM for combustion are based on a progress variable directly [83]. In OpenFOAM, the flame front propagation is modelled by solving a transport equation for the regress variable ***(b)*** instead of the progress

variable c, where b = 0 represents the products and b = 1 represents the reactants and:

$$b = 1 - c \tag{4.7}$$

Henceforth, Eq. (4.6) can be written in terms of the regress variable b as follows:

$$\frac{\partial(\bar{\rho}\,\tilde{b})}{\partial t} + \frac{\partial(\bar{\rho}\;\tilde{u}_i\,\tilde{b})}{\partial x_i} = \frac{\partial}{\partial x_i}\left(\rho^{-}\alpha + \frac{\mu_t}{SC_t}\frac{\partial\,\tilde{b}}{\partial\,x_i}\right) - \dot{\omega_c} \tag{4.8}$$

Eq. (4.8) is the equation used in OpenFOAM and, in particular, in XiFoam solver.

4.3.5 Turbulence Modeling Using the Standard k - ϵ Model

Compressible fluid is highly affected by any minor changes in the energy level, most of the compressible fluid problems requires to be corrected by the turbulence models to calculate the fluid properties especially in case of combustion or chemical reactions models. The basic model developed is the Reynold-Averaged Navier Stock Equation (RANS). This model is unable to capture the smallest vortex robs in the flow. Therefore, new model called by LES (Large Eddy Simulation) was developed to capture the intermediate vortex robs in the flow. However, the smallest robs still cannot be captured by LES filters. Thus, new developed model called by DNS (Direct Numerical Simulation) was created to capture the smallest generated vortex in the system. DNS requires a highly computing resources as well as the complexity in applying the DNS model in the complex domain.

In the current numerical work, RANS turbulence model was implemented using the standard *k* - ϵ turbulence model. In this model, two important parameters are considered for the calculations, *k* or what is called by turbulent kinetic energy which represents the measure of turbulence production. The other important parameter in this model is the dissipation rate

which is characterized by ϵ. This parameter represents the loss in the turbulence energy.

This section presents the required steps to develop the standard k - ϵ turbulence model in the current computation model. The first step is set by averaging each parameter in the Navier-Stock equation through the time where each parameter would be separated into two parts: time-averaged term and fluctuating term as below:

$u = \bar{u} + \acute{u}$, where $\bar{u} = \lim_{T\to\infty} \frac{1}{T}\int_0^T u(x,t)dt$

$\bar{u}$ represents the time – averaged term while $\acute{u}$ represents the fluctuating term. However, as the fluid is compressible, density change should be considered through simplifying the transport equation as below:

$u = \tilde{u} + \acute{u}$, where $\tilde{u} = \frac{\overline{\rho u}}{\bar{\rho}}$

Such a method is called by Favre-Averaging when the density change is being taken into account. This method is applicable for the other parameters of the flow, pressure, density, specie, and temperature. Now, by applying the Favre-Averaging on the abovementioned governing equations, they would be reformed as below:

1-) Averaged Continuity Equation:

$$\frac{\partial \bar{\rho}}{\partial t} + \frac{\partial(\bar{\rho}\tilde{u}_j)}{\partial x_j} = 0 \qquad (4.9)$$

2-) Averaged Momentum Equation:

$$\frac{\partial(\bar{\rho}\tilde{u}_i)}{\partial t} + \frac{\partial(\bar{\rho}\tilde{u}_i\tilde{u}_j)}{\partial x_j} = \frac{\partial \bar{P}}{\partial x_i} + \frac{\partial}{\partial x_j}\left[\mu\left(\frac{\partial \tilde{u}_i}{\partial x_j} + \frac{\partial \tilde{u}_j}{\partial x_i} - \left(\frac{2}{3}\delta_{ij}\frac{\partial \tilde{u}_k}{\partial x_k}\right)\right) - \overline{\rho \ddot{u}_i \ddot{u}_j}\right] \qquad (4.10)$$

$(-\overline{\rho \ddot{u}_i \ddot{u}_j})$ Parameter is called by Reynold stresses which can be modelled using what is called by Boussinesq eddy-viscosity model as below:

$$(-\overline{\rho \ddot{u}_i \ddot{u}_j}) = \mu_t \left(\frac{\partial \tilde{u}_i}{\partial x_j} + \frac{\partial \tilde{u}_j}{\partial x_i} - \left(\frac{2}{3} \delta_{ij} \frac{\partial \tilde{u}_k}{\partial x_k} \right) \right) - \left(\frac{2}{3} \bar{\rho}\, \breve{k} \delta_{ij} \right) \quad (4.11)$$

Where *k* represents the turbulent kinetic energy while μ_t is the eddy viscosity.

μ_t can be calculated as below:

$\frac{C_\mu \bar{\rho} \widetilde{k^2}}{\breve{\epsilon}}$ where $\breve{\epsilon}$ is the dissipation rate while C_μ is a constant.

k and ϵ are scalars which can be evaluated using specific scalar transport equation or scalar conservation equation as below:

for *k* the transport equation is derived as:

$$\frac{\partial (\bar{\rho} \breve{k})}{\partial t} + \frac{\partial (\bar{\rho} \breve{k} \tilde{u}_j)}{\partial x_j} = \frac{\partial}{\partial x_j} \left[\left(\mu + \frac{\mu_t}{Pr_k^t} \left(\frac{\partial \breve{k}}{\partial x_j} \right) \right] + P - \bar{\rho} \tilde{\epsilon} \right. \quad (4.12)$$

While the derived transport equation for ϵ is:

$$\frac{\partial (\bar{\rho} \breve{\epsilon})}{\partial t} + \frac{\partial (\bar{\rho} \breve{\epsilon} \tilde{u}_j)}{\partial x_j} = \frac{\partial}{\partial x_j} \left[\left(\mu + \frac{\mu_t}{Pr_\epsilon^t} \left(\frac{\partial \breve{\epsilon}}{\partial x_j} \right) \right] + \frac{\tilde{\epsilon}}{\tilde{k}} (C_{\epsilon 1} G - C_{\epsilon 2} \bar{\rho} \breve{\epsilon}) - \left(\frac{2}{3} C_{\epsilon 1} + C_{\epsilon 3} \right) \bar{\rho} \breve{\epsilon} \frac{\partial \tilde{u}_k}{\partial x_k} \right. \quad (4.13)$$

P is the production rate of the turbulent kinetic energy, and be calculated as below:

$$P = G - \frac{2}{3} \bar{\rho} \breve{k} \frac{\partial \tilde{u}_k}{\partial x_k} \quad (4.14)$$

$$G = 2\mu_t \left(S_{ij} S_{ij} - \frac{1}{3} \left[\frac{\partial \tilde{u}_k}{\partial x_k} \right]^2 \right) \quad (4.15)$$

$$S_{ij} = \frac{1}{2} \left(\frac{\partial U_i}{\partial x_j} + \frac{\partial U_j}{\partial x_i} \right) \quad (4.16)$$

Pr_k^t and Pr_ϵ^t are the turbulent Prandtl number for k and ϵ respectively while $C_{\epsilon 1}$, $C_{\epsilon 2}$, C_μ, and $C_{\epsilon 3}$ are the model constants. All these constants were already calculated as below:

$Pr_k^t = 1$ $Pr_\epsilon^t = 1.3$ $C_\mu = 0.09$,

$C_{\epsilon 1} = 1.44$ $C_{\epsilon 2} = 1$ $C_{\epsilon 3} = -0.33$

4.3.6 Combustion Model

In most of the flame propagation problems, the reaction rate is controlled by the turbulent time scale for each specie rather than the reaction time scale. Such a model which controls the combustion rate is called by Eddy Dissipation Model (EDM). The original model from which the abovementioned model was derived is developed by Spalding [91]. The model derived by Spalding [91], called by "Eddy-Break-Up" (EBU) model, was set first to calculate the reaction rate of the premixed turbulent flame, and states that:

$$\overline{\omega_f} = -C_{EBU}\frac{\sqrt{\widetilde{Y_f''^2}}}{\tau_f} \tag{4.17}$$

Where $\overline{\omega_f}$ is the reaction rate or combustion rate while C_{EBU} is the model coefficient, and $\widetilde{Y_f''^2}$ is the variance of the mixture fraction. τ_f represents the characteristic turbulent time which is equal to:

$$\tau_f = \frac{\tilde{k}}{\tilde{\epsilon}}$$

Later, new model was introduced by Magnussen and Hjertager [92] to develop the Eddy Dissipation Model (EDM) in which, the variance of the mixture fraction ($\widetilde{Y_f''^2}$) is replaced by the mass fraction of the deficient species which represents the fuel for the lean mixture and the oxidizer for rich mixture. Thus, the Eddy Dissipation Model can be reformed as below:

$$\overline{\omega_f} = -C_{EBU}\frac{\min\left\{\widetilde{Y_f}, \frac{\widetilde{Y_o}}{s}, \frac{\widetilde{Y_p}}{1+s}\right\}}{\tau_f} \tag{4.18}$$

$\widetilde{Y_f}$, $\widetilde{Y_o}$, and $\widetilde{Y_p}$, are fuel, oxidizer, and product Favre-Averaged mass fractions while (s) represents the stoichiometric mass ratio of oxidizer to the fuel.

To calculate the reaction rate for any specific specie, the below equation can be used:

$$\widetilde{\omega_{\dot{S}}} = -\frac{\gamma^2}{1-\gamma^2}\frac{\bar{\rho}(\widetilde{Y_S}-\widetilde{Y_S^*})}{\tau^*} \quad (4.19)$$

Where $\widetilde{Y_s}$ and $\widetilde{Y_s^*}$ are the species mass fraction which is calculated from the species transport equation and species fraction which is calculated chemically. Here reminded again that the overbar ¯ and the tilde ˜ refer to the Reynolds and Favre averaging, respectively

$$\tau^* = 0.4083\sqrt{\frac{\upsilon}{\tilde{\epsilon}}}$$

where υ is the kinematic viscosity.

$$\gamma = 2.1377\,(\frac{\upsilon\tilde{\epsilon}}{\tilde{k}^2})^{\frac{1}{2}}$$

4.3.7 Radiation Model

The energy transport equation (Eq. 4. 4) includes two source terms: the combustion term, and the radiation term (S_{rad}). The radiation term can be derived originally from calculating the net radiation heat ($\nabla.\bar{q}_R$) flux where:

$$\nabla.\bar{q}_R = \int_{4\pi} \nabla.(\hat{s}I)d\Omega \quad (4.20)$$

$\hat{s}$ is the direction along which the radiation rays are propagating while I, and Ω are the spectral intensity and the entire spherical solid angle respectively. One of the assumptions set in the current computational model is that the medium is gray so that $\nabla.(\hat{s}I)$ can be integrated along the radiation wavelength (λ) as below:

$$\int_\lambda \nabla.(\hat{s}I)d\lambda = k_p \int_\lambda \left(I_{p\lambda} - I_\lambda\right)d\lambda = \nabla.(\hat{s}I) = k_p\left(I_p - I\right) \quad (4.21)$$

By substituting Eq. (4.21) in Eq. (4.20), it is found that:

$$\nabla.\bar{q}_R = \int_{4\pi} \nabla.(\hat{s}I)d\Omega = k_p 4\pi\, I_p - k_p \int_{4\pi} I\, d\Omega = k_p(\,4\sigma T^4 - G) \quad (4.22)$$

Where k_p is the spectral absorption coefficient. The term $(4\sigma T^4)$, and (G) are the energy resealed rate per unit area and the total irradiation received from

domain directions. σ is Stefan- Boltzmann constant which is equal to (5.67×10^{-8} W/m^2. K). Equations (4.21) and (4.22) represent the Radiative Transfer Equation (RTE) which determines the spectral radiation rate in specific medium.

To solve the RTE which has been derived above, there are two methods; first, the PI-approximation method in which the incident irradiation is calculated using spherical harmonics. In the present computational model, the common widely used Finite Volume Discrete Ordinates Method (fvDOM) is implemented as a solution to the radiative transfer equation (RTE). In this method, the irradiation field is splitting into a specific number of solid angles. Then, the irradiation intensity (I_i)would be calculated at each solid angle (Ω_i) at each direction. Finally, the net radiation (G) can be calculated using numerical integration for the predict irradiation intensities along the solid angle as below:

$$G = \int_{4\pi} (I) d\Omega \approx \sum_i I_i \,.\, \Delta\, \Omega$$

k_p can be calculated by weighting the individual k_p for each specie (i) at each partial pressure as below:

$$k_p = \sum_{i=1} k_{p,i} \,.\, p_i, \quad p_i = \frac{M\tilde{Y}}{M} \bar{p}$$

4.4. Strategies For Predicting the Required Values

In this section the procedure for the prediction and determination of flame height as well as the mole fraction for the reactant and products are illustrated. After completing the required simulation process for a particular fuel /air mixture under certain conditions, some computational and post processing steps are performed as described below:

4.4.1 Flame Height Prediction

As mentioned previously, the solver which is used is supplied with a model for predicting the energy as well as the temperature at each cell across the computational domain. After getting the temperature contour for a specific case, the temperature distribution is plotted over the computational domain's center line. C. S. Mcenally [18] et. al. & G. Zhang et. al. [93] reported that the flame height located at the point of peak temperature on the center line. This methodology has shown good results and a high matching with the experimental results of the current study, as will be presented in chapter five later.

4.4.2 Prediction of Species Mole Fractions

As stated earlier, the XiFoam solver has its model for predicting the transportation of species at each cell across the computational domain. The mole fraction for the species is calculated through a post calculation for the regress variable (b) and progress variable (c) according to the chemical reaction balance. The regress variable (b) has been used to trace the reactants while the progress variable (c) has been used to trace the products.

4.5 Mesh Generation and Mesh Convergence Study

OpenFOAM code has its own tool for mesh generation called by "blockMesh" where all the vertices govern the domain are constructed to create the domain mesh blocks and boundaries. All these details are written as a code in a journal file called by "blockMeshDict". However, in the current study the whole geometrical domain of the studied control volume was constructed from structured mesh with hexa-blocks using the abovementioned tool. Thus, a uniform structured mesh was generated using different blocks as being shown in Fig. (4. 1). The computational domain has been generated such

that the cells are larger on both sides while it becomes finer as it moves towards the center line to take the effects of flame into accounts, see Fig. (4. 1, B).

Four mesh sizes are set in the simulations to perform the mesh convergence study and approach the mesh independence, namely 20000 cells (coarse mesh), 25000 cells (medium mesh), 30000 cells (fine mesh), as well as 35000 cells (very-fine mesh size) are tested. Fig. (4. 2) demonstrates the temperature distribution along the center line above the burner tip at the abovementioned four mesh sizes and all are for the combination of the stoichiometric LPG/air mixture at 5 Lt/min. It's worth mentioning that the difference in temperature values between the different mesh sizes appears in figure to be greater than it is in reality since the figure is zoomed to be able to notice the difference, otherwise the difference in the values is slight specially between the fine & the very-fine mesh. The figure also shows that the temperature distribution approaches its mesh independency at the very-fine mesh size where the curve in the very-fine mesh size matches the curve in the fine mesh size concluding that any further increase in the mesh would not affect the results significantly. Accordingly, the fine mesh size has been chosen for all the simulations of the present work.

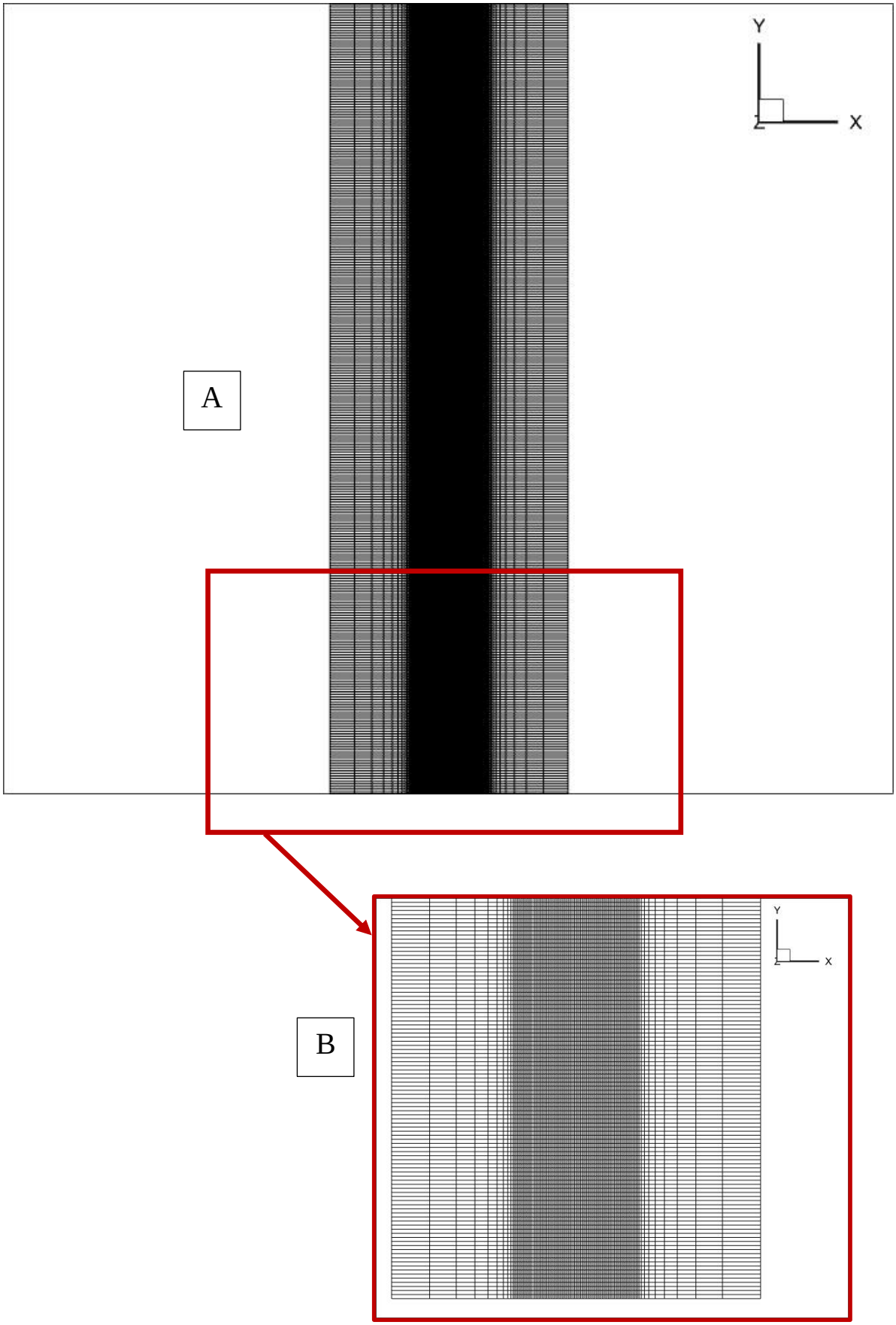

Fig. (4. 1) Computational domain and mesh details used in the current simulation: A) the full domain, B) zoomed view for a region of the domain

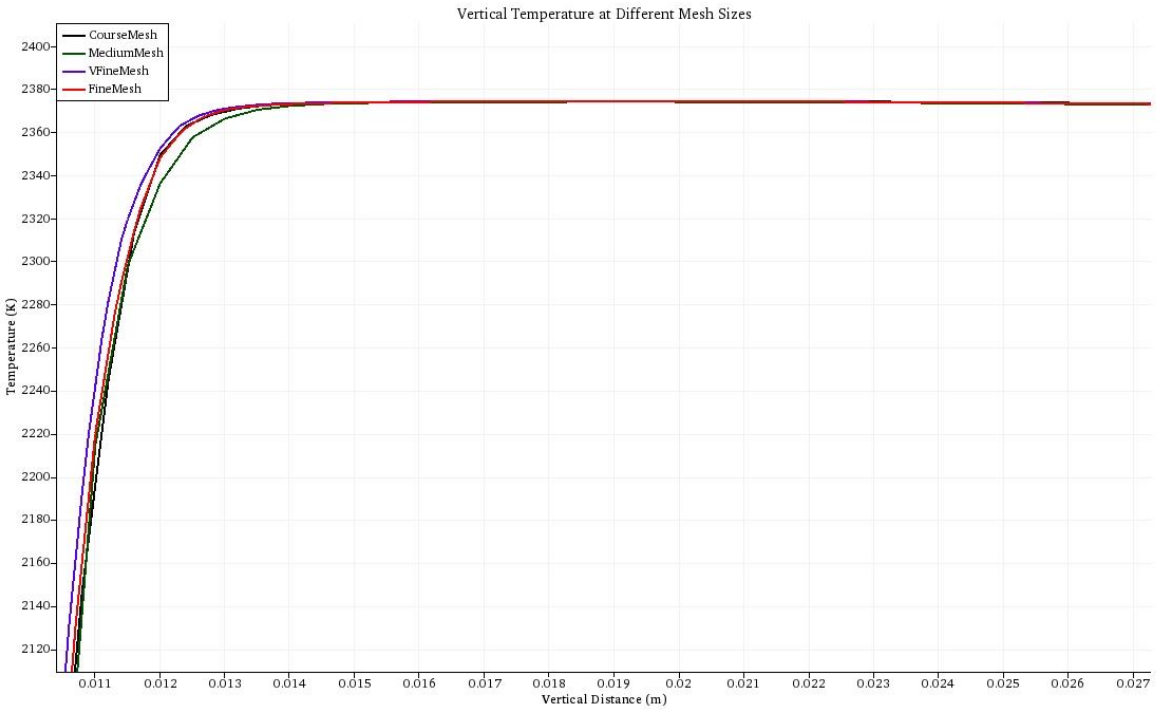

Fig. (4. 2) Temperature distributions along center line at different mesh sizes

4.6 Boundary Conditions

There are different types of boundary conditions used in the current computational model. Generally, the boundary conditions in the current numerical simulation are divided into four categorizes; boundary conditions involved in the turbulence model parameters, boundary conditions involved in the species of the chemical reaction, boundary conditions related to the energy transport parameters, and finally, the conditions involve the momentum equation parameters. Fig. (4. 3) shows the physical domain, where figure A illustrates the domain pointer to it the boundary conditions corresponding to each region. These boundary conditions were used for the solution of the problem through the discretization of the partial differential equations of the abovementioned model governing equations. Fig. (4. 3, B) show the regions of the physical domain. Table (4. 1) show all these boundary conditions for each patch under each of the aforementioned categorizes.

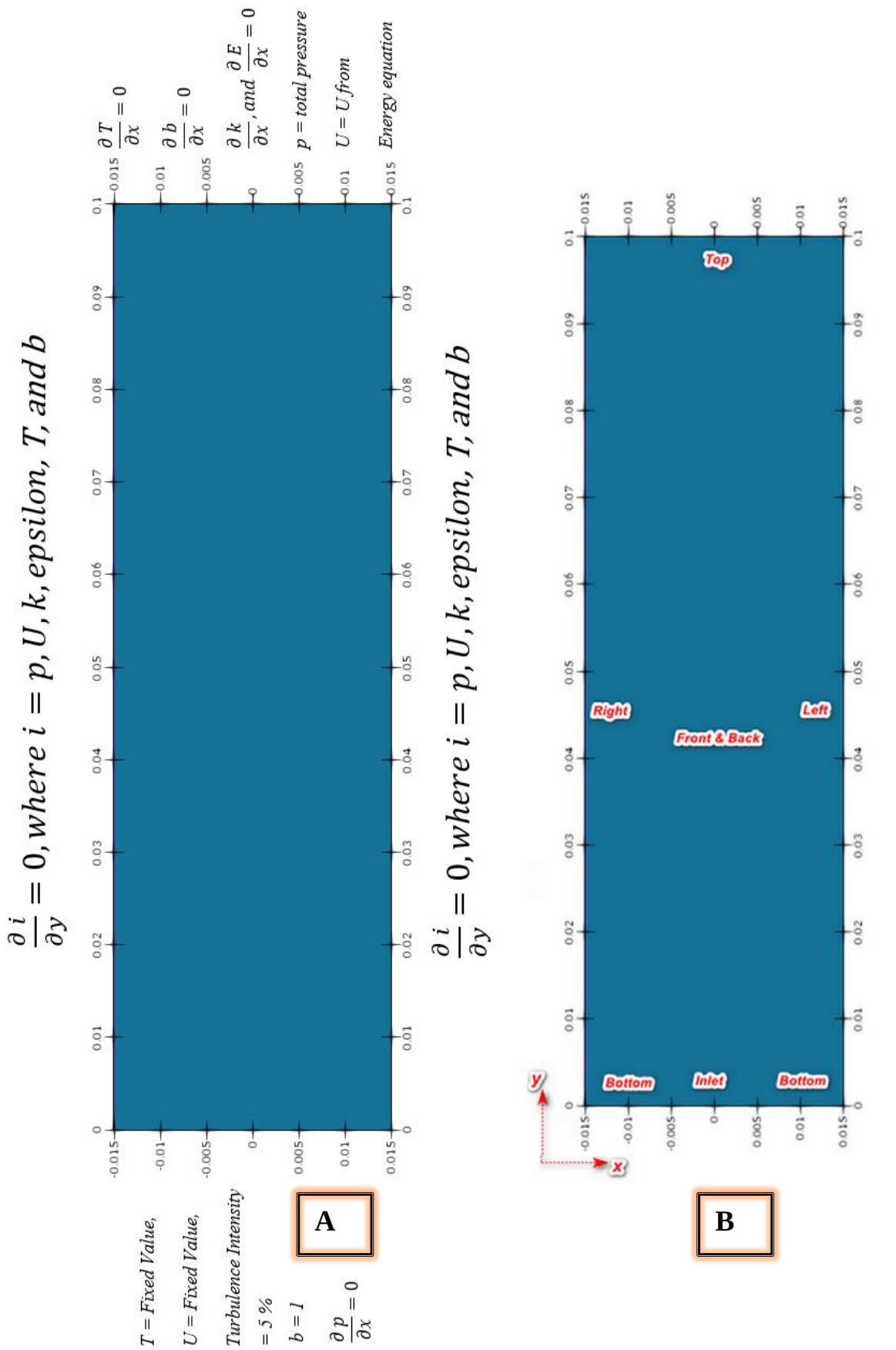

Fig. (4. 3) The physical domain and its Boundary conditions: A) types of Boundary conditions, & B) Regions of the domain

Table (4. 1) Boundary conditions specifications for main properties under each category of the gov. Eqs.

Turbulence Model Parameters						
	Front and Back	**Left**	**Inlet**	**Right**	**Bottom**	**Top**
∈	Empty	Periodic	Turbulent Mixing Length Dissipation Rate Inlet	Periodic	Symmetry Plane	Zero Gradient
k	Empty	Periodic	Turbulent Intensity Kinetic Energy Inlet	Periodic	Symmetry Plane	Zero Gradient
nut	Empty	Periodic	calculated	Periodic	Symmetry Plane	calculated
Momentum and Continuity Parameters						
u	Empty	Periodic	Fixed Value	Periodic	Symmetry Plane	Pressure Inlet Outlet Velocity
p	Empty	Periodic	Zero Gradient	Periodic	Symmetry Plane	Total Pressure
Energy Equation Parameters						
Alphat	Empty	Periodic	Calculated	Periodic	Symmetry Plane	Calculated
T	Empty	Periodic	Fixed Value	Periodic	Symmetry Plane	Zero Gradient
Species Transport Equation Parameters						
b	Empty	Periodic	Fixed Value	Periodic	Symmetry Plane	Zero Gradient

where alphat is the turbulent thermal diffusivity and nut is the turbulent kinematic viscosity.

4.7 Present Numerical Code Validation

In order to give validity to the present numerical study and its procedure and details, the present code validated with some previous related works using the code and procedure of the present study. The operating condition which used by (Kutkan and Guerrero 2022) [67] are used in the present code in order to conduct its validity.

Fig. (4. 4 A) shows the flame shape resulting from the present simulation, measured in meters, while Fig. (4. 4 B) is the flame shape obtained by Kutkan and Guerrero 2022 [67] measured in millimeters. The comparison

between the two results indicates that the present numerical code is and valid as it gives results with good agreement with Ref. [67] who studied the premixed flame modeling using OpenFOAM also. H. Kutkan and J. Guerrero [67] compared their results with experimental results of (Siewert, P. 2006) [94] and take all the experimental conditions and values from it. The predicted flame height, is equal to 104, 126.5, and 140 mm for [67], the present simulation results, and for [94] respectively. This means that the predicted flame height by the current numerical code is close the average of predicted flame height of [67] & [94] with a deviation of 3.6% and with the same general flame shape.

This validation process for the present numerical code means that its setup is true and valid to be implemented for the simulation of the different cases in present work.

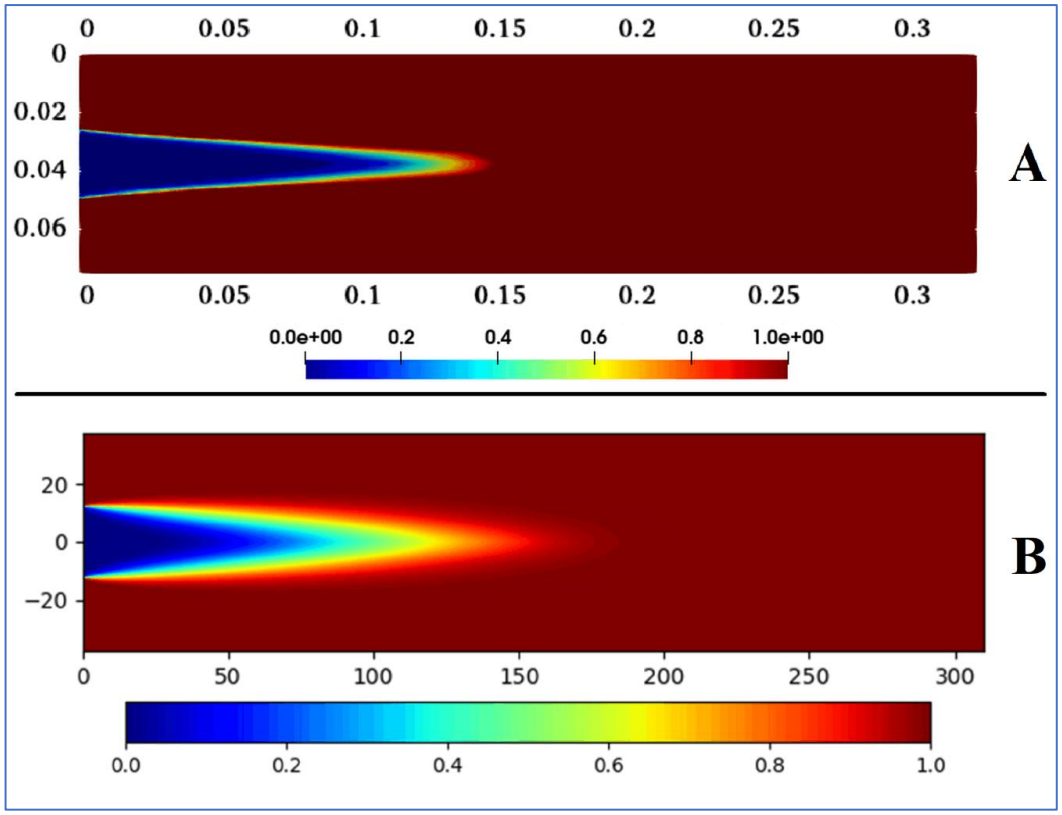

Fig. (4. 4) comparison of flame shape: A) the result of the present numerical code, & B) is the result of H. Kutkan and J. Guerrero 2022 [67].

CHAPTER FIVE

RESULTS & DISCUSSION

5.1 Introduction

In this chapter, the most prominent results and observations which were obtained from the current study, with all its details and methods, will be reviewed. First, the results will be presented for the practical study part, which include the effect of many operating parameters on flame height and structure (such as equivalence ratio, flow rate, H_2 blending ratio, mixture dilution, and the use of swirling burner). A repeatability test was performed to ensure the validity of the experimental equipment and measurement accuracy. After that, the results of the theoretical part of this study are presented, which include simulations of the combustion of LPG/air mixture and the flame height and structure including the effect of the above parameters. A validation for the numerical simulation is conducted by comparing the results of the present work with the results of a previous one. Then the experimental & numerical results are compared with each other and with some previous works.

5.2 Results of the Experimental Work

5.2.1 Repeatability of the Experimental tests:

An experimental apparatus is specifically fabricated and built to perform the details of this study. Before proceeding with the practical tests, a repeatability test has been carried out to approve the experimental apparatus validity and measurement accuracy. As it was mentioned earlier, the fuel/air mixture is prepared inside the mixing chamber based on the partial pressure method. Three different experiments were carried out, each repeated three times to get the repeatability test results. The results of flame height with

respect to flow rate for these three experiments are shown in Fig. (5. 1), where Fig. 5.1. a is for LPG/air mixture at ϕ=1, Fig. 5.1. b is for LPG/air mixture at ϕ=1.2, and Fig. c is for LPG/air mixture at ϕ=1.4 and all are for the burner of 8 aspect ratio. These figures show that the results of the repeatability are reasonable, since all the curves obtained have the same trend and the values are very close. The cumulative percentage error is about 1% or less, while the maximum difference in the measured flame height among the different repeated tests for each experiment is about 1.1 mm which represents 1.5% of the length of the flame. The difference in the results could be attributed to due to the errors in measuring devices, the difference in ambient conditions and human errors. The comparison shows good agreement, verifying the high accuracy of the experimental procedure and the measurement methodologies.

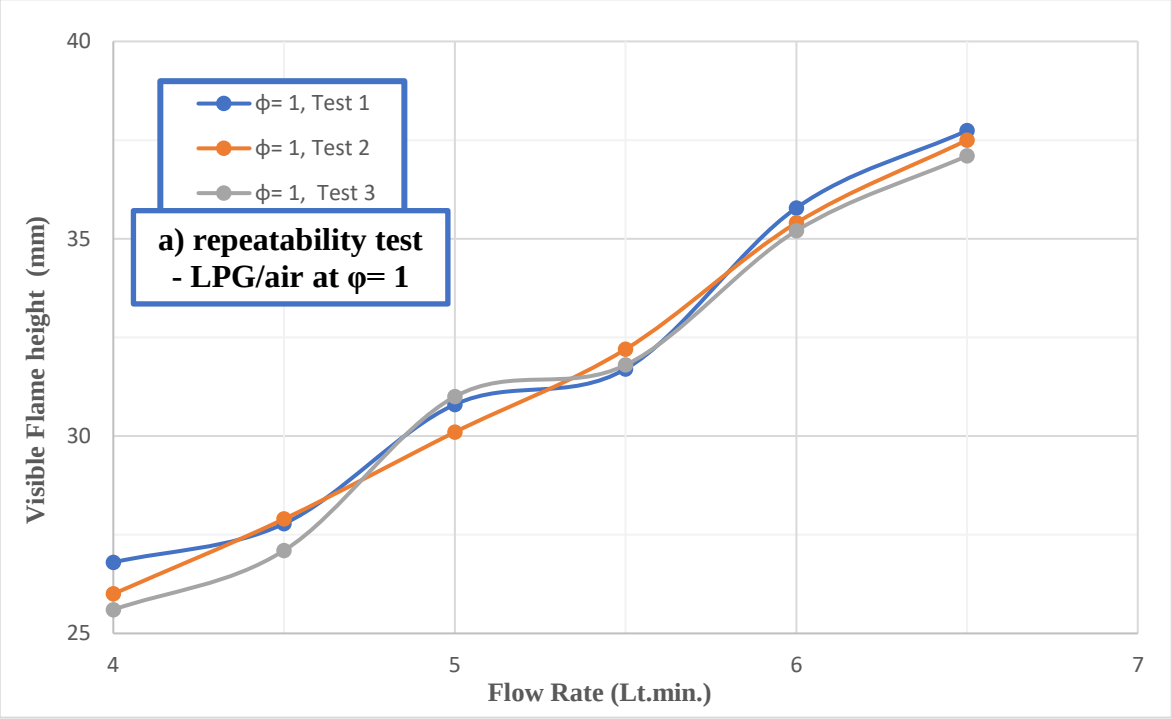

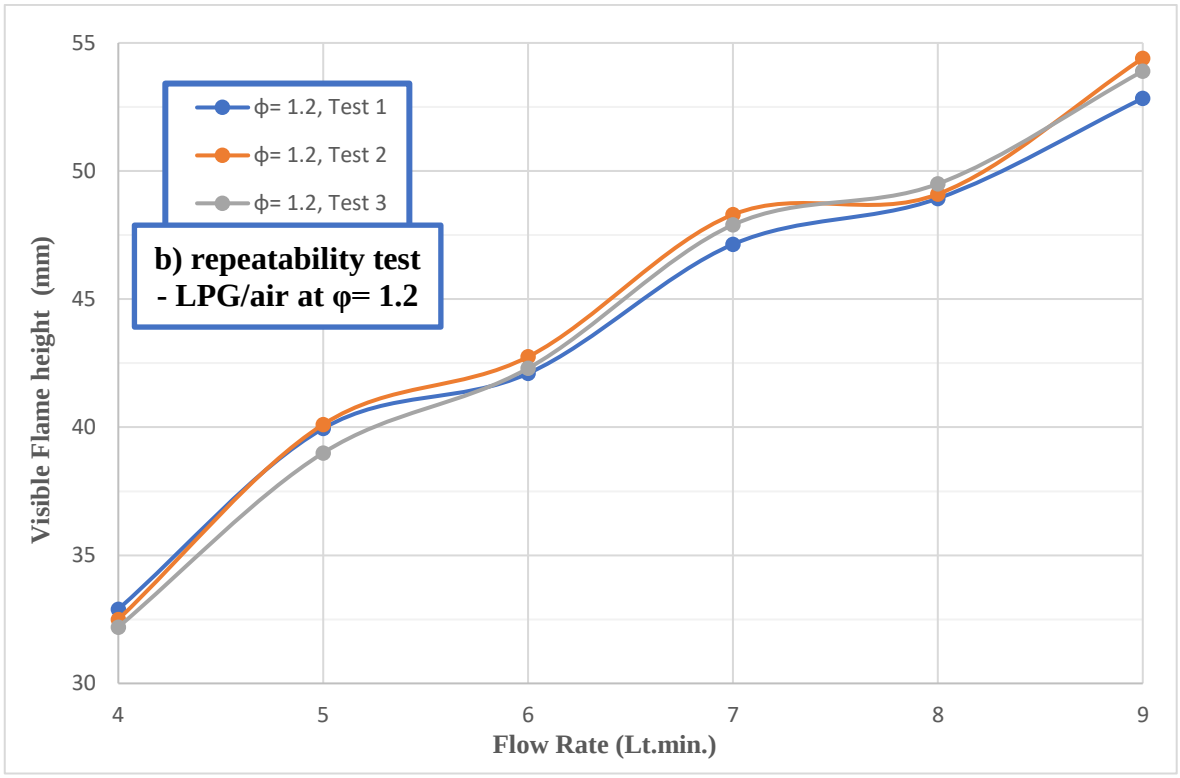

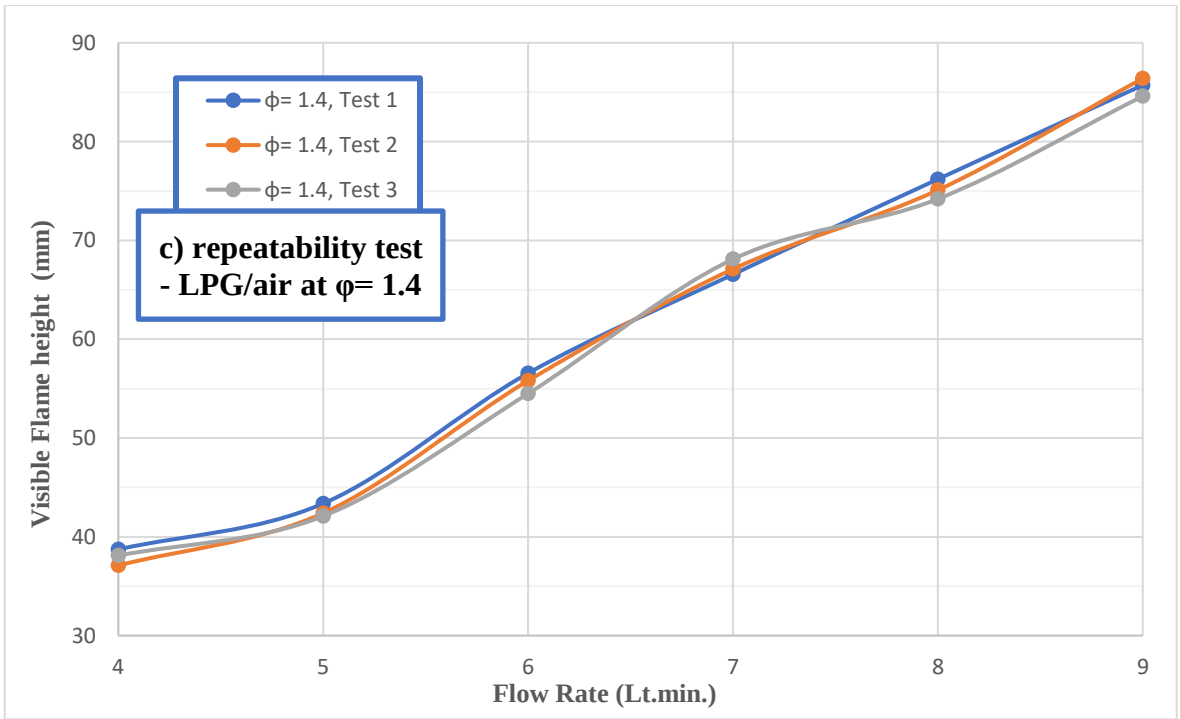

Fig. (5. 1)Results of the repeatability test: a) LPG/air at ϕ =1, b) LPG/air at ϕ =1.2, and c) LPG/air at ϕ =1.4

5.2.2 Procedure of Flame Height Determination:

After capturing the flame, the image is saved and renamed up to the case and experimental conditions. Two procedures were used to determine the height of the flame. The first method is conducted by image processing analysis for flame image by a MATLAB code [29], [72] & [13]. The second method is conducted by scaling the length of the flame that displayed in the image [95]–[97]. These methods show comparable matching in values for the measured flame height with each other for a large number of images and for different cases see Fig. (5. 2) below. The details of each method are illustrated below:

5.2.2.1 Measuring Flame Height by MATLAB Image Processing:

The flame image is first processed with an image extraction software and then its height is calculated by relating the flame pixel position with the burner pixels seen in the image. The number of pixels of the burner is calculated. The actual diameter of the burner is 12 mm. Thus, the resolution of pixel (millimeters /pixel) is obtained for the image. Through the image processing, the pixels where the flame root and the flame tip were located are detected. The flame height could be calculated by multiplying the difference in flame pixels by the resolution of burner pixels.

5.2.2.2 Measuring Flame Height by AutoCAD Scaling:

The image of the flame is inserted into AutoCAD using the raster image reference tool. Then the image is rescaled with a reference value for the burner diameter equal to its actual diameter. Now all dimensions of the image become identical to the actual dimension including flame height.

Fig. (5. 2) is a sample for the comparison of the results of MATLAB image processing & AutoCAD scaling methods for the determination of the height of the flame for LPG/air mixture at the stoichiometric condition for different flow rates for the burner of 8 aspect ratio. The difference in the

measured height between the two methods is with the order of 0.4 mm, i.e., about 1% of the total length of the flame. According to the great congruence in the measured flame height values by the two methods, the scaling method by AutoCAD has been adopted to measure the length of the flame.

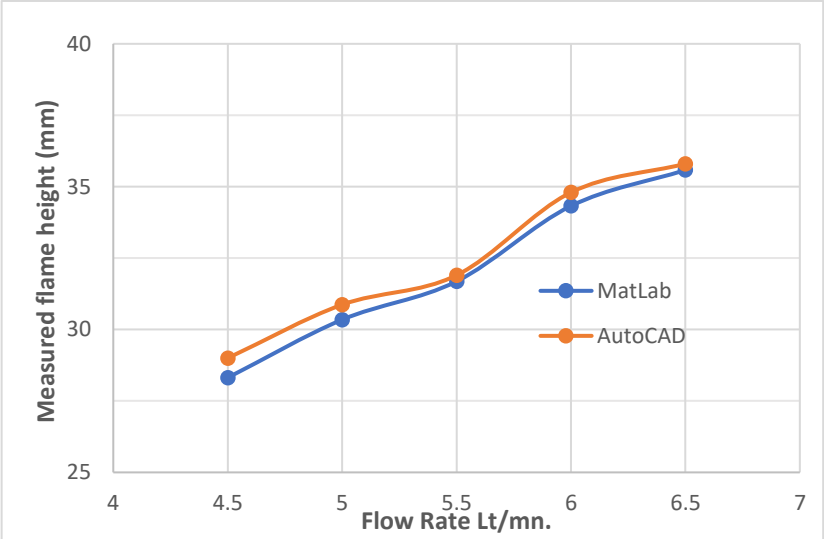

Fig. (5. 2) Comparison of the measured flame height for (LPG/air at ϕ=1) by methods of MATLAB image processing & AutoCAD scaling

5.2.3 Results of LPG/ air mixture:

The LPG/ air mixture was tested with respect to different equivalence ratios (0.6, 0.8, 1, 1.2 1.4), flow rates (from flashback to blowout limits), and the burner's aspect ratios (2, 4, 6, 8, 10). This section includes the results for the effect of these parameters on flame structure and flame stability limits as shown below:

5.2.3.1 Effect of Equivalence Ratio:

Fig. (5. 3) & Fig. (5. 4) show the measured flame height for LPG/air mixture at different equivalence ratios. It is obvious that the higher equivalence ratio the taller flame and for both the inner zone height and visible height. When the fuel and air are mixed with a higher equivalence ratio, the fuel mole fraction in the mixture increases while the oxidant mole fraction decreases. In

this situation, the additional amount of fuel requires more distance to react with the oxidant and complete combustion reactions.

The reaction zone of a flame can be divided into two layers, the inner layer & the oxidation layer [98]. In the inner layer all the fuel is preheated and degraded into intermediate radicals and chain-branching reactions that form combustion radicals and keep the reaction running are initiated. In the oxidation layer, the species are oxidized to form the final product see Fig. (5. 5).

A pivotal issue has been noticed from the experimental tests, where there is a high attachment and interdependent relationship between the equivalence ratio and the valid flow rate range for combustion. As the equivalence ratio decreases, the range of flow rates valid to achieve the combustion is oriented toward smaller values, see Fig. (5. 3) & Fig. (5. 4). When the flow rate falls below that ranges, the flame experiences a flashback, and when the flow rate exceeds the ranges, the flame blowoffs. This matter is very important and effective; thus, it is not possible to choose the same value for the flow rate at all equivalence ratios especially for lean mixture.

Fig. (5. 6) shows a series of photographs of flames of LPG/air mixture for equivalence ratios at 6 Lt/min. The figure illustrates the flame height and inner structure. It shows that the flame aspect ratio (the ratio of flame height to flame width at the base) increases with equivalence ratio.

Several experimental tests were conducted with equivalence ratio of 0.6. It is noticed that the flame is very short, not stable and very hard to adjust with flow rate. The same was observed with the all mixtures for LPG/air, LPG-H_2/air, LPG-CO_2/air, and LPG-H_2-CO_2/air mixtures. Accordingly, it is difficult obtain stable flames at ϕ = 0.6 or less for all types of mixtures. Thus, the experimental results are presented only for equivalence ratios of 0.8, 1, 1.2, 1.4.

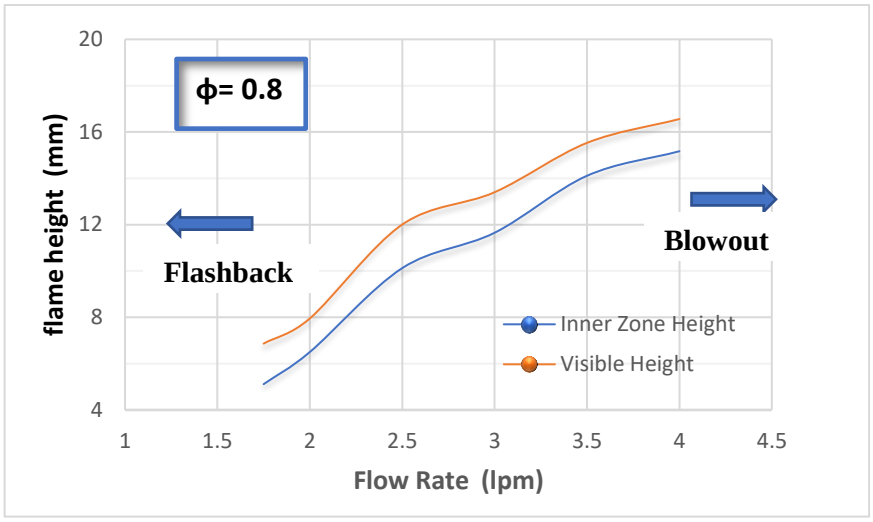

Fig. (5. 3) Effect of flow rate on flame height for LPG at φ = 0.8.

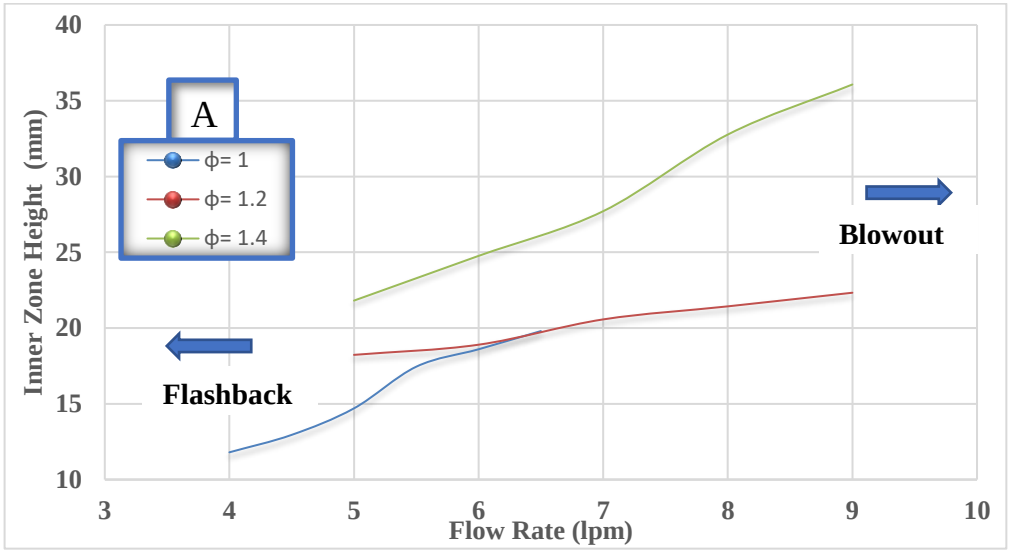

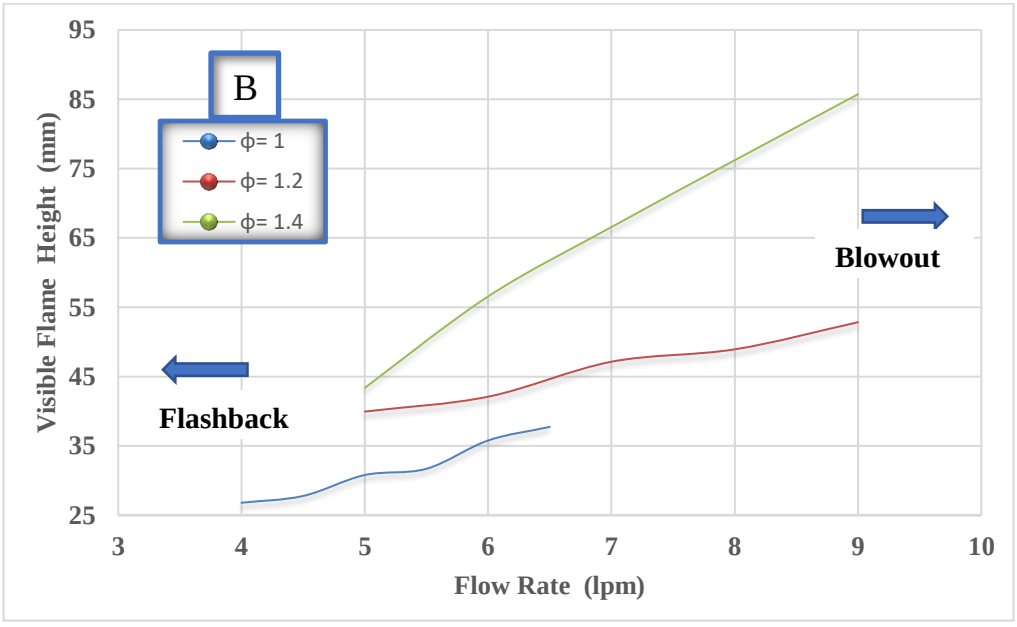

Fig. (5. 4) Effect of flow rate on flame height for LPG at φ =1, 1.2 & 1.4: A) height of inner zone and B) visible flame height

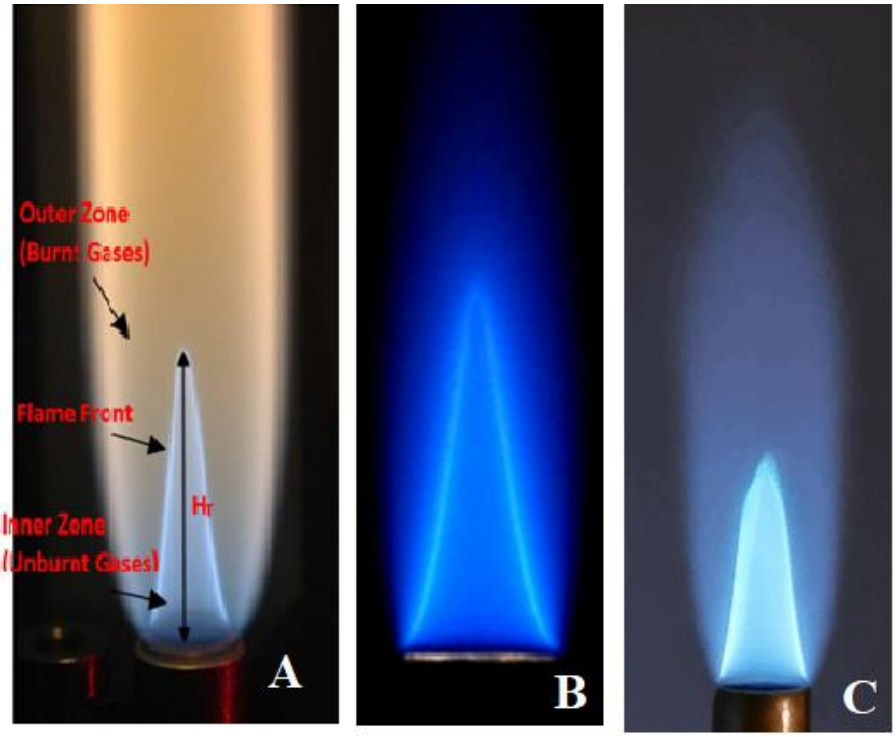

Fig. (5. 5) photography of flame with two regions: Fig. A is from [98], *Fig. B is from* [21], *and Fig. C is the present study flame.*

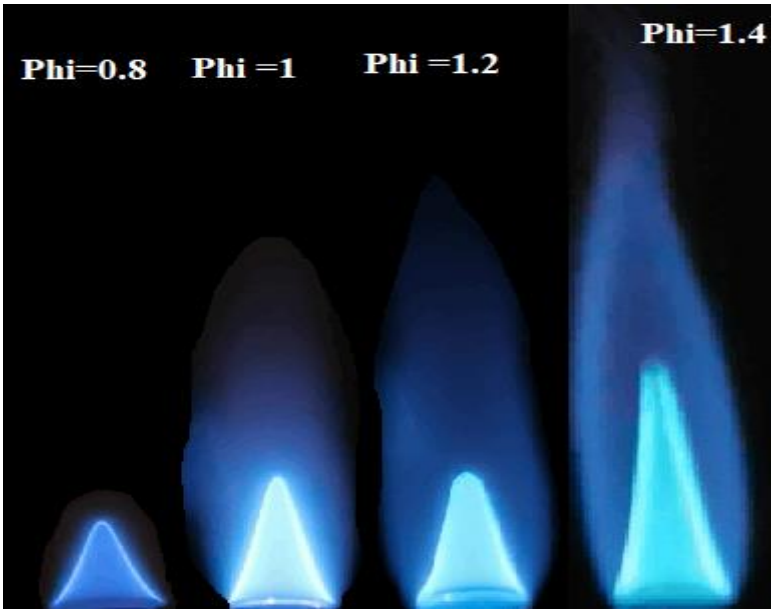

Fig. (5. 6) Photography of flames at different φ for (LPG/Air) mixture at 6 Lt/min.

5.2.3.2 Effect of Flow Rate:

The effect of flow rate of the LPG/air mixture on flame height were investigated and the results are shown in Fig. (5. 3) & Fig. (5. 4) above for different equivalence ratios and for both flame zones, inner zone and visible

height. It is obvious that the flame height increases as the flow rate increase. The higher flow rate of fuel/air mixture the larger amount of the combustible mixture, and thus the combustion process needs additional distance for the fuel and oxidant to react. This will make the flame extended to a farther location until the maximum possible amount of fuel is reacted through the combustion process. As mentioned in section 5.2.3.1, the equivalence ratio affects to change the values of the flow rate for the same fuel/air mixture. For example, if the flow has been doubled from 2 to 4 Lt/min. in Fig. (5. 3) then the visible height of the flame increase from 7.95 to 16.56 mm. This increase does not continue in the same manner in cases when ϕ = 1 & 1.2 while approximately the same increase is repeated when ϕ = 1.4 see Fig. (5. 4B).

Fig. (5. 7) shows a series of photographs of flames of stoichiometric LPG/air mixture at different flow rates. The effect of mixture flow rate on flame height is similar to that of equivalence ratio which mentioned above. The flame aspect ratio increases with respect to flow rate increase.

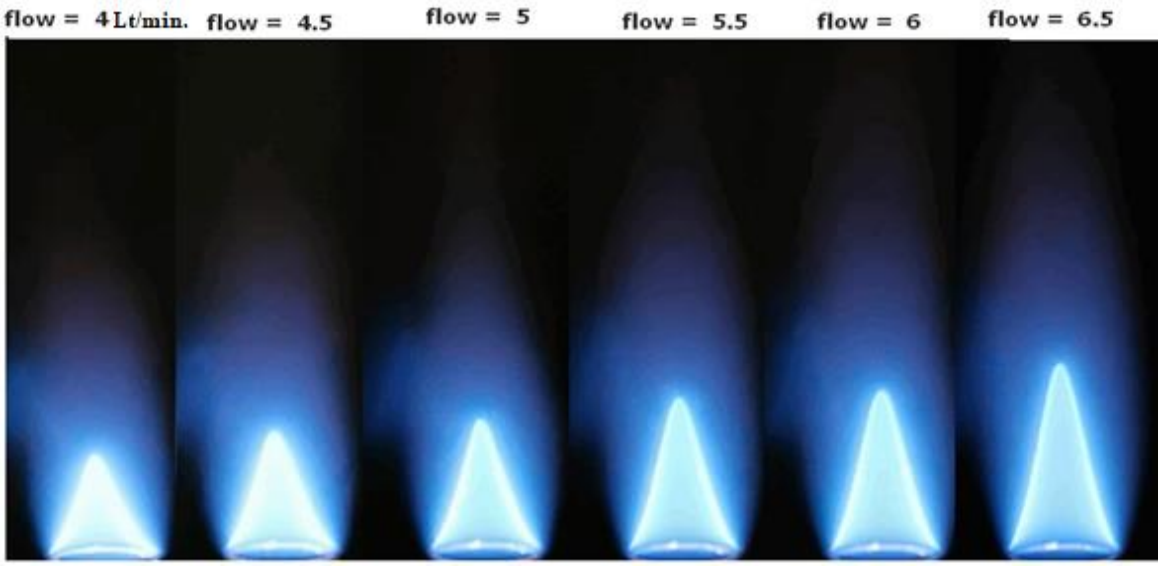

Fig. (5. 7) Photography of flames at φ =1 at different flow rates for (LPG/Air) mixture

5.2.3.3 Effect of Burner's Aspect Ratio

Fig. (5. 8) indicates the effect of changing the aspect ratio of the burner on the flame height with different equivalence ratios for (LPG/Air) mixture for the visible flame height. Fig. (5. 8, A) is for equivalence ratio of 0.8 at 3 Lt/min., while Fig. (5. 8, B) is for an equivalence ratio of 1, 1.2, & 1.4 at 6 Lt/min common to the three cases. The burner aspect ratio effect is less significant than that of equivalence ratio ϕ. This illustrates that, while the mean flow rate of the air/fuel mixture are the same, the interaction between the mixture and their mixing differs depending on the burner length [99].

Both figures indicate that increasing ϕ lead to elongating the flame, especially for a high equivalence ratio. Higher ϕ means that the fuel/air mixture contains more fuel fraction and thus with the increase of ϕ, there was not enough time for all the fuel to be burned completely with the same distance above the burner tip and the reaction extends far away producing a longer flame.

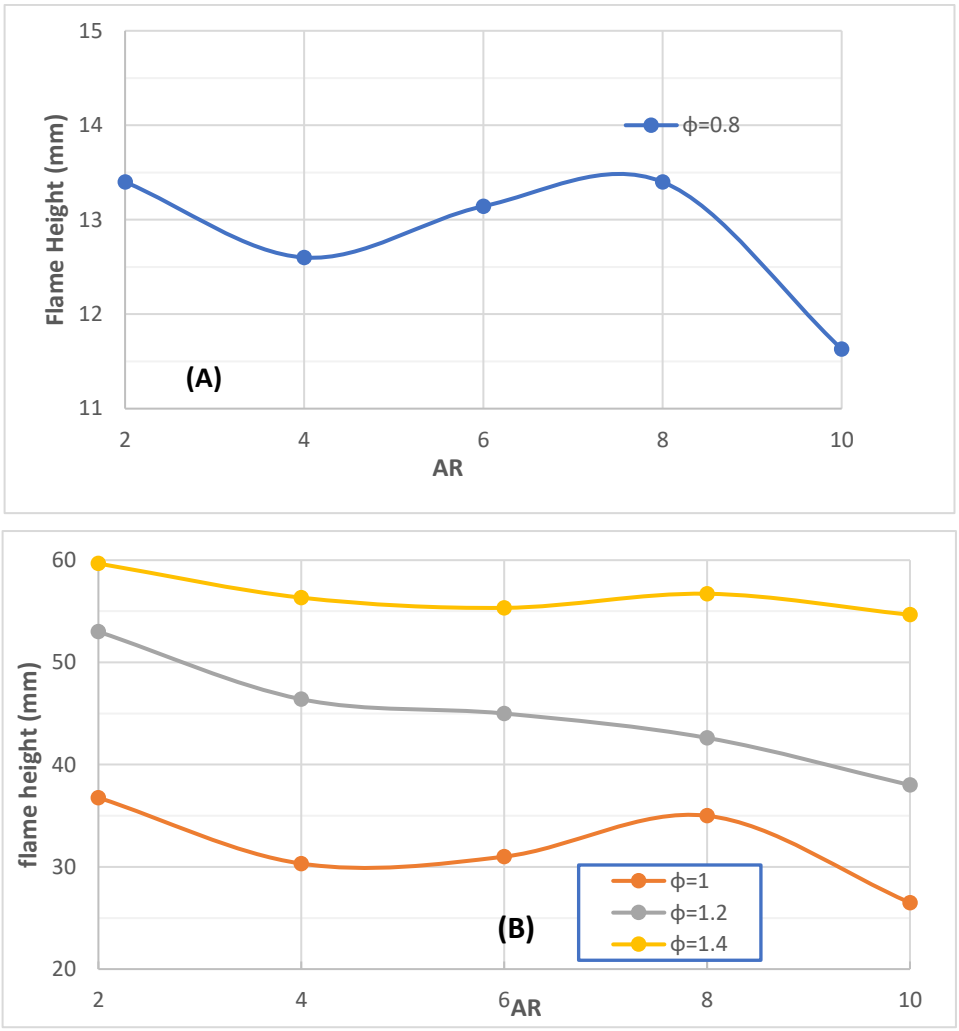

Fig. (5. 8) Effect of aspect ratio on flame height for different φ : A) for φ = 0.8 and B) for φ =1, 1.2 & 1.4 for (LPG/Air) mixture

5.2.3.4 Effect of Flow Rate & ϕ on Flame Stability Limits:

As mentioned previously in section 5.2.3.1, there is a coherent effect between the equivalence ratio and flow rate. Changing the equivalence ratio will lead to a change in flow rate values where flashback and blowout are taken place. Increasing the equivalence ratio will increase the flashback and blowout flow rates as shown in Fig. (5. 9) while on the other hand, the stability limits (values and ranges for flow rate that producing a stable flame) increases significantly as shown in Fig. (5. 10).

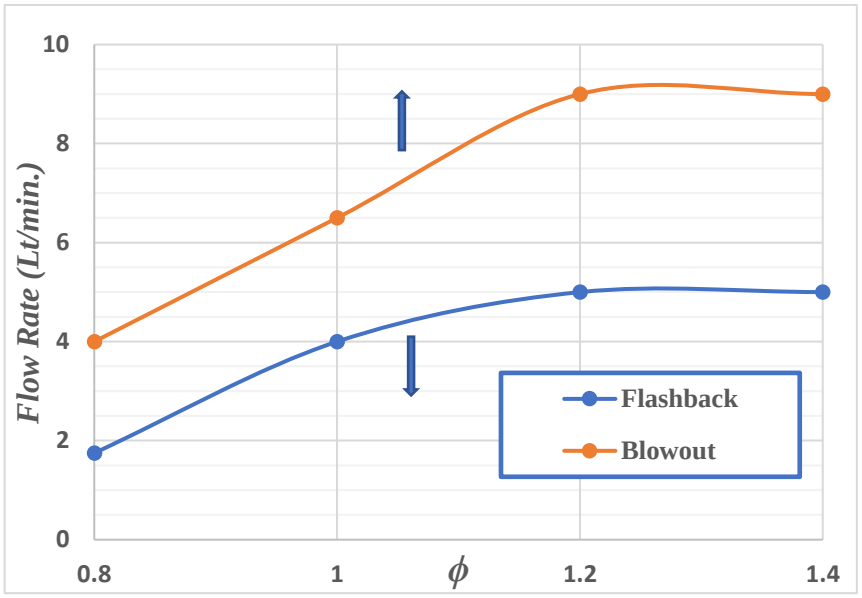

Fig. (5. 9) Flow rate of flashback and blowout limits for LPG/air at different ϕ

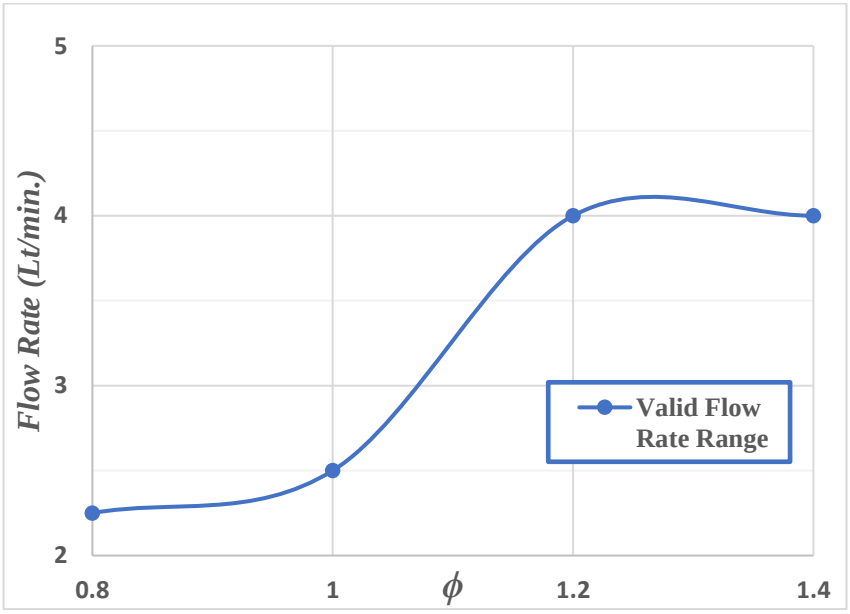

Fig. (5. 10) Stability limit for LPG/air at different equivalence ratios

5.2.4 Results of LPG- H_2/ air mixture:

This section includes the results for the influence of LPG- H_2/ air flames structure by hydrogen blending ratio (0%, 10%, 20%, 30%, & 40%), equivalence ratio (0.8, 1, 1.2, &1.4), and flow rate (from flashback to blowout limits), as well as the effect of hydrogen blending ratio on flame stability limits, as shown below:

5.2.4.1 Effect of Hydrogen Blending Ratio:

Fig. (5. 12) indicates the effect of hydrogen blending ratio on the visible flame height for stoichiometric LPG-H2/air mixture at different flow rates. It is clear that the flame shortens as a result of hydrogen blending.

In Fig. (5. 13) & Fig. (5. 14) the results for the influence of visible flame height by hydrogen blending ratios (0%, 10%, 20%, 30%, and 40%) are shown. Fig. (5. 13) is for different equivalence ratios where the flow rate is fixed at 3 Lt/min. for the case ϕ = 0.8 and at 6 Lt/min. for the cases when ϕ = 1, 1.2, & 1.4. Fig. (5. 11) is for different flow rates of the mixture at ϕ =1. These figures illustrate that the addition of H_2 to the fuel/ air mixture led to flame height reduction. Another finding is that the flame height monotonically decreases when the fraction of blended H_2 is 30% and more. As the diffusivity of hydrogen is too high, then the diffusivity of the fuel blended with hydrogen will increase somewhat. This means an increase in the rate of the chemical reaction and its occurrence within a shorter space, which leads to a decrease in the length of the flame. The entrainment area, mixing area, reaction zone, and post-combustion area were all reduced by hydrogen blending, resulting in a shorter flame [54]. Another justification is that the laminar burning velocity shows a monotonic increase at higher hydrogen fraction [100] and this led to reduce flame height.

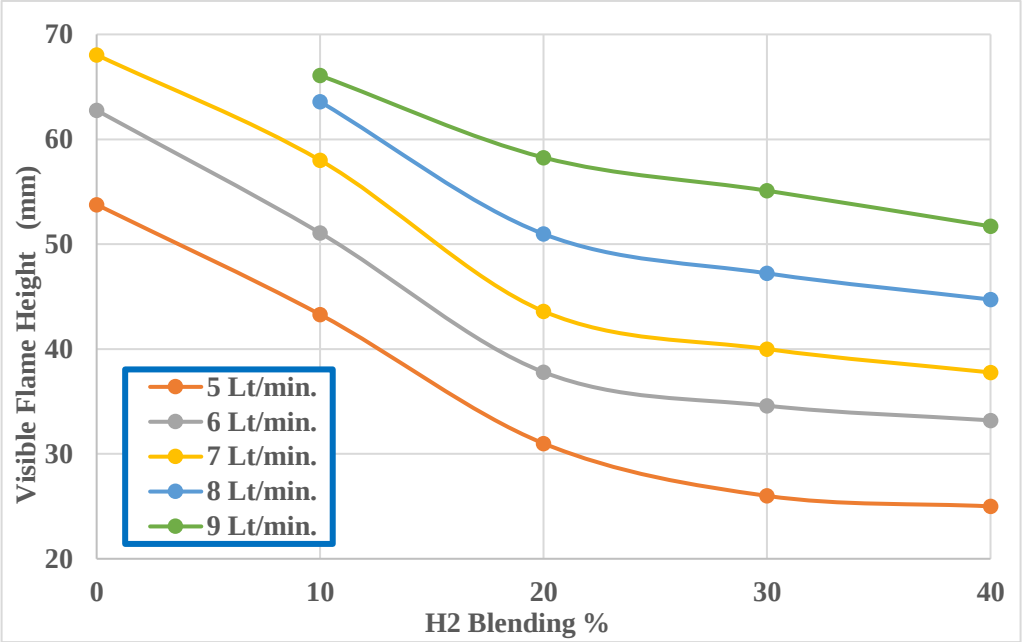

Fig. (5. 12) Effect of H_2% on visible flame height for stoichiometric LPG-H_2/air mixture

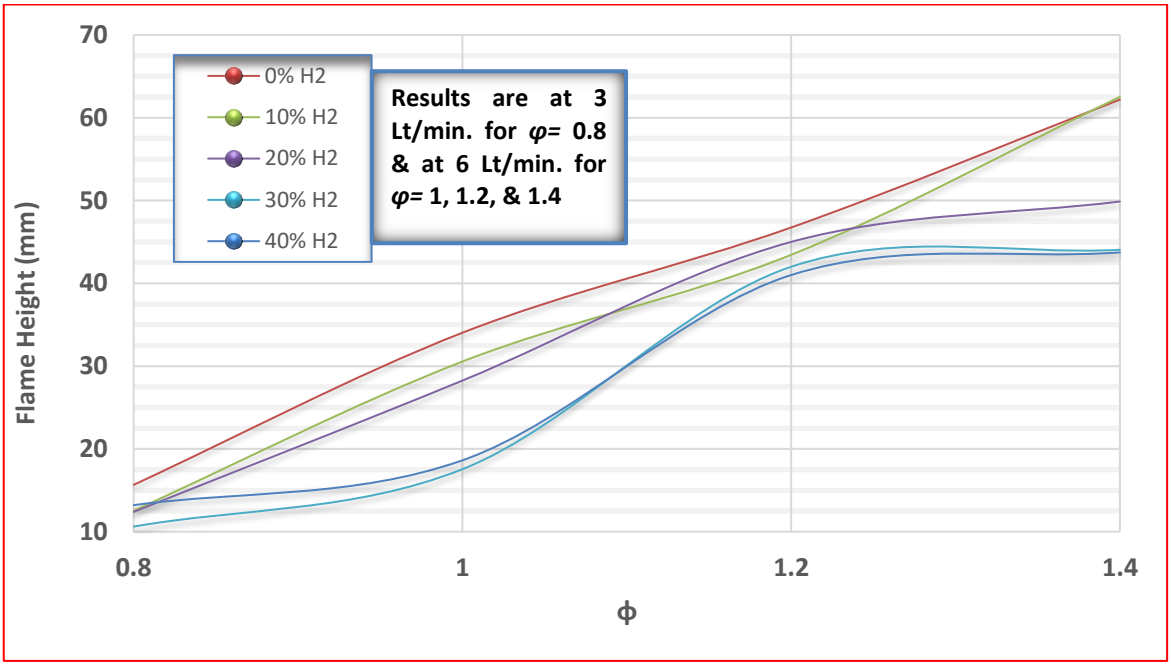

Fig. (5. 13) Effect of φ on visible flame height for different hydrogen blending for (LPG-H2 / Air) mixture

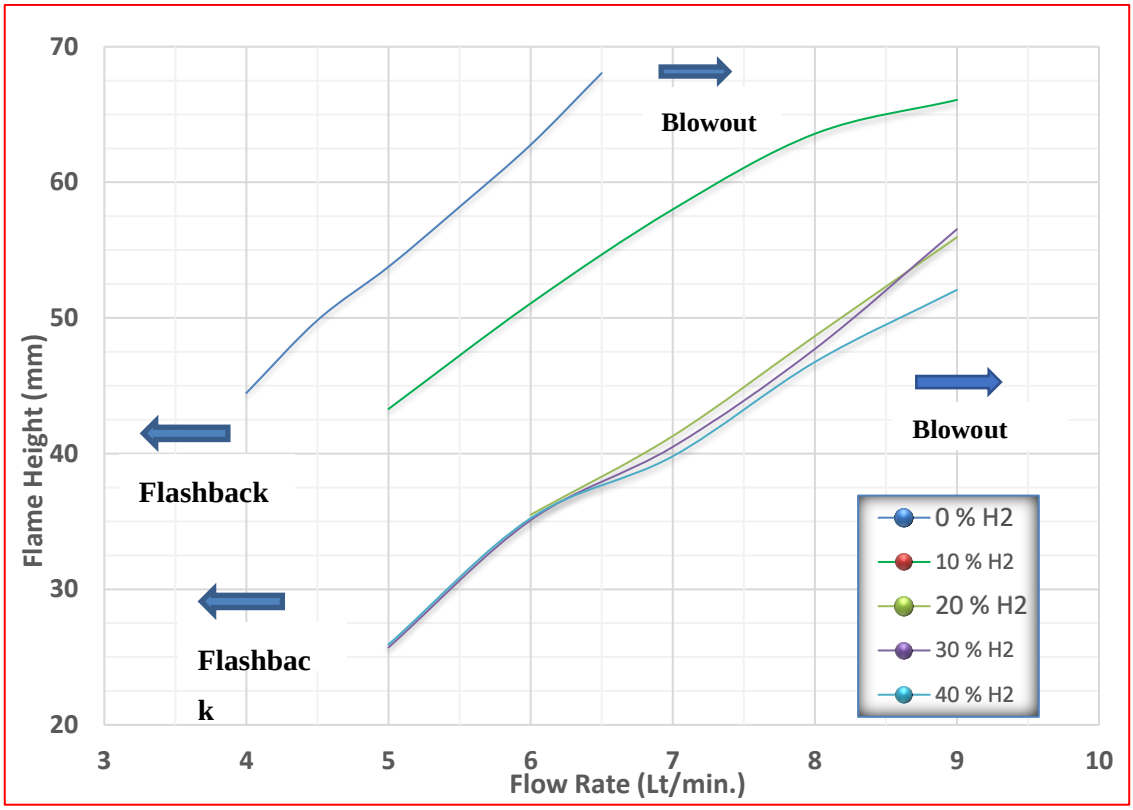

Fig. (5. 14) Effect of flow rate on visible flame height for different hydrogen blending ratios for (LPG-H2 / Air) mixture at ϕ =1

5.2.4.2 Effect of Equivalence Ratio:

The effect of equivalence ratio on flame height for the LPG-H_2/air mixture is shown in Fig. (5. 13) above. On the contrary of the effect of H_2, the flame height steadily increases when the mixture's equivalence ratio goes up. Generally, the increase in flame height as a result of increasing the equivalence ratio is more compared to the reduction in flame height as a result of increasing H_2 blending ratio.

5.2.4.3 Effect of Flow Rate:

The effect of varying flow rate of the mixture on flame visible height is shown in Fig. (5. 14) above for LPG fuel with hydrogen blending ratio of (*0%, 10%, 20%, 30%, and 40%)* at ϕ *=1*. The flame height elongated continuously while increasing the mixture flow rate. This result is the same when increasing the flow rate for the LPG/air mixture previously. The greater the flow rate,

requires more distance for the fuel and oxidant to react. This will cause the flame elongation until the maximum quantity of fuel is reacted and.

On the other hand, when a slight hydrogen is blended to fuel, the flame shortens. This decrease continues in the flame height up to 20% hydrogen blending ratio, after that the flame shortens slightly with extra hydrogen blending at 30% & 40%. For example, at a flow rate of 6 Lt/min., if 40% H_2 is added to the mixture, then the flame undergoes a reduction by nearly 50% in its height as it compared with the height of LPG/air mixture flame. Briefly, the net effect is that the increase in the height of the flame due to the increase in mixture flow rate outmatches its decrease with the increase in the percentage of hydrogen blending.

Fig. (5. 15) shows some flame images at stoichiometry. The first & second images from the left are for LPG flame, while the third & fourth images are for LPG-20%H_2 flames. It is clear from the figure that LPG-air mixture blended with hydrogen produces a shorter flame, especially at the level of the visible length, and also increases the width of the flame, especially at the inner zone tip. The flame aspect ratio is increased with higher flow rate while it decreased at higher hydrogen blending ratio.

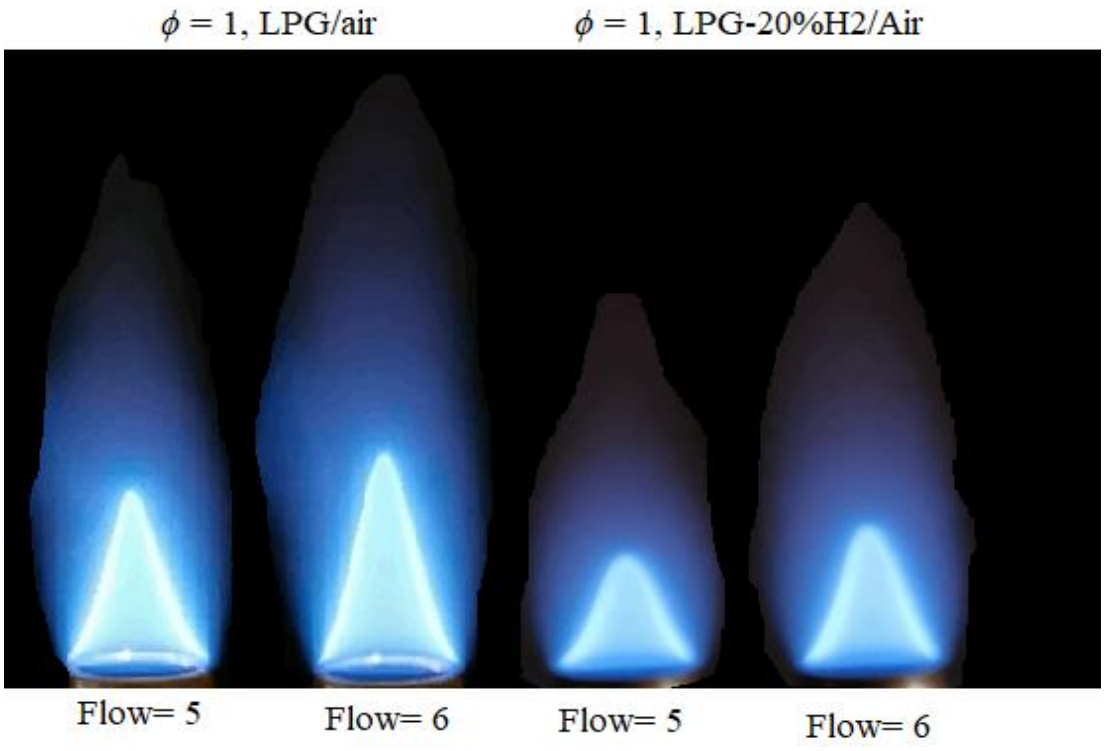

Fig. (5. 15) photography of flames with and without H_2 blending

5.2.4.4 Effect of Flow Rate & ϕ on Flame Stability Limits:

The addition of hydrogen improves flame stability and expands the range between the flow rates which causing flame flashback and blowoff, see Fig. (5. 14) above. At 0% H_2, this range is about 2.5 Lt/min (4-6.5 Lt/min.), while this range has been approximately doubled if H_2 added to the mixture. On a related note, from the figure, the addition of H_2 shifted the curves to begin with flow rate of 5 Lt/min. instead of 4 Lt/min. for the LPG/air mixture to avoid flame flashback. This can be attribute to the fact that H_2 has high flame speed. If the flame speed is higher than the flow velocity, the flame starts to propagate upstream leading to flashback [25].

5.2.5 Results of LPG- CO_2/ air mixture:

Carbon dioxide (CO_2) is used as a diluent to the LPG/air mixture to investigate the effect of dilution on flame height of a premixed mixture. This section includes the results for the influence of LPG- CO_2/ air flames structure by CO_2 dilution

ratio (0%, 5%, 7.5%, & 10%), equivalence ratio (1, & 1.2), and flow rate (from flashback to blowout limits), as well as the effect of CO_2 dilution ratio on flame stability limits, as shown below:

5.2.5.1 Effect of CO_2 Dilution Ratio:

Fig. (5. 16) shows flame height versus CO_2 dilution ratio for stoichiometric (LPG-CO_2 /Air) mixture. It is obvious that the diluted LPG flame is longer than the LPG flame without dilution for the same flow rate. The addition of CO_2 elongating the flame and this elongation keeps going as CO_2 dilution ratio increased. This result coincides with the observations of H. Xu et. al. [70] for the syngas flames and J. Min et. al. [101] for the methane/air flames.

Conversely with the effect of H_2 addition that discussed previously, the addition of CO_2 to the fuel/ air mixture increases flame height. The addition of CO_2 to the mixture leads to reduce the oxygen mole fraction in the fuel/ air mixture as CO_2 is diluted instead of a part of the air. This means that the fuel needs more further downstream to get the oxygen required for the combustion which leads to a longer flame. On the other hand, the addition of CO_2 may also produce more soot formation in the flame since that part of fuel may undergo pyrolysis process due to oxygen insufficiency.

This causes the reaction and combustion to continue for a longer distance, resulting in an increase in the flame height. For rich mixture Fig. (5. 18), the flame elongation responses more directly to a slight addition of CO2 as compared with stoichiometric mixture. This can be attributed to the double effect of both equivalence ratio & CO2 in prolonging the flame.

5.2.5.2 Effect of Equivalence Ratio:

By comparing Fig. (5. 17) & Fig. (5. 18), the effect of equivalence ratio on flame height is concluded for LPG- CO_2/ air mixture. An increase in the

equivalence ratio leads to an increase in flame height but with a higher rate than that presented in the mixtures which discussed previously, as both equivalence ratio and / or CO_2 dilution ratio elongate the flame. For example, the flame elongates by about 4.7 mm if 7.5% CO_2 is diluted to the stoichiometric LPG/air mixture at 5 Lt/min. this increase in flame height jump to about 12 mm at $\phi=1.2$ under the same conditions. For a rich mixture, the oxidant mole fraction in the fuel/ air mixture decreases. This decrease in the oxidant molar fraction will be more effective when carbon dioxide is added.

5.2.5.3 Effect of Flow Rate:

The flame height shows a steady increase with the increase of flow rate in fuel/air mixtures but with a higher rate of increase than that mentioned in the previous cases. For example, the flame at ϕ =1 elongated, at 0% CO_2, by about 9 mm (from 26.8 to 35.8 mm) as a result of rising the mixture flow rate from 4 to 6 Lt/min. while the flame lengthened by about 16.2 mm (from 16.9 to 33.1 mm) if mixture flow rate increased from 2 to 4 Lt/min in the case of 10% CO2, see Fig. (5. 17).

Fig. (5. 19) shows a collocation of flame images at stoichiometry for LPG/air & LPG-CO_2/air mixtures for three different flow rates for each mixture. The figure indicates that LPG/air mixture diluted with CO_2 combustion could start at a lower flow rate as it compared with the not diluted mixture. Using CO_2 with LPG/air mixture give a taller flame for both the inner zone and the visible flame. Fig. (5. 19) endorses and confirms the results of Fig. (5. 17) & Fig. (5. 18). Also, the figure indicates that the flame aspect ratio is doubled increase when both flow rate and CO_2 dilution ratio are increased.

5.2.5.4 Effect of Flow Rate & ϕ on Flame Stability Limits:

Regarding to the flow rate range for stable flame, the addition of CO_2 enables the flame to overcome the flashback and begins at lower flow rates as

the fuel/ air mixture diluted with CO_2 has less flame speed. On the other hand, the flow rate of flame blowoff case declines if CO_2 added to the mixture. In other words, the addition of CO_2 to the mixture shifts the flow rates toward lower values as the dilution ratio increases, but in the aggregate, it increases the flow rate range by about 40% and 25% for ϕ = 1 and 1.2 respectively, see Fig. (5. 17) & Fig. (5. 18).

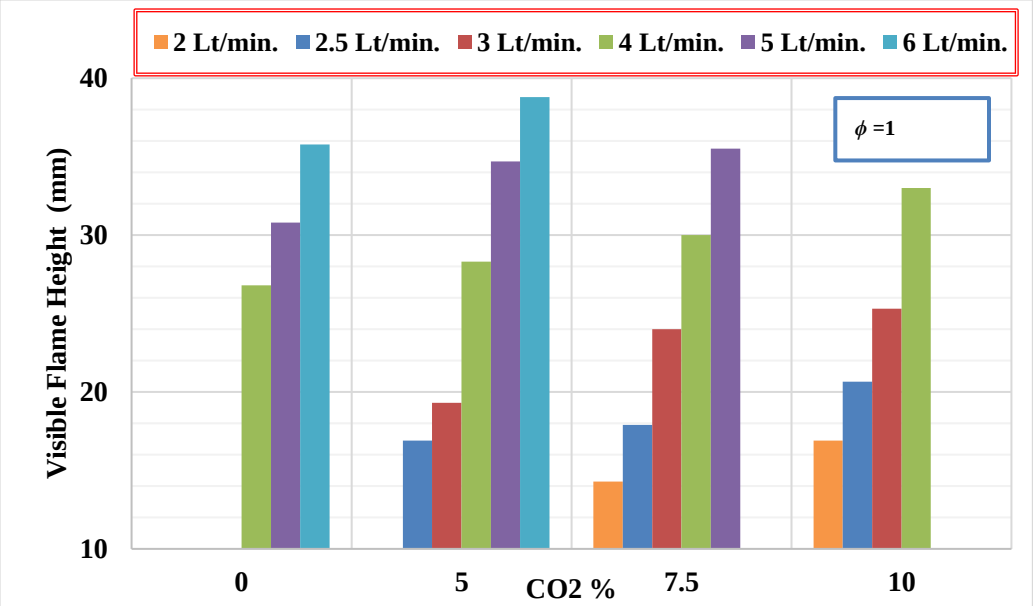

Fig. (5. 16) Flame height VS. CO_2% for stoichiometric (LPG-CO_2 /Air) mixture

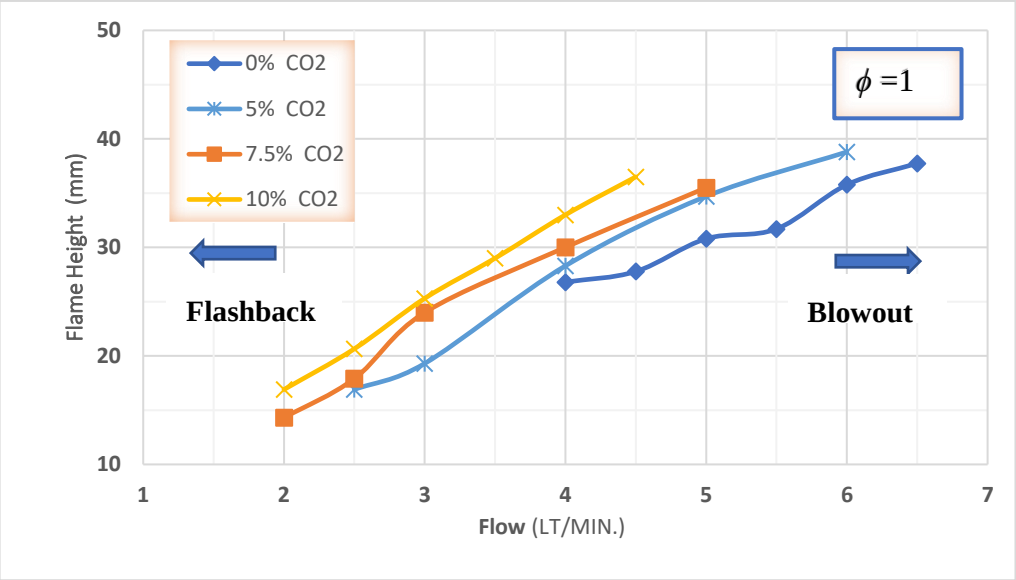

Fig. (5. 17) Effect of flow rate on visible flame height for (LPG-CO2 /Air) mixture at φ =1

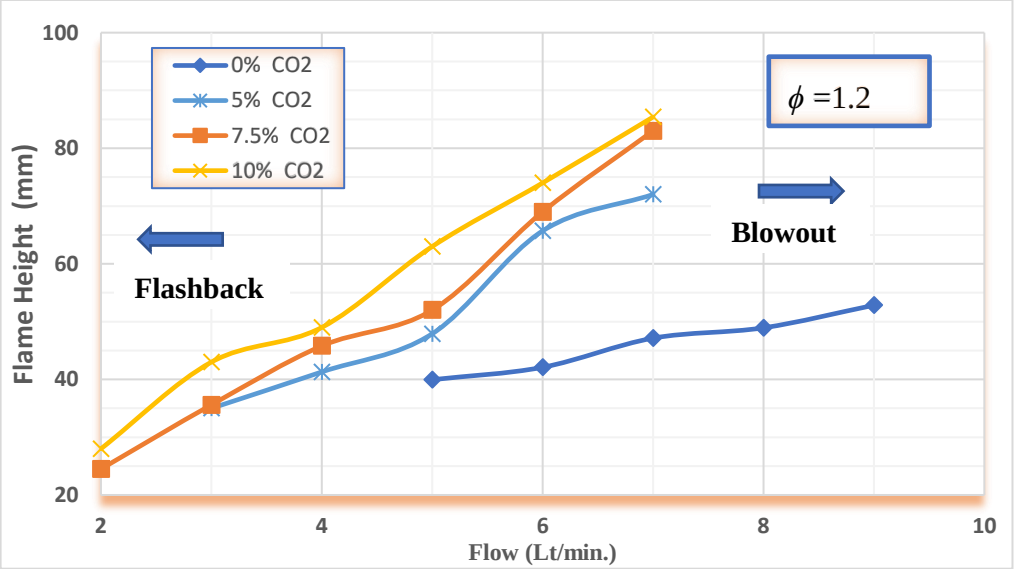

Fig. (5. 18) Effect of flow rate on visible flame height for (LPG-CO2 /Air) mixture at φ =1.2

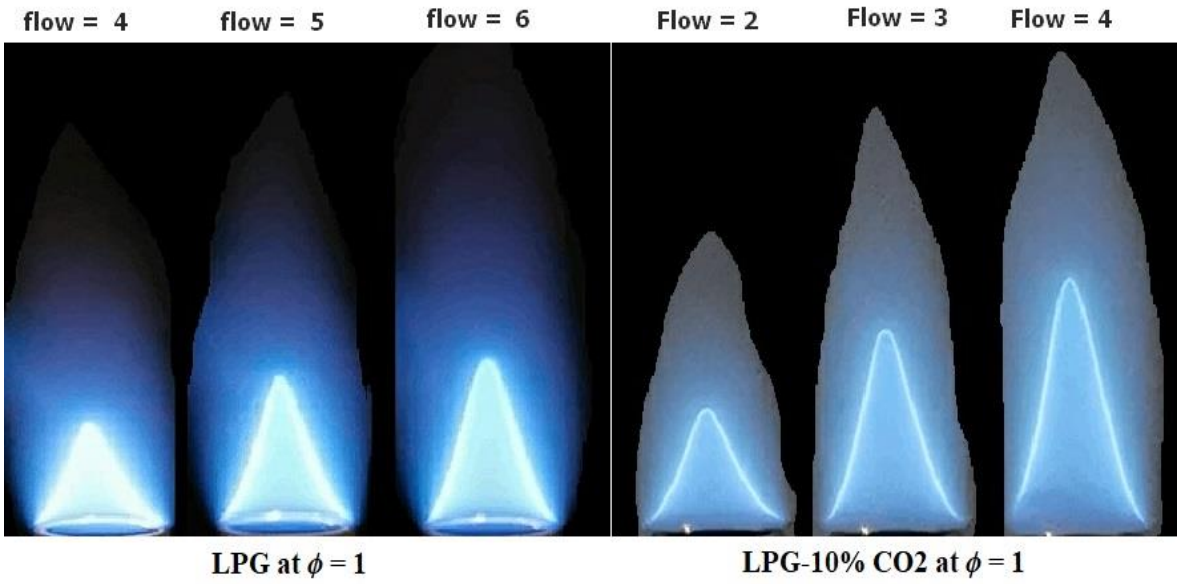

Fig. (5. 19) Photography comparison between LPG/air & LPG-CO2/air mixtures

5.2.6 Results of LPG- H_2 - CO_2/ air mixture:

In this section the LPG/air mixture is blended with H_2 and diluted with CO2 to test dual fuel/ air diluted mixture. The results involve the effect of H_2 blending ratio (0%, 10%, & 30%), CO_2 dilution ratio (0%, 5%, & 10%), equivalence ratio (1, & 1.2), as shown below:

5.2.6.1 Dual Effect of H_2 With CO_2:

Fig. (5. 20) & Fig. (5. 21) illustrate the results for the experiments of LPG/air mixtures diluted with carbon dioxide as well as blended with hydrogen. Fig. (5. 20) indicates the results for the stoichiometric mixture, and Fig. (5. 21) indicates the results for the fuel rich mixture and all are at 6 lt/min. The flame height augmented when CO_2 added while it shortened when H_2 added to the mixture. In this mixture, CO_2 is added to the mixture as a diluent gas instead of a part of the oxidant while H_2 is added to the mixture as a blended fuel instead of a part of LPG. As a result, the oxygen mole fraction decreases resulting in getting a taller flame while the diffusivity of the mixture

enhances and the chemical reaction rate increases resulting in getting a shorter flame.

The decline in flame height is obvious if 10% H_2 blended as it compared with the case of 0% H_2. This reduction keeps going when 30% added to the mixture but with a smaller percentage change than before. If it compared with the basic mixture, LPG/air, it is noticed that the mixture of LPG-5%CO_2-10%H_2 elongates the flame height with about 3% & 12% at ϕ = 1 & 1.2, respectively. On a related note, the effect of carbon dioxide in increasing the length of the flame is significantly more than the effect of hydrogen in decreasing it for the mixture of LPG-10%CO_2-30%H_2. The flame of the last mixture is longer than the basic LPG/air mixture with about 20% & 30% at ϕ = 1 & 1.2, respectively.

5.2.6.2 Effect of Equivalence Ratio:

Fig. (5. 20) & Fig. (5. 21) indicate that the flame height increases monotonically with respect to the equivalence ratio. For example, the flame height of the stoichiometric mixture (LPG-5%CO_2-10%H_2) increases by about 18.3 mm if the ϕ increases to 1.2. This increase becomes about 12.3 mm for the mixture of (LPG-10%CO_2-30%H_2) at ϕ =1.2 as it compared to the stoichiometric condition.

The increase in flame height with respect to CO_2 addition at ϕ = 1 continues in roughly the same manner for 5% and 10% CO_2 dilution ratio. At ϕ = 1.2 the flame elongated rapidly with a slight CO_2 addition and then the flame height increases a bit with more CO_2 addition.

Fig. (5. 22) gives a real comparison by images for the mixtures of LPG-5%CO_2-10%H_2, LPG-5%CO_2-30%H_2, LPG-10%CO_2-10%H_2, & LPG-10%CO_2-30%H_2 respectively. These pictures display the same details and results that appear in the Fig. (5. 20) & Fig. (5. 21).

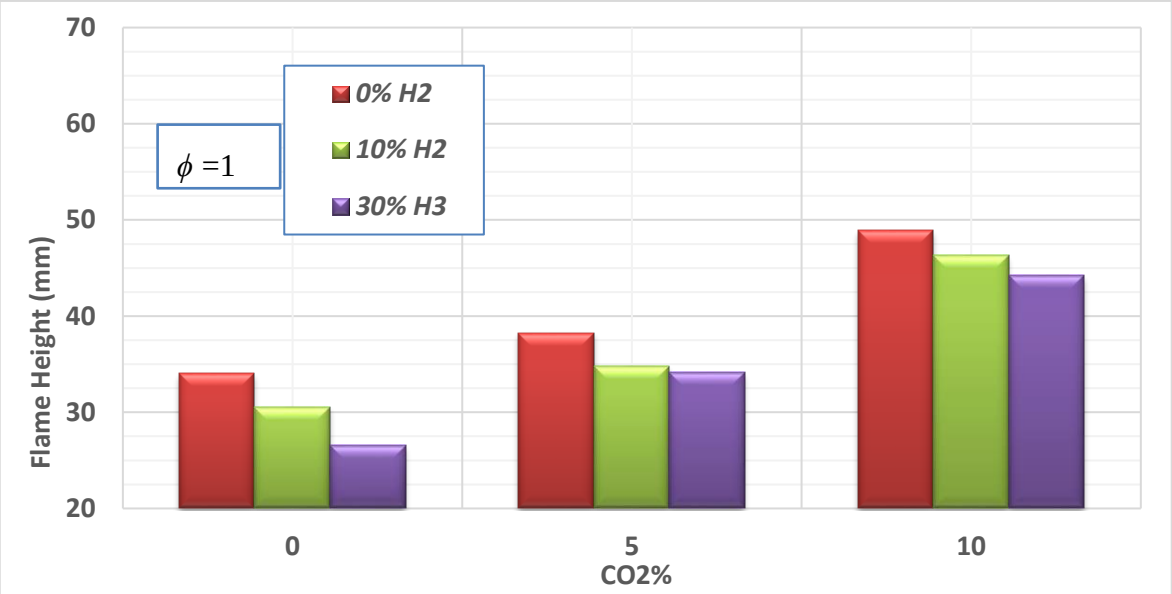

Fig. (5. 20) Visible flame height for (LPG-CO_2 /Air) mixture for different H_2 blending ratios at stoichiometric condition

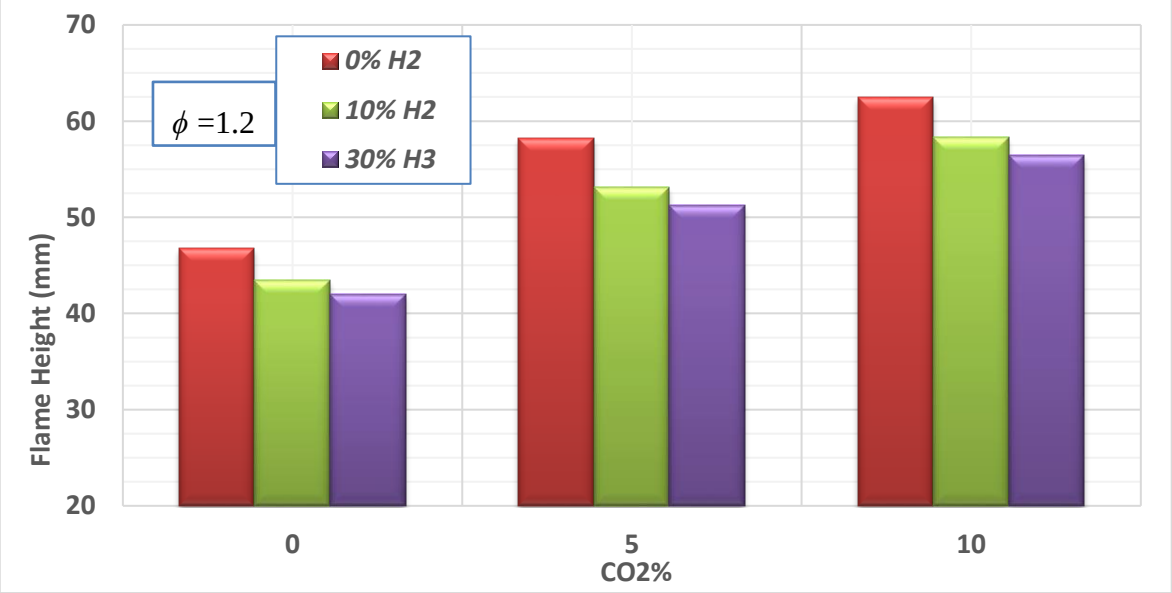

Fig. (5. 21) Visible flame height for (LPG-CO_2 /Air) mixture for different H_2 blending ratios at φ =1.2

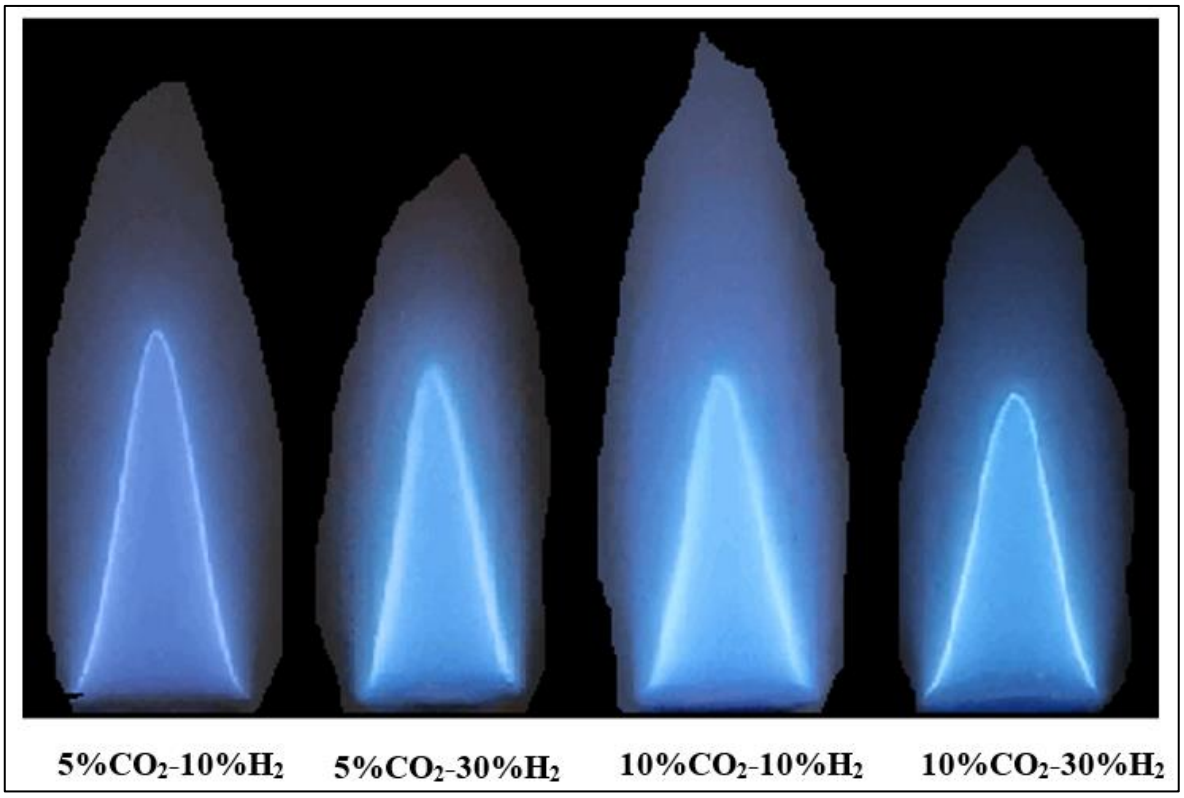

Fig. (5. 22) Flames photography for (dual fuel LPG-H_2)/air mixture- diluted with CO_2 at stoichiometric condition.

5.2.7 Results of the Swirling Burners:

The burners employed in the experimental rig are non-swirling and swirling burners of the same diameter and substance in order to evaluate the influence of the swirling flow.

Fig. (5. 24), Fig. (5. 25), & Fig. (5. 26) show the comparison for the effect of flow rate on measured flame height of LPG/air mixture between the swirling & the non- swirling burners for lean, stoichiometric, and rich mixtures respectively. The first matter these results show is that the length of flame extends with an increased Φ and/ or flow rate. On the other hand, it is also marked that with the same Φ and flow, the height of the flame is shortened when the swirling burner used. Generally, flame height shows slight reduction when decreasing the swirler number. These details seem clearer and more prominent for stoichiometric and rich mixtures. In the case of lean mixture, the difference is less as the length of the flame is generally short and the changes are not noticeably visible. Patel and Shah [43] reported similar effects of the swirling burner and Φ on the flame length.

For the swirling flame, the inner recirculation zone plays an important role in shortening the length of flame. The swirling air expands radially outwards due to the angle of vanes of the swirler. Because of this, the fuel and air particles flow tangentially under the centrifugal effect. This leads to the disintegration of the axial velocity of air-fuel mixture and results in the reduction of swirling flame height [43].

Regarding to flame stability and the limit between the flow rates that causing flame flashback and flame blowout, it could be concluded from Fig. (5. 25) & Fig. (5. 26) that the swirling burner of 0.78 swirl number shows better flame stability and enable the flame to overcome the flashback and starting with a lower flow rate. Besides, the flame blowout occurs at a higher flow rate as it compared with the non-swirling burner. Overall, the limit between the

flow rates which causing flame flashback and flame blowout increased to about 280% and 250% for the swirling burner of 0.78 swirl number when Φ =1 and 1.2 respectively as it compared to the non-swirling burner but with higher mixture consumption rate, see Fig. (5. 25) & Fig. (5. 26). The swirling burner of 9 vanes show the same trend but with lower flame height and lower flow rate limit as it compared with the swirling burner of 5 vanes. The abovementioned changes are shown inversely in the case of Φ =0.8, as the use of the swirling burner reduces this limit, as shown in Fig. (5. 24).

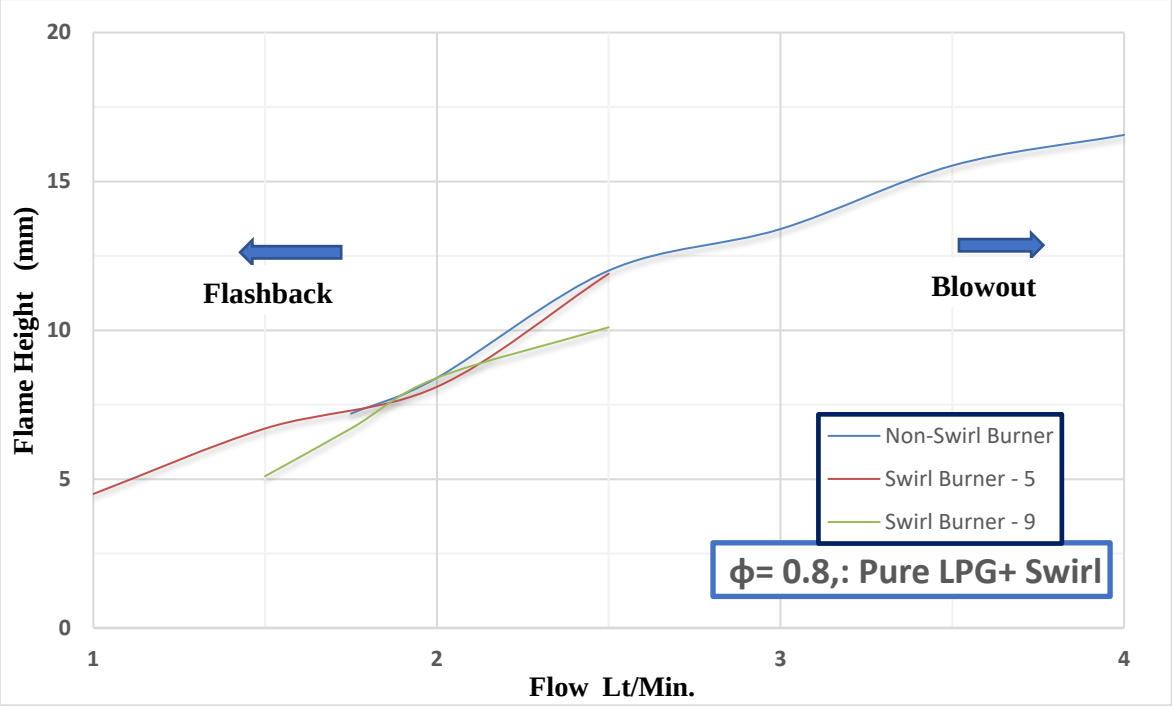

Fig. (5. 24) Effect of flow rate on measured flame height for swirling & non- swirling burners for LPG at $\phi = 0.8$

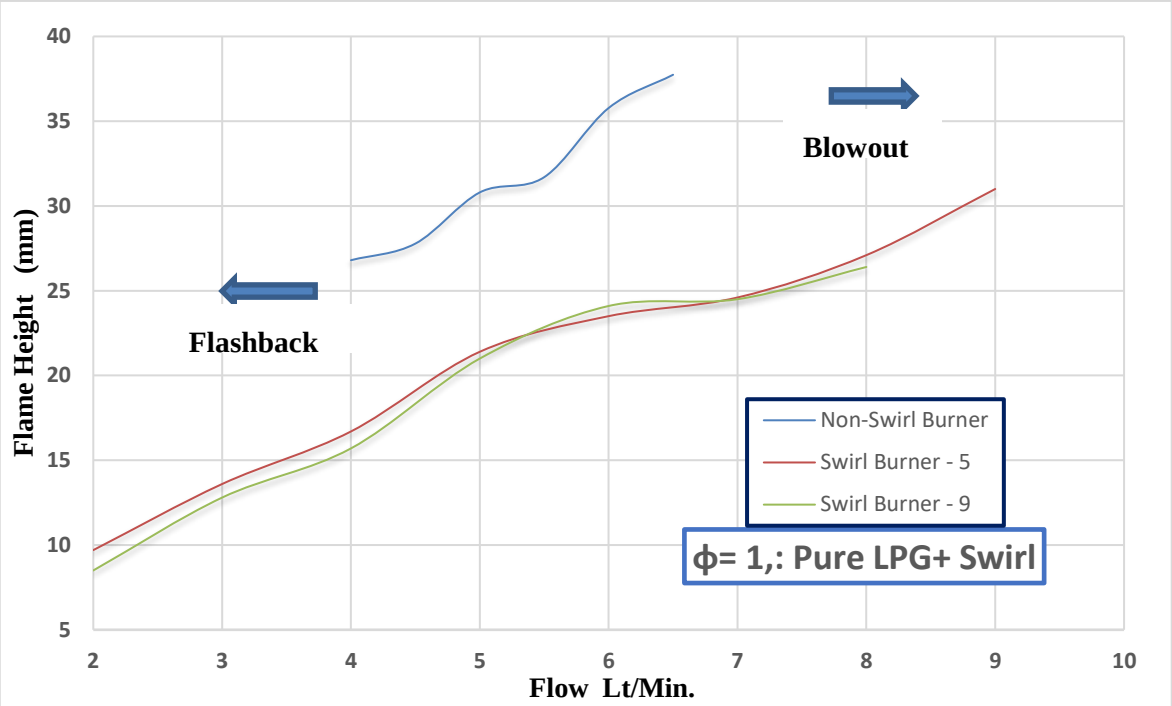

Fig. (5. 25) Effect of flow rate on measured flame height for swirling & non- swirling burners for LPG at $\phi = 1$

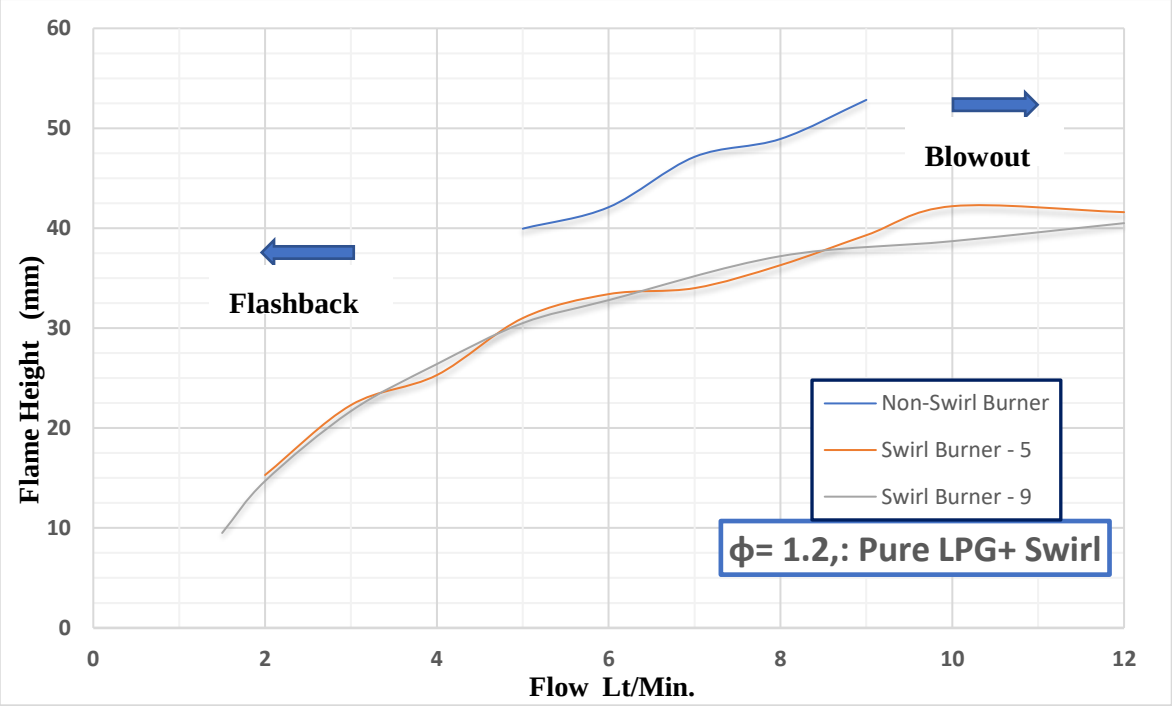

Fig. (5. 26) Effect of flow rate on measured flame height for swirling & non- swirling burners for LPG at $\phi = 1.2$

Fig. (5. 27) & Fig. (5. 28) show flame photography for the non-swirl and swirl burners of 5 vanes and 9 vanes at Φ =1 for LPG/air mixture. Fig. (5. 27) indicates that when using the swirling burner, flame's inner core is divided

into segments equals to the number of swirl vanes, and the flame shape is similar to a flower at lower flow rates. Also, a decrease in the flame length can be observed when using the swirling burner. This can attribute to the increase in the surface area of the flame and thus leads to a better mixing process and a greater entry of the required oxygen into the flame, so the reaction occurs faster and thus shortens the flame. On the contrary, when the flame does not take enough oxygen which needed for the chemical reaction, the flame forces to advance to a farther distance in order to complete the reaction and burn as much fuel as possible in the presence of the external oxygen.

Fig. (5. 28) show flame photography for the swirl burners of 5 vanes at Φ =1 for LPG/air mixture at different flow rates. The inner cone is consisted of five segments at lower flow rate. When the flow rate is increased to a higher level, it is noticed that the flame segments begin to merge with each other, as well as the flame inner zone merges with the outer zone so that the inner core of the flame is no longer clearly diagnosed.

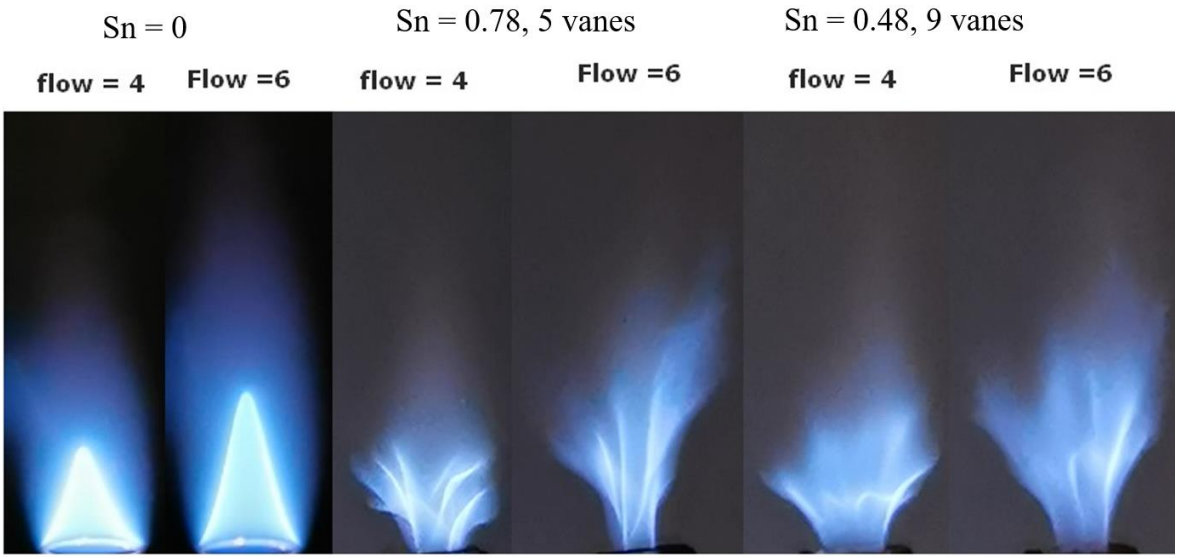

Fig. (5. 27) Flame photography comparison between swirl & non-swirl burners at Φ =1 LPG/air mixture

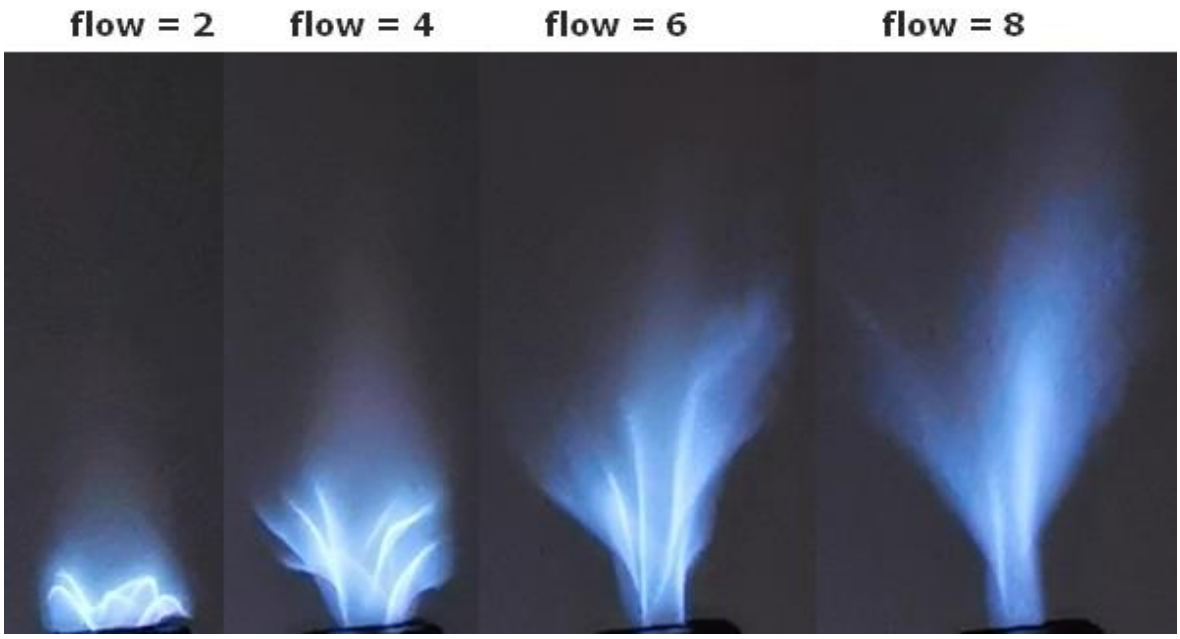

Fig. (5. 28) Flame photography for the swirl burner of 5 vanes at Φ =1 LPG/air mixture at different flow rates

5.2.8 Flame History

In order to track the process of the instantaneous formation of the flame, starting from spark ignition until the formation of the full flame and its stability, some experiments have been carried out for the LPG/air mixture for different equivalence ratios. Fig. (5. 29, 30, 31, & 32) show the series of flame history selected frames for LPG/air mixture at equivalence ratio of 0.8, 1, 1.2, & 1.4 respectively. These frames are obtained by the ultra-speed camera and then the recorded video has been converted to a series of frames using a special animation EZGIF programs. The figures also illustrate the real-time for each frame and for each equivalence ratio in a percent of a second.

All figures show that the flame starts its propagation from the position of ignition near the burner-tip, and then the flame begins to spread unsteadily until it reaches a state of stability and attached to the burner. Part of the fuel/ air mixture which already exists around the burner before the spark will initially burn and detached from the burner. The obvious change in the shape of the flame appears during this process, which forms the prominent part during the flame propagation process. Therefore, a larger number of frames

have been selected within this part of the videos. This process definitely varies according to the equivalence ratio. As the equivalence ratio increases, the time interval that this process takes will increase, in addition to the increase in the size of the part that will randomly burn and detach from the burner.

By comparing these four figures, it could be concluded that the higher equivalence ratio is the longer flame. On the other hand, as the equivalence ratio increases more pollution and soot will be produced. In addition, the number of frames of incomplete combustion increase and this incomplete combustion goes on until the last frame especially when equivalence ratio is 1.4.

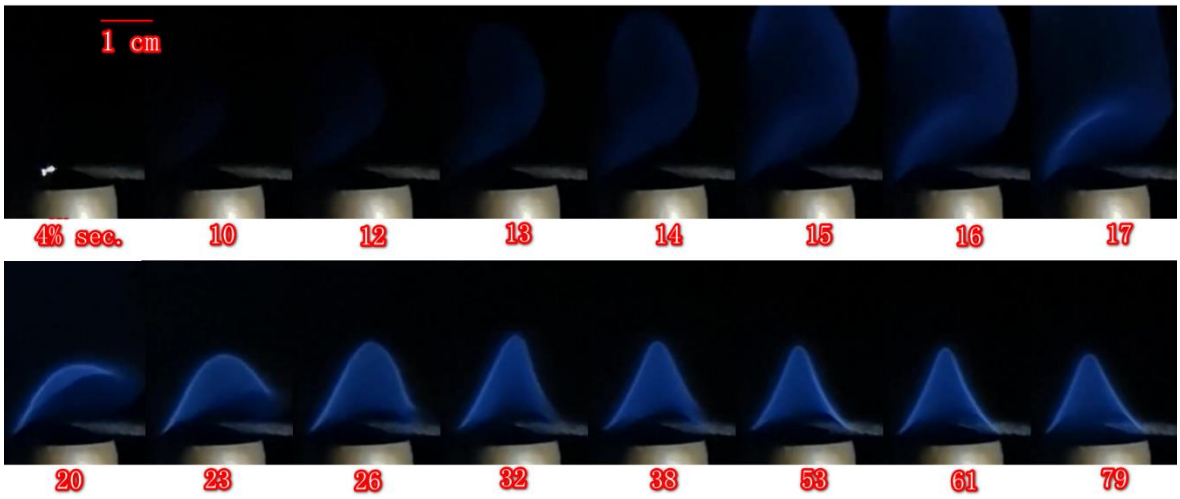

Fig. (5. 29) Series of frames for flame history for LPG/air mixture at ϕ=0.8

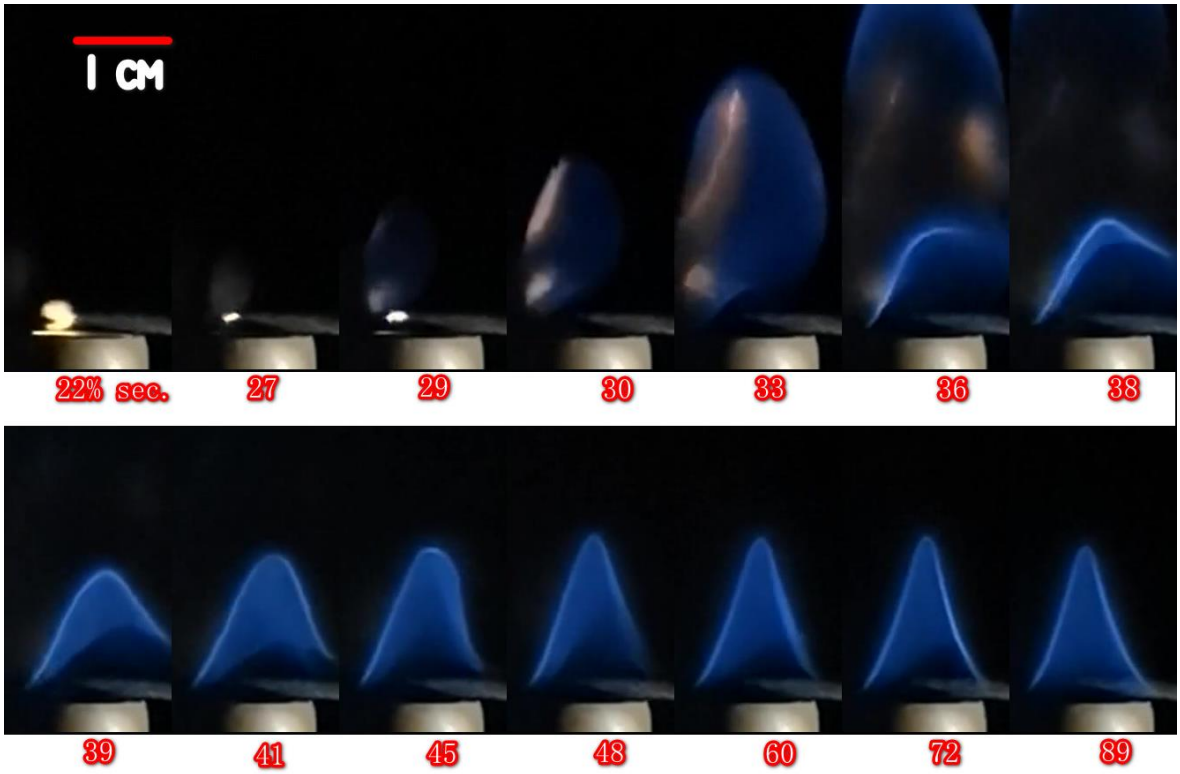

Fig. (5. 30) Series of frames for flame history for LPG/air mixture at ϕ=1

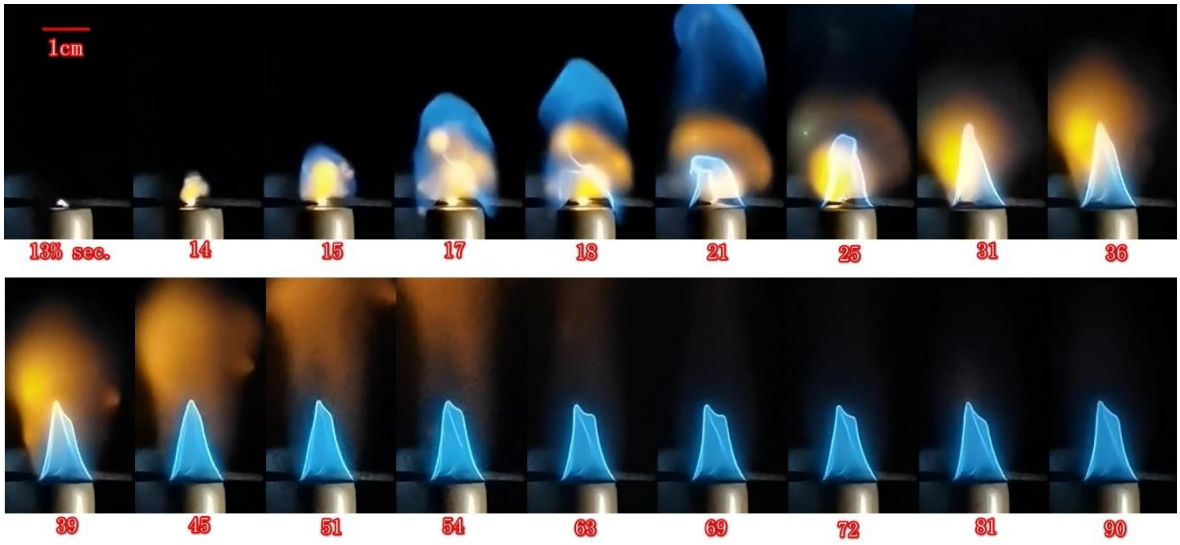

Fig. (5. 31) Series of frames for flame history for LPG/air mixture at ϕ=1.2

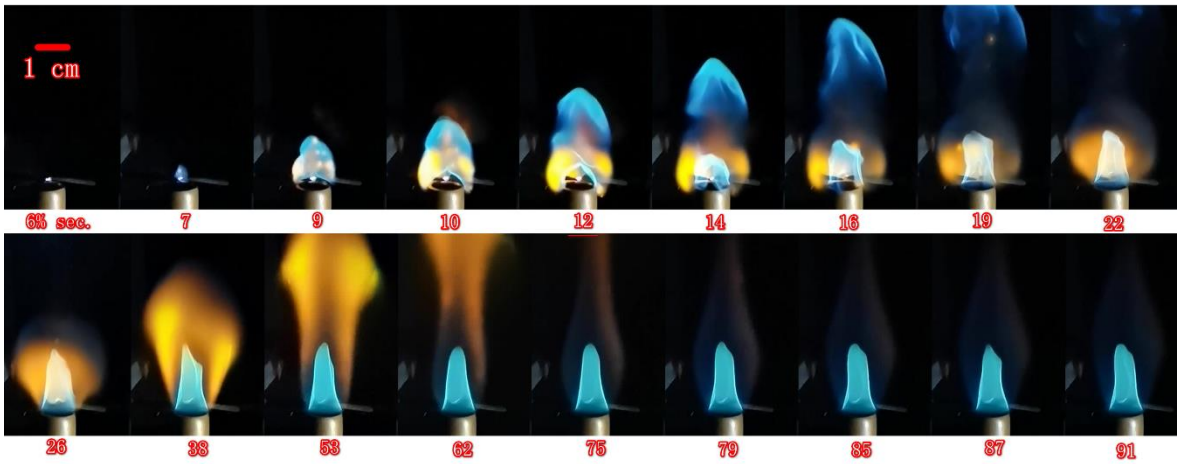

Fig. (5. 32) Series of frames for flame history for LPG/air mixture at ϕ=1.4

5.3 Results of the Numerical Work

5.3.1 Experimental Data Validation by Numerical Cases:

As shown in Table (5. 1) there are three different sets of simulations were performed in the current work. First, performing sets involved in studying are the effect of equivalence ratio ϕ using four values: 1, 1.2, 1.4, and 1.6 for the LPG/ air mixture all are at 6 Lt/min. The second sets of simulation relate the effect of changing the flow rate (mixture feeding velocity) is studied for stoichiometric LPG/ air mixture at five flow rate values: 4, 5, 6, 7, and 8 Lt/min. Finally, the effect of H_2 blending ratio is simulated with five cases: 0%, 5%, 20%, 40%, and 50% for LPG-H_2/ air mixture at stoichiometric conditions at 6 Lt/min.

All the simulations are performed using Intel® Xeon(R) CPU ES-2650 v3 @ 2.30 GH × 20 processors. Parallel computation was performed to accelerate the simulation using the OpenMPI tool.

Table (5. 1) Shows all the cases sets for the performed simulation in the current work

Case No.	ϕ	Reactants				Products					Notes	
		O_2	N_2	H_2 (k)	LPG (1-K)	CO2	N_2	H_2O	CO	O_2		
SET NO. 1 Effect of φ For *only LPG* 0%H2, Flow = (6 lt/min.)											Flow Rate=	
1	1	5.528	20.79	0	1	3.358	20.79	4.34	0	0	6 Lt/min	Exp. & Num.
2	1.2	4.60667	17.32			1.515	17.32	4.34	1.843	0		
3	1.4	3.94857	14.85			0.1991	14.85	4.34	3.159	0		
4	1.6	3.45	12.99			0.01	12.99	4.34	3.358	0		Num only
SET NO. 2 Effect of *Flow rate* For *only LPG* 0%H2, Const. φ= 1											Flow Rate (lt/min.)	
5	1	5.528	20.79	0	1	3.358	20.79	4.34	0	0	4	Exp. & Num.
6											5	
7											6	
8											7	Num. only
9											8	
SET NO. 3 Effect of H2 % For *LPG- H2 Blended* Flow = 6 lt/min. Const. ϕ= 1											H2 %	
10	1	5.528	20.79	0	1	3.358	20.79	4.34	0	0	0%	Exp. & Num.
11		5.2766	19.84	0.05	0.95	3.1901	19.84	4.173	0	0	5%	Num only
12		4.5224	17	0.2	0.8	2.686	17	3.672	0	0	20%	Exp. & Num.
13		3.5168	13.22	0.4	0.6	2.015	13.22	3.004	0	0	40%	
14		3.014	11.3326	0.5	0.5	1.679	11.3326	2.67	0	0	50%	Num only

5.3.2 Numerical Results of LPG/air Mixture:

Several simulations are conducted for the LPG/air mixture to investigate the effect of equivalence ratio and the effect of the low rate. Below are the results for these two parameters on the combustion and flame characteristics:

5.3.2.1 Effect of Equivalence Ratio:

In this simulation, five cases for the combustion of the LPG/air mixture were carried out for five different equivalence ratios namely 0.8, 1, 1.2, 1.4, and 1.6 all at 6 Lt/min. using OpenFOAM code. Below are the results of these simulations:

Fig. (5. 33) shows temperature distribution contours for the combustion simulation of LPG/air mixture for different equivalence ratio at 6 Lt/min. It is

noticed that the higher temperature is for the stoichiometric mixture. The temperature tends to decrease monotonically when the equivalence ratio moves away from unity and in the both sides, lean and rich. The figure indicates that the length of the preheated zone increases with equivalence ratio. The temperature increases along the flame center line as the mixture is heated in the preheat zone and the combustion starts. The temperature reaches its maximum value in the stoichiometric zone along the flame (reaction zone) and drops further downstream.

On the other hand, the flame height increases and reaches further points by increasing the equivalence ratio. As the equivalence ratio getting close to unity, the complete combustion will take place and thus, the biggest possible amount of the fuel/air mixture will burn, producing the greater heat release through a shorter distance as it compared with those values in the case of other equivalence ratios more than unity. It is noted that the temperature ranges between 300 and 2400K at the stoichiometric mixture. These temperature ranges descend towards 1700K when ϕ = 1.6 see Fig. (5. 33). The temperature for the lean side , ϕ = 0.8, is higher than that of the rich side, ϕ = 1.2.

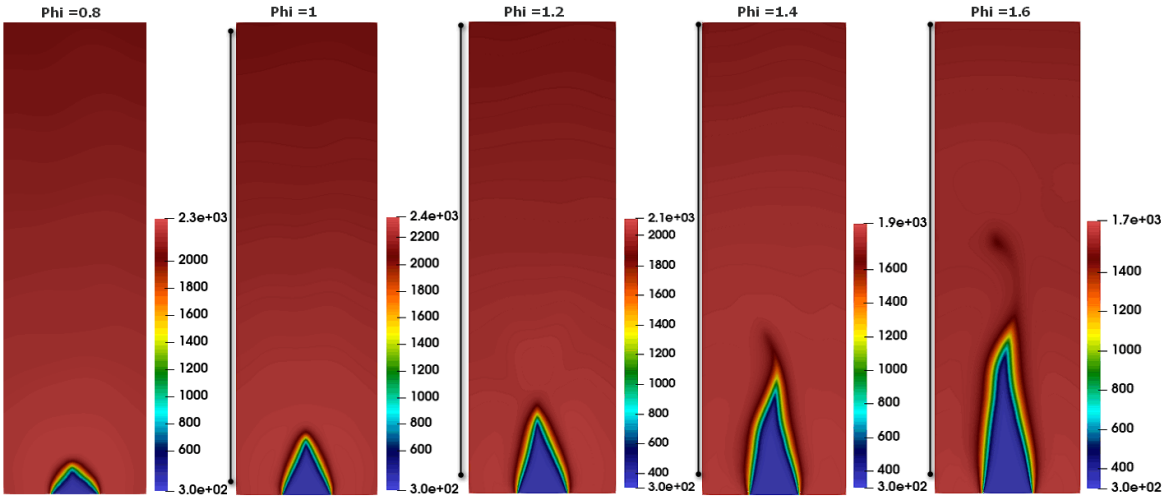

Fig. (5. 33) Temperature distribution contours for the effect of equivalence ratio (LPG/air mixture) at 6 Lt/min.

Fig. (5. 34) shows the temperature distribution results along the flame center line for different equivalence ratios. The higher temperature values

appear at stoichiometric condition and decrease for the lean and/ or rich mixture. The temperature rises with a rate of change that is very rapid in the reaction zone, and then the temperature begins to decrease monotonically with a lower rate of change as when moving away from flame tip. The figure also reveals that the reduction in the temperature after the reaction zone is not identical for the different equivalence ratios. For a higher equivalence ratio, this drop will be less valuable. This can be explained by two reasons: the first is that the higher equivalence ratio produces longer flame which means that the remaining distance between flame region and the end of the computational domain is less and so this drop does not appear complete. The second reason is that the temperature values are generally less for a higher equivalence ratio and therefore the decreasing value is lower. Comparing the curve for $\phi = 0.8$ with rich mixture curves, it is clear that its temperature is less than that for stoichiometric conditions but higher than that when $\phi > 1$. On the other hand, this curve reaches its maximum value in short distance before the other cuvres which give another indication that the flame is shorter for a lower equivalence ratio.

The flame had been divided by Karaminejad et. al. 2018 [98] into three zones: the preheat zone, the reaction zone, and the equilibrium zone. Heat transfer from hot products heats reactants to ignition temperature in the preheat zone. It is chemically inert, and no considerable heat is produced. Chain-branching reactions that keep the reaction going are begun in the reaction zone. This layer consumes all of the fuel and releases the majority of the heat. All species achieve their equilibrium states without significant heat release in the equilibrium zone.

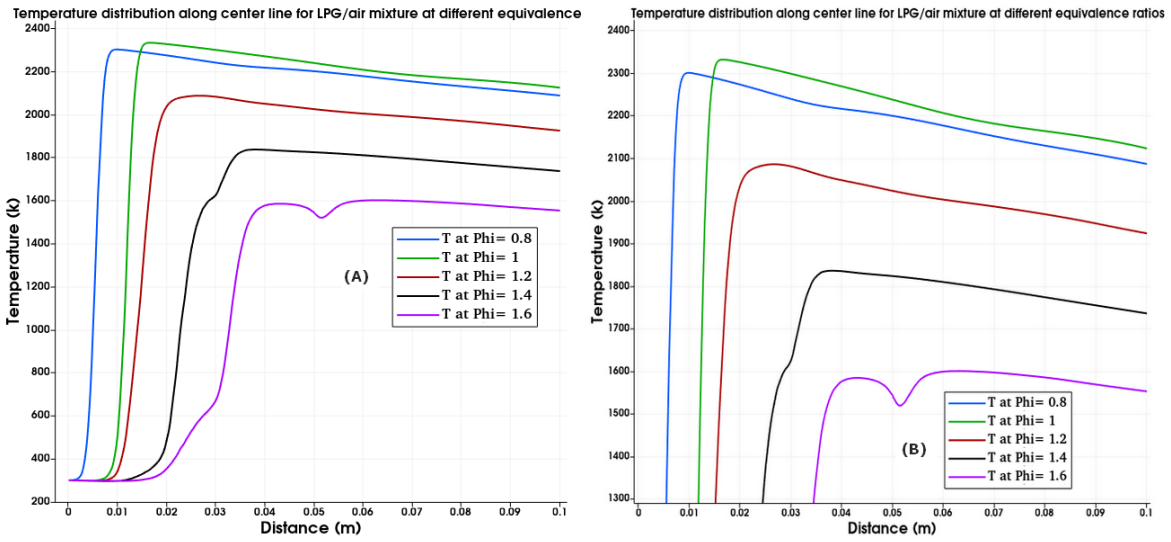

Fig. (5. 34) Predicted temperature distribution along the center line for LPG/air mixture with different equivalence ratios: A) full curves view, & B) zoomed view.

Fig. (5. 35) show the temperature distribution results across different cross sections above burner tip for LPG/air mixture with different equivalence ratios. It is noticed that minimum temperature occurs at the flame center line where the preheat zone is located. The temperature is maximum at the flame periphery where the reaction takes place see figures A & B. This trend is also observed in Fig. (5. 34). Another matter could be observed through figures C, D, & E. The deviation in temperature values becomes less at a longer distance above the burner tip away from the reaction zone especially when ϕ = 0.8, 1& 1.2 when the flame and its reaction zone are shorter. When going further downstream, the temperature at the flame center line region becomes little higher than that at flame periphery when ϕ = 0.8, 1& 1.2, see & Fig. (5. 36) & Fig. (5. 37). This belongs to the effect of the maximum temperature at the center line in the reaction zone few millimeters below these points. The asymmetry in some values sometimes on both sides of the axial axes is due to that the computational domain is not carried out symmetrically.

Fig. (5. 36) shows the predicted temperature distribution at ϕ =0.8 & 1 at 20 mm above the burner tip, i.e., outside the flame region. The figure indicates that the temperature distributes in a parabolic shape outside of the flame and it is at its maximum at center line while it tends to decrease towards

the flame periphery. This result is repeated in Fig. (5. 37) at ϕ = 0.8, 1 & 1.2 at 30 mm above the burner tip and the temperature values for stoichiometry are higher than that for the other.

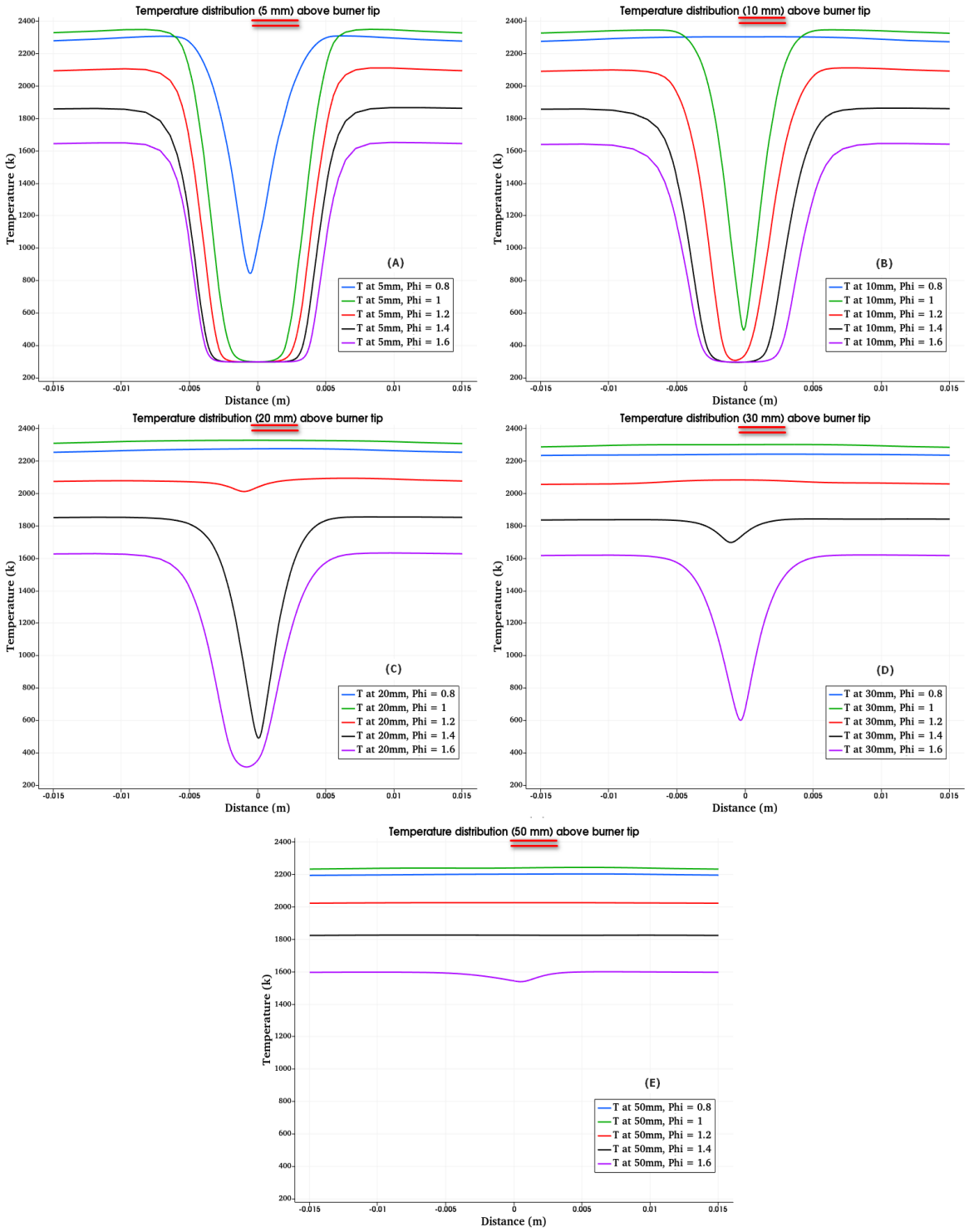

Fig. (5. 35) Predicted temperature distribution at different distances over burner tip for LPG/air mixture with different equivalence ratios

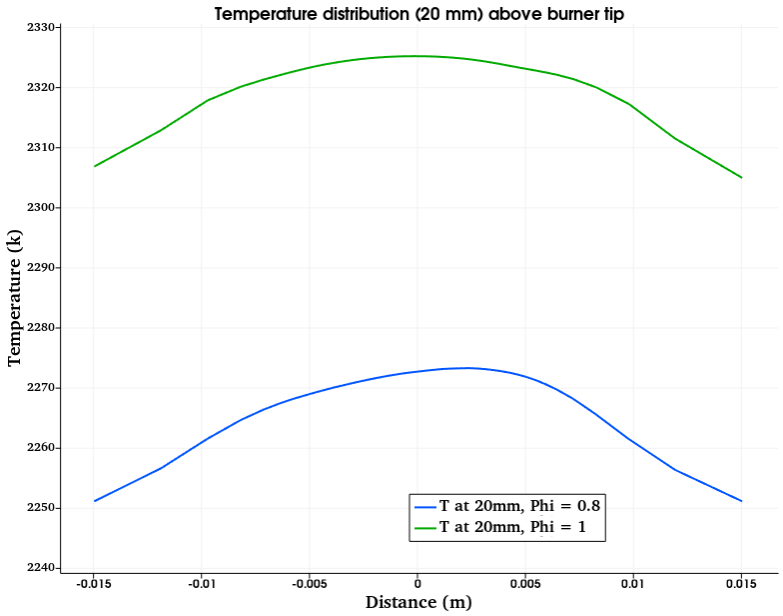

Fig. (5. 36) Predicted axial temperature distribution above the flame tip at ϕ =0.8 & 1

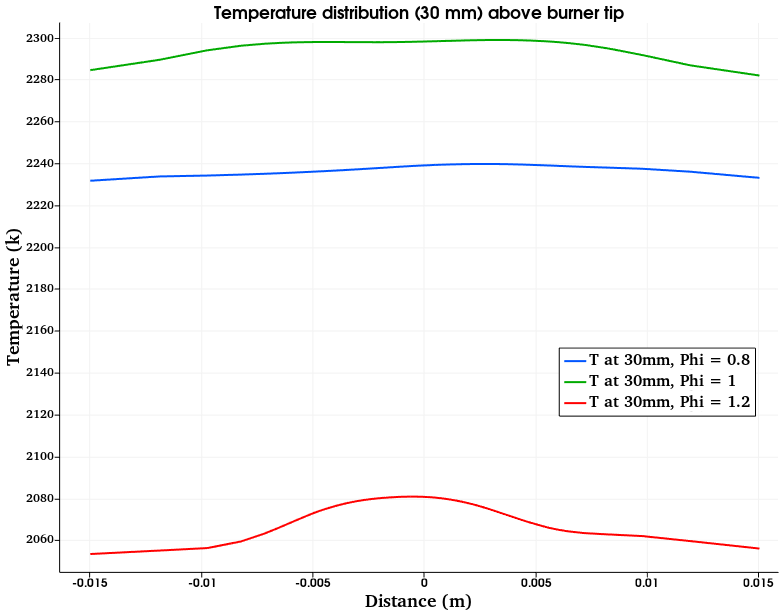

Fig. (5. 37) Predicted axial temperature distribution after flame region at ϕ =0.8 & 1 & 1.2

Fig. (5. 38) shows the variation of inner zone length predicted by OpenFOAM with equivalence ratio. It shown that flame height increases with equivalence ratio. The rich mixture getting longer flame since the fuel needs to move further downstream to get the required quantity of air for combustion. There is in an agreement with the experimental findings for the inner zone region.

The distribution of progress variable (C) along center line is shown in Fig. (5. 39) for different equivalence ratios. The progress Variable had been defined by [90] & [67] as a variable describes the thermochemical state of the mixture and combustion at any point in space and time (products and reactants). This variable is confined between zero and unity, if c = 0 represents the reactants (unburned state) while if c = 1 represents the products (burned state). This variable can be used to represent the flame progression process. The reaction takes place slowly & directly above burner tip and then the reaction will take its turn and intensify where the largest proportion of the fuel/air mixture will begin to burn and turn into products and the progress variable values are close to one. After that the progress variable will be in a relative balance. It is noticed that curves of $\phi = 1.4$ & 1.6 are located below the other curves. This is belonged to the access fuel in the rich mixtures which are not burnt completely leading to a decrease in the values of variable C. It is also noticed that the curves shifted to higher distance throughout the domain as equivalence ratio increases. This is what supports that the flame height increases as a result of equivalence ratio increase as the chemical reaction needs a long path to consume the fuel rich mixture. When looking at the length of reaction zone up to progress variable, Fig. (5. 39), it is noticed that this length is little less than that shown in Fig. (5. 38). This difference belongs to that the progress variable is related to the chemical reaction and it shows the flame location where the mean mixture fraction on the flame axis is at a stoichiometric value which less than the length shown in Fig. (5. 38) which predicted up to maximum temperature along the flame center line. R. T. Stephen [11] stated that the flame height based on temperature tends to be larger than those based on concentration measurements.

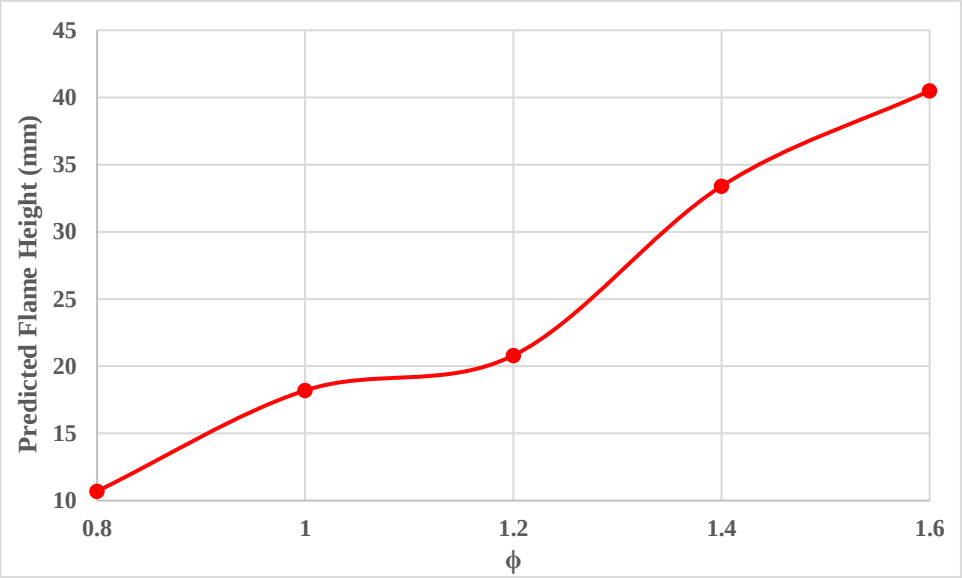

Fig. (5. 38) predicted flame height for the inner zone by OpenFOAM for LPG/air mixture

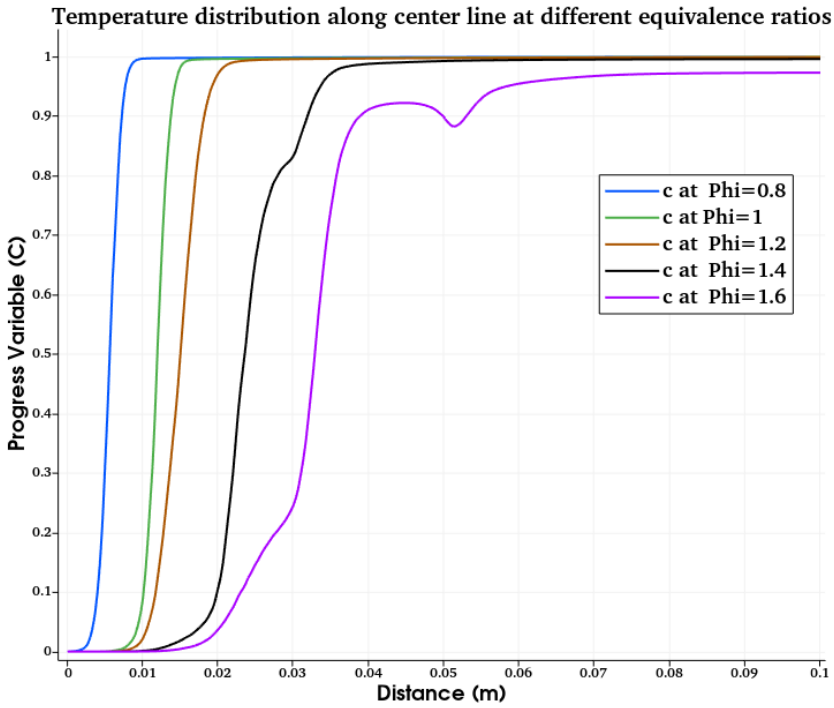

Fig. (5. 39) Distribution of progress variable (C) along center line for different equivalence ratios for LPG/air mixture

5.3.2.2 Effect of Flow Rate:

In this simulation, five cases were carried out for the combustion of the stoichiometric LPG/air mixture with five different mixture flow rates of 4, 5, 6, 7, and 8 Lt/min. using OpenFOAM software. Below are the results of these simulations:

Fig. (5. 40) shows the temperature distribution contours for the combustion simulation of stoichiometric LPG/air mixture at different flow rates. It is noticeable that the higher the flow rate the taller flame. On the other hand, the higher the flow the larger flame aspect ratio. These results are similar to those results obtained experimentally. This is another validation for the present code.

Fig. (5. 41) shows the temperature distribution along the center line for different flow rates. As flow rate increases, the maximum flame temperature decreases and the point of the maximum temperature moves further downstream. Along the center line, the flame temperature increases slightly in the preheated zone and then its increases sharply and rapidly after its decreases monotonically further downstream above the flame region. The reduction in flame temperature after the flame region is affected by the height of the flame associated with the flow rate. For a lower flow rate the maximum temperature is higher but the flame is shorter, hence the temperature reduction starts previously leading to make the temperature for the lower flow rate is less than that of higher flow rate in downstream regions.

The predicted inner zone length of the flame is shown in Fig. (5. 42) for different flow rates. The higher the flow rate the longer flame inner zone. These results agreed with that obtained by [42] & [27]. The rate of increase in flame height becomes smaller at higher flow rates. Overall, the results of this figure reveals that the average of the rate of increase in flame inner zone height is about 17% per each 1 Lt/min. increment of flow rate.

Fig. (5. 43) shows progress variable (C) distribution along center line at different flow rates for LPG/air mixture. The curves of progress variable shifted to longer distance throughout the domain when flow rate increases. This is what supports that the flame height increases as a result of increasing the flow rate. The values of the progress variable do not vary dramatically when flow rate changed.

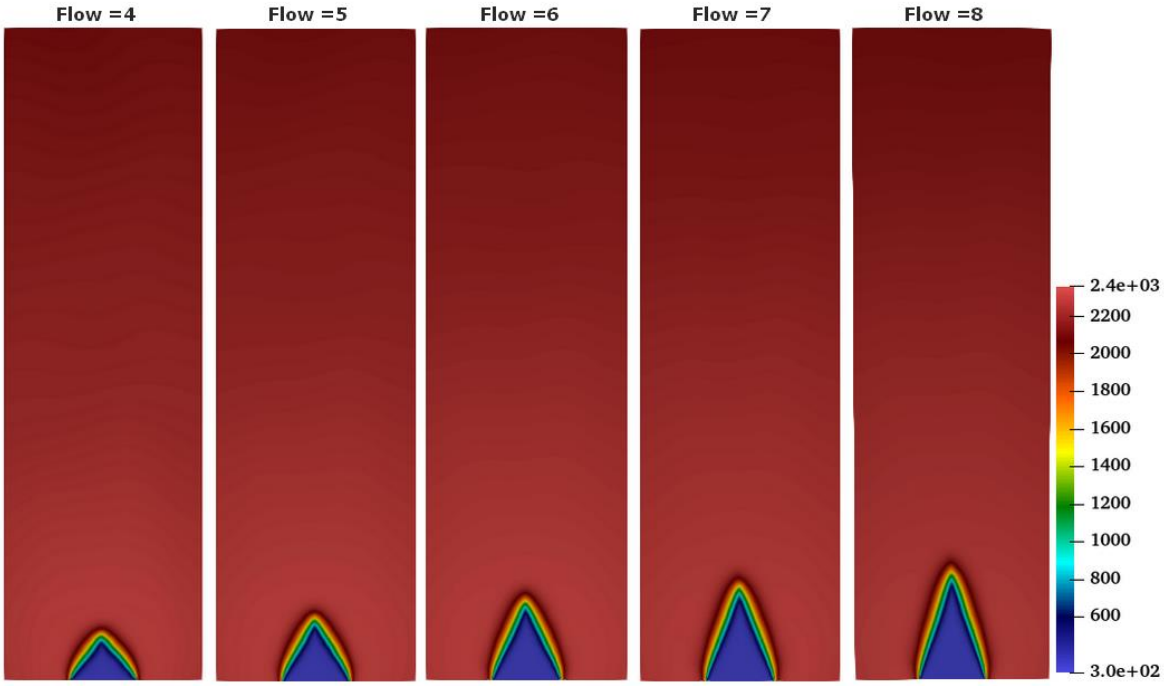

Fig. (5. 40) Temperature distribution contours for the stoichiometric LPG/air mixture at different flow rates

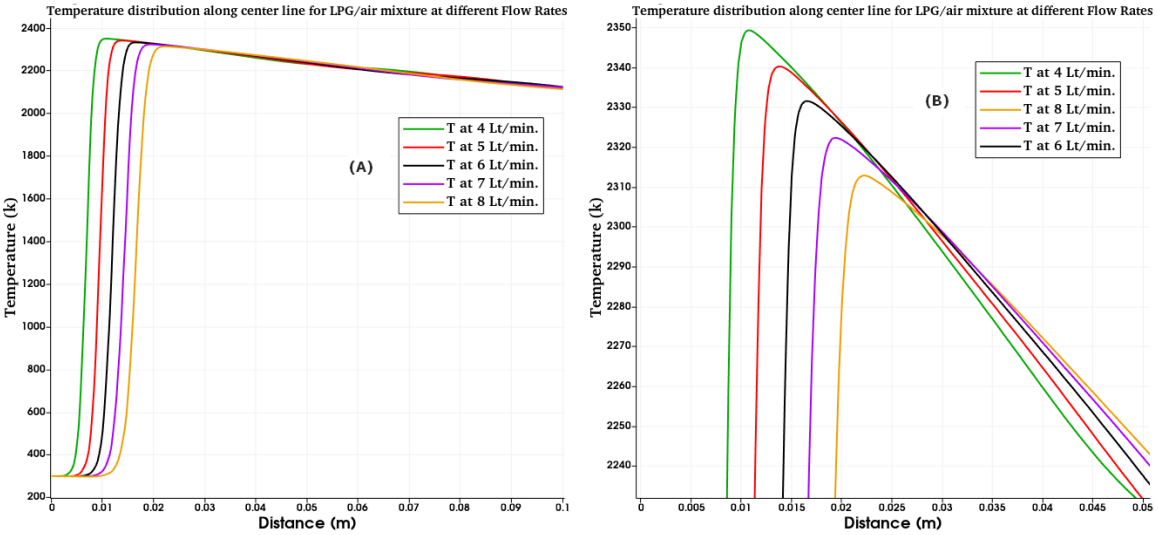

Fig. (5. 41) Predicted temperature distribution along the center line for stoichiometric LPG/air mixture at different low rates: A) full curves view, & B) zoomed view.

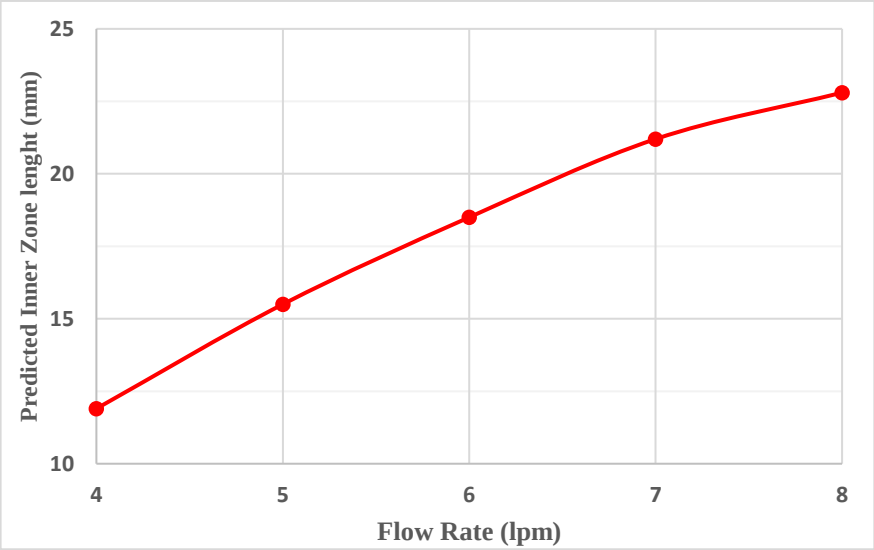

Fig. (5. 42) predicted flame height for the inner zone at different flow rates for the stoichiometric LPG/air mixture

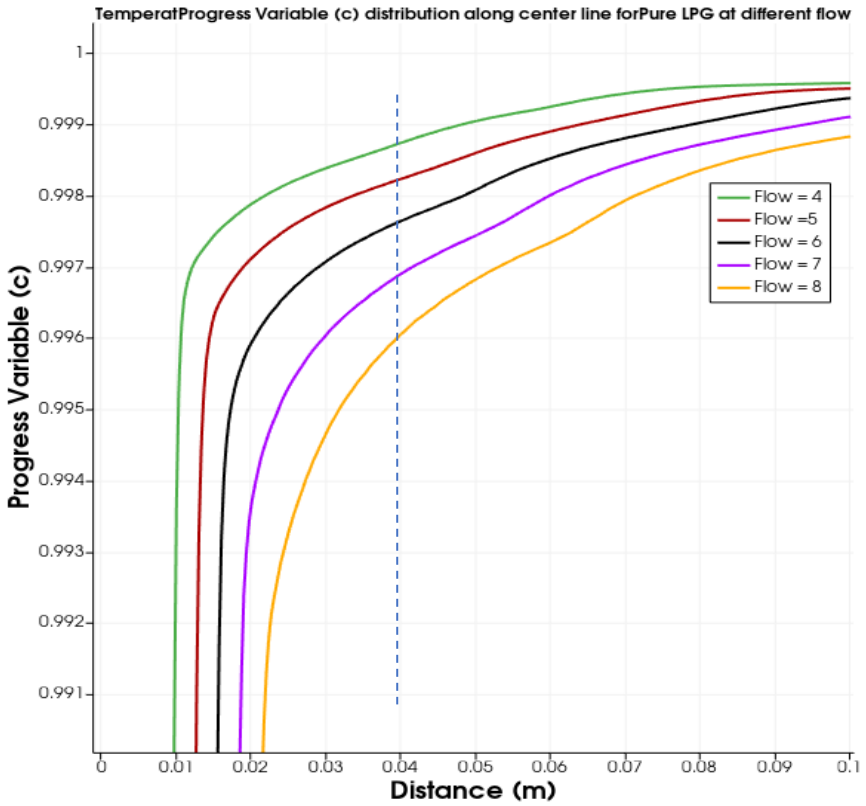

Fig. (5. 43) Progress variable (C) distribution along center line at different flow rates for stoichiometric LPG/air mixture

5.3.3 Numerical Results of LPG-H_2 Mixture, Effect of H_2%:

In this simulation, the combustion of the LPG/air mixture blended with hydrogen are carried out for stoichiometric condition at 6 Lt/min. using OpenFOAM code. Five different H_2 blending ratios: 0%, 5%, 20%, 40%, and 50% are studied. Below are the results of these simulations:

Fig. (5. 44) shows the temperature distribution contours for the combustion simulation of LPG-H_2/air mixture at different hydrogen blending ratios. The addition of H_2 in the fuel/air mixture affects flame height inversely. As H_2 percentage increase the length of the flame decreases monotonically. Furthermore, the higher the hydrogen blending ratio, the smaller is the flame aspect ratio. This is due to the higher flame speed of H_2 and the large H_2 diffusivity.

Fig. (5. 45) shows the temperature distribution along the center line for LPG-H_2/air mixture with different hydrogen blending ratio. It noticed that, as the hydrogen blending ratio increases the flame maximum temperature increases a bit to since more heat is liberated which is due to the higher hydrogen heating value see figure b. This result is agreed with that presented by [25]

The predicted flame inner zone for the LPG-H_2/air mixture is shown in Fig. (5. 46). The length of flame inner zone decreases as a result of hydrogen addition to the fuel/ air mixture. This is agreement with the findings obtained by [24], [102]. The rate of inner zone reduction with respect to hydrogen addition becomes smaller for higher H_2 blending. If 5% hydrogen is blended with the fuel/ air mixture, the inner zone length decreases by about 10% while for 50% H_2 blending ratio the length of the inner zone shortened by about 16%. J. Miao et. al. 2019 [27] indicated that for 50% addition of H_2 contributed about 14% reduction in flame length.

Fig. (5. 47) shows the progress variable (C) distribution along center line for LPG-H_2/air mixture at different blending ratios. It is noticeable that the rates of products formation represented by the progress variable are something increased as a result of H_2 addition. It is also notice that the addition of hydrogen shifted the towards the burner tip which give another indication that the addition of hydrogen shortened the flame.

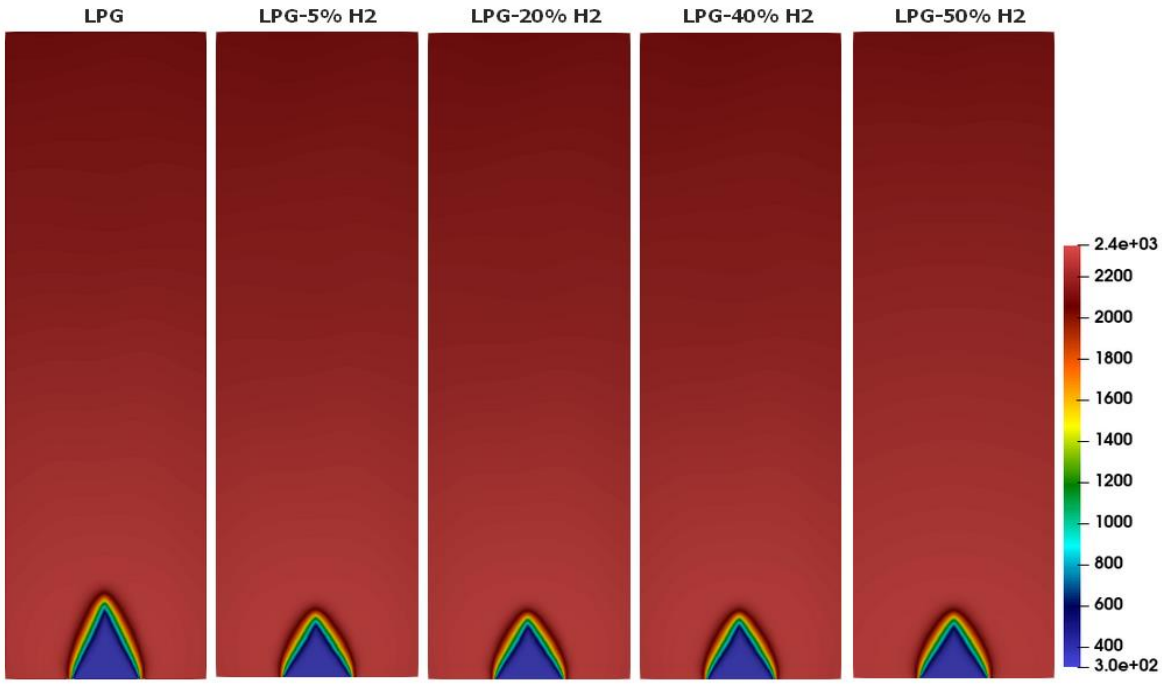

Fig. (5. 44) Temperature distribution contours for stoichiometric LPG-H_2/air mixture at different H_2 blending ratio at 6 Lt/min.

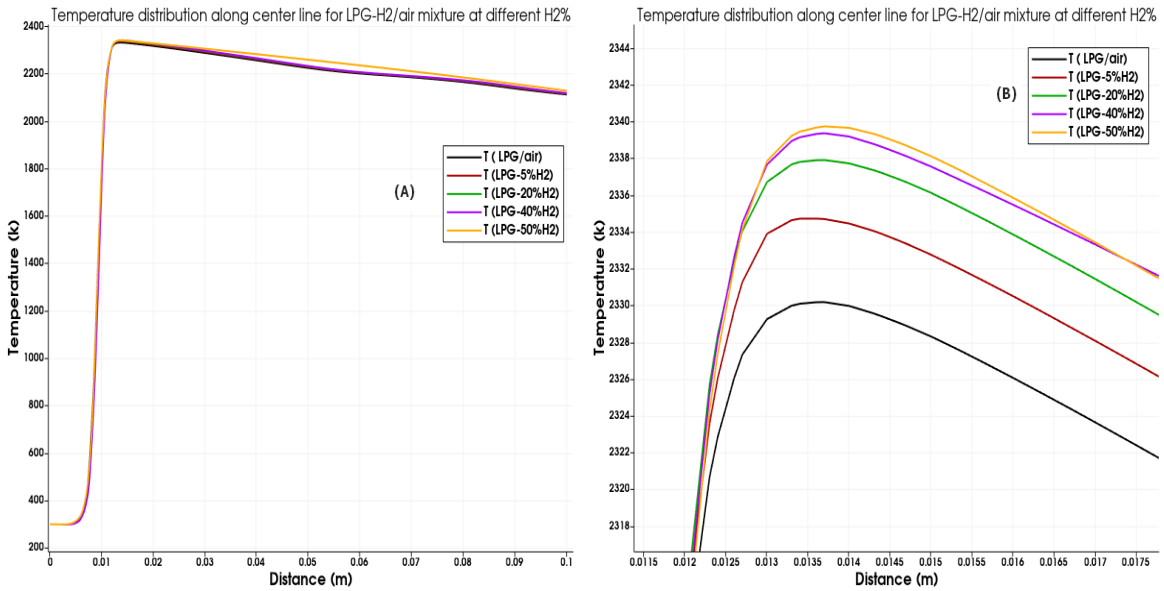

Fig. (5. 45) Predicted temperature distribution along the center line for stoichiometric LPG-H_2/air mixture at different H_2 blending ratio at 6 Lt/min. a) full view & b) zoomed view

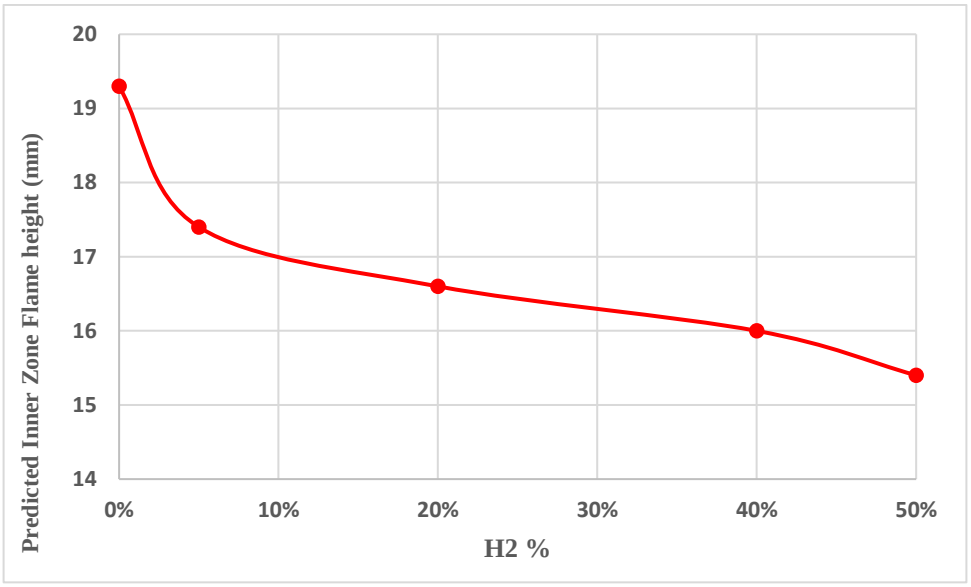

Fig. (5. 46) Predicted flame height for the inner zone by OpenFOAM simulations set No. 3, LPG-H_2/ air mixture

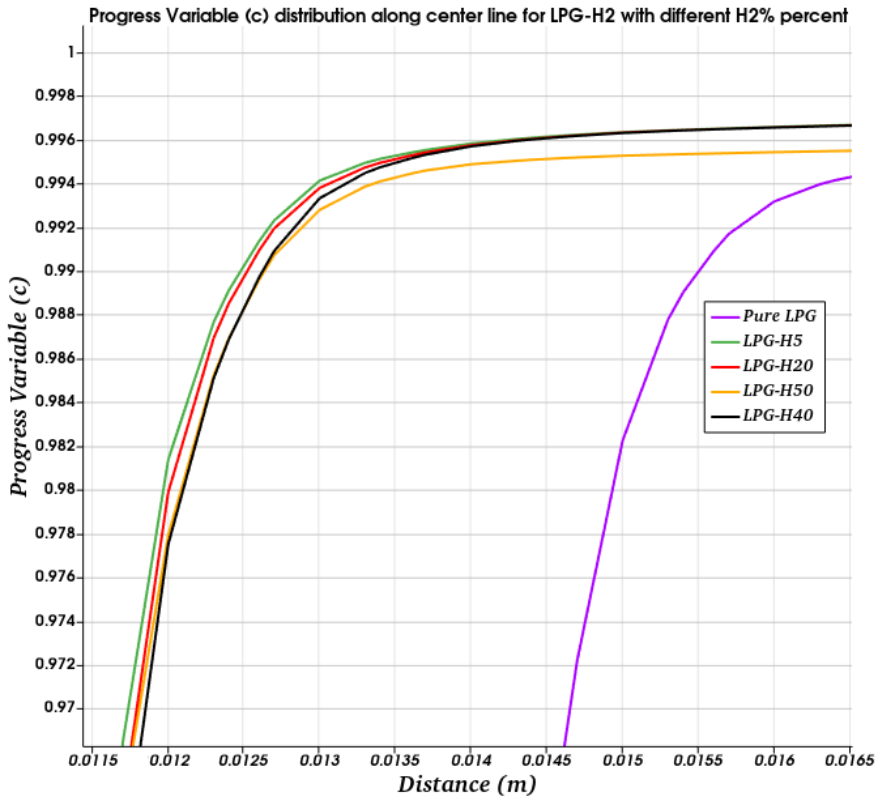

Fig. (5. 47) Progress variable (C) distribution along center line for LPG-H_2/air mixture at different blending ratio

5.3.4 Numerical Results for pollutants Formation:

In addition to the analysis of flame characteristics that presented in section 5.3, the present CFD simulations involve the prediction of the combustion species (O_2, fuel, CO_2, CO) formation both quantitatively and qualitatively as presented below:

5.3.4.1 Effect of Equivalence Ratio:

The effect of equivalence ratio on the combustion species formation is investigated for LPG/air mixture at 6 Lt/min. Mole fraction of species (O_2, fuel, CO_2, CO) predicted along the center line (in meters) are shown in Fig. (5. 48). This figure indicates the following details:

The curves of mole fraction move further downstream for all species as the equivalence ratio increases. These changes are agreed with that shown in Fig. (5. 34) for the temperature distribution along the center line. This is due to the growing fuel amount when the equivalence ratio increases which make the chemical reaction continues for a longer distance throughout the flame center line. This is another indication for the fact that flame height increases as the equivalence ratio increases.

It is concluded that the mole fraction (for all species and at any equivalence ratio Figure A, B, C, D, or E) starts to change at a slight rate in the first 10-25 mm above the burner tip, this change is hardly noticeable. Then the values change rapidly in the next few millimeters. After this rapid change, the values of mole fraction will approximately remain constant within the same values at each equivalence ratio. On the other hand, the distance which these changes take place will extends as the equivalence ratio increases and this is the same notice that mentioned in the above paragraph. This difference in the rate of change of mole fraction means that the flame chemical reactions could be divided into three zones: the preheated zone, the reaction zone and the equilibrium zone according to the rates of change, which are mentioned above.

This could be considered as another validation for the present numerical code as this agreed with fact of [98] which mentioned previously in section 5.3.2.1.

The mole fractions moving along the flame's center line are decrease for the oxidant and fuel while increase for CO & CO_2. This outcome is considered inevitable. The oxidant and the fuel are reactants; thus, they are consumed throughout the center line and their mole fractions decrease. On the other hand, CO & CO_2 are produced as the combustion takes place and therefore their mole fractions increase. This truth persists regardless of the equivalence ratio.

Comparing Fig. (5. 48A, B, C, D, & E), it could be concluded that as the equivalence ratio increase, the Oxygen mole fractions somewhat decrease. This behavior related to the fact that LPG/air mixture with a higher equivalence ratio contains less Oxygen amount for the same amount of LPG. Another notice could be concluded, that the ratio of LPG to Oxygen mole fractions changes approximating to the same change in the equivalence ratios. Concerning the CO_2 & CO mole fractions, when increasing the equivalence ratio CO_2 mole fractions decrases while CO mole fractions increases. On the other hand, as the equivalence ratio increase more than unity, the mole fractions of CO_2 significantly decreasing while CO mole fractions increasing. This behavior is due to the Oxygen deficiency when increasing the equivalence ratio [103].

Fig. (5. 49) & Fig. (5. 50) shows the effect of equivalence ratio on mole fraction along the center line for CO_2 & CO respectively. It can be seen from these figures that for a stoichiometric fuel/ air mixture the maximum CO_2 and with no CO occurs. This is due to the stoichiometric quantities of fuel and air. In the same time, the maximum CO_2 mole fraction occur at the stoichiometric condition and is less for lean side. The rich mixture producing lower fraction of CO_2. The complete combustion at stoichiometric conditions converting all carbon atoms into CO_2 while for lean mixture there is a lower ratio of fuel

which means the little carbon atoms and some portion of the oxidant doesn't react. On the other hand, for rich mixture there is a fuel deficiency.

Regarding the CO mole fraction, it's the exact opposite. For the lean and stoichiometric mixtures, there are no CO production. For the rich mixtures CO mole fraction increases monotonically as the equivalence ratio increases. A rich mixture contains more carbon and less oxidant. Thus the combustion in this situation is incompleted which makes carbon atoms react with insufficient amount of oxygen. This makes CO_2 mole fraction decreases while CO mole fraction increases as the equivalence ratio increases, compare Fig. (5. 49) & Fig. (5. 50).

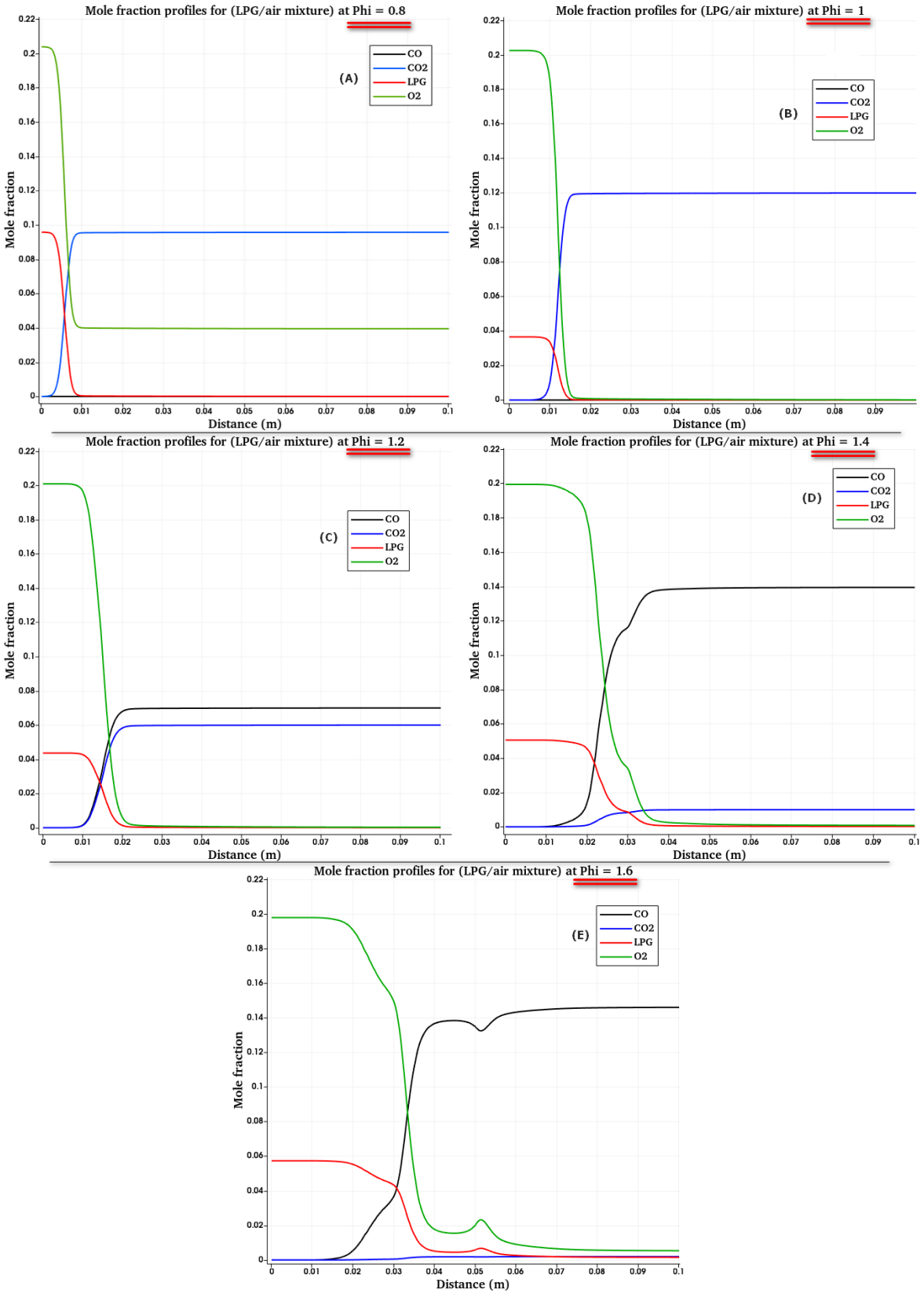

Fig. (5. 48) Species mole fraction profiles along the center line for LPG/air mixture at different equivalence ratio

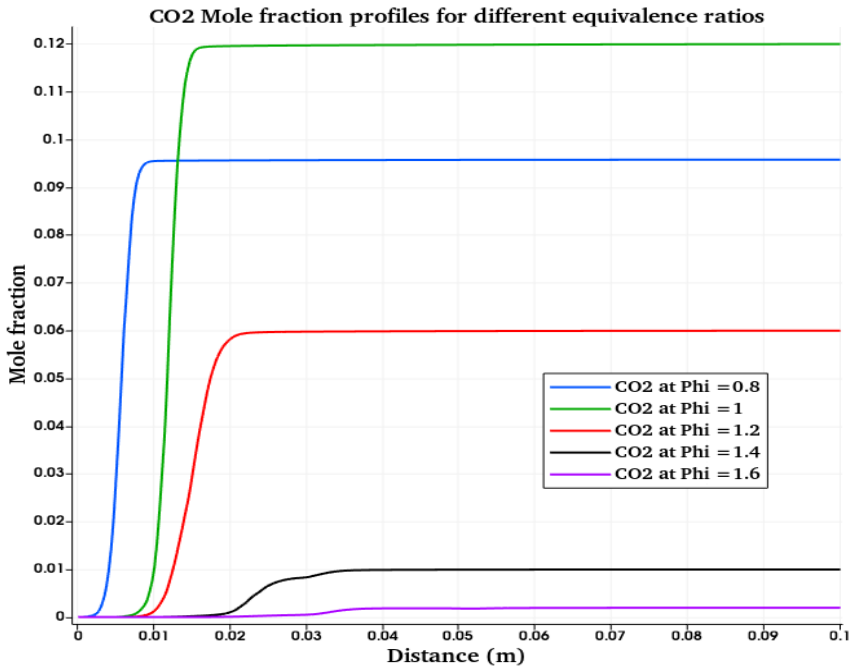

Fig. (5. 49) comparison of CO_2 mole fraction distribution along the center line for LPG/air mixture at different equivalence ratio

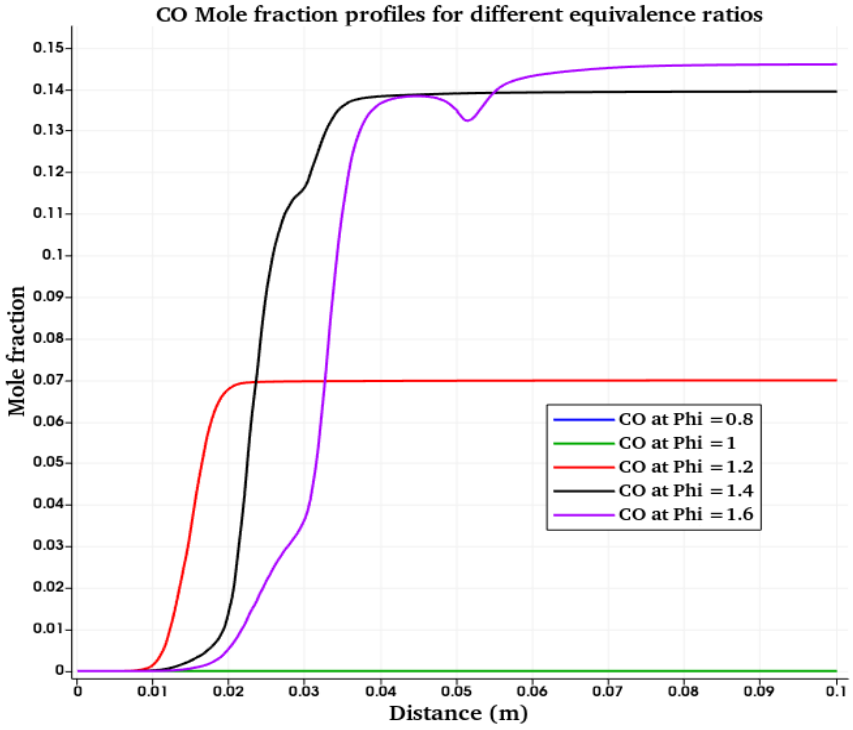

Fig. (5. 50) comparison of CO mole fraction distribution along the center line for LPG/air mixture at different equivalence ratio

5.3.4.2 Effect of Flow Rate:

The effect of mixture flow rate on the combustion species formation has been simulated for stoichiometric LPG/air mixture. The predicted mole

fraction of the reactants (O_2 & LPG) and CO_2 along the center line are shown in Fig. (5. 51) & Fig. (5. 52). The abscissa shows the distance above the burner tip (in meters) and the ordinate shows the mole factions. These figures indicate the following details:

The values of mole fractions assume the same values for all of the mass flow rates generally as all the cases are for the same chemical composition and the same amounts of species. Both LPG and O2 are completely consumed in the reaction zone and they are disappearing in the post flame region. The mole fraction values of CO_2 do not change with the flow rate.

Fig. (5. 52) shows the difference in mole fractions along the center for stoichiometric LPG/air mixture when changing the mixture flow rate from 4 to 8 Lt/min. It is shown that the location of the reaction zone shifted further downstream regarding to increasing the flow rate. This is comparable to obtained experimentally and numerically findings previously for the effect of flow rate on flame height, see Fig. (5.7), Fig. (5. 40), Fig. (5. 42) & Fig. (5. 43). On the other hand, this agreed with findings of U. Atmaca 2021 [104]. It also can be seen from the figure that the length of the reaction zone increases in proportion to the rate of increase in flow rate.

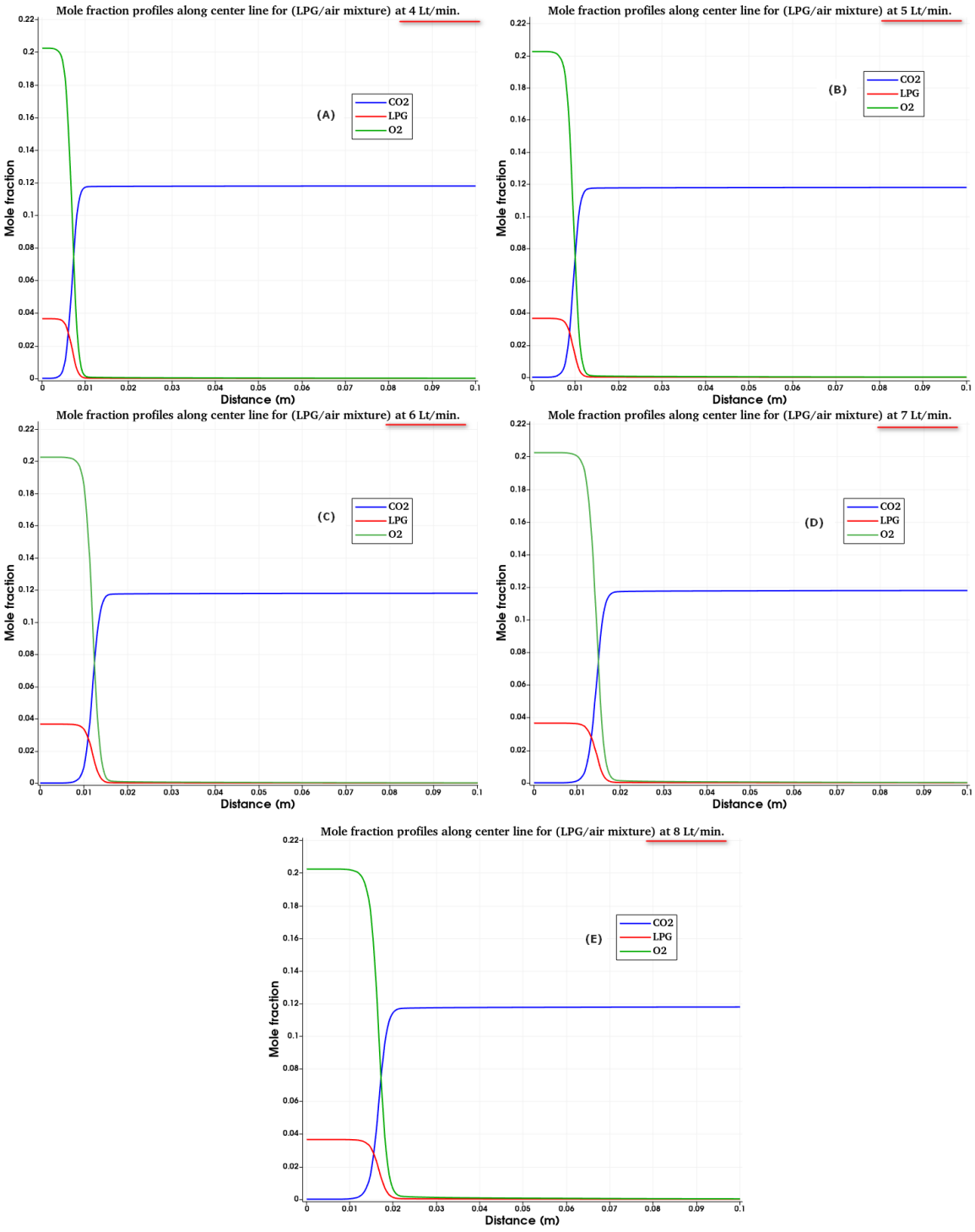

Fig. (5. 51) Species mole fraction profiles along the center line for stoichiometric LPG/air mixture at different flow rates

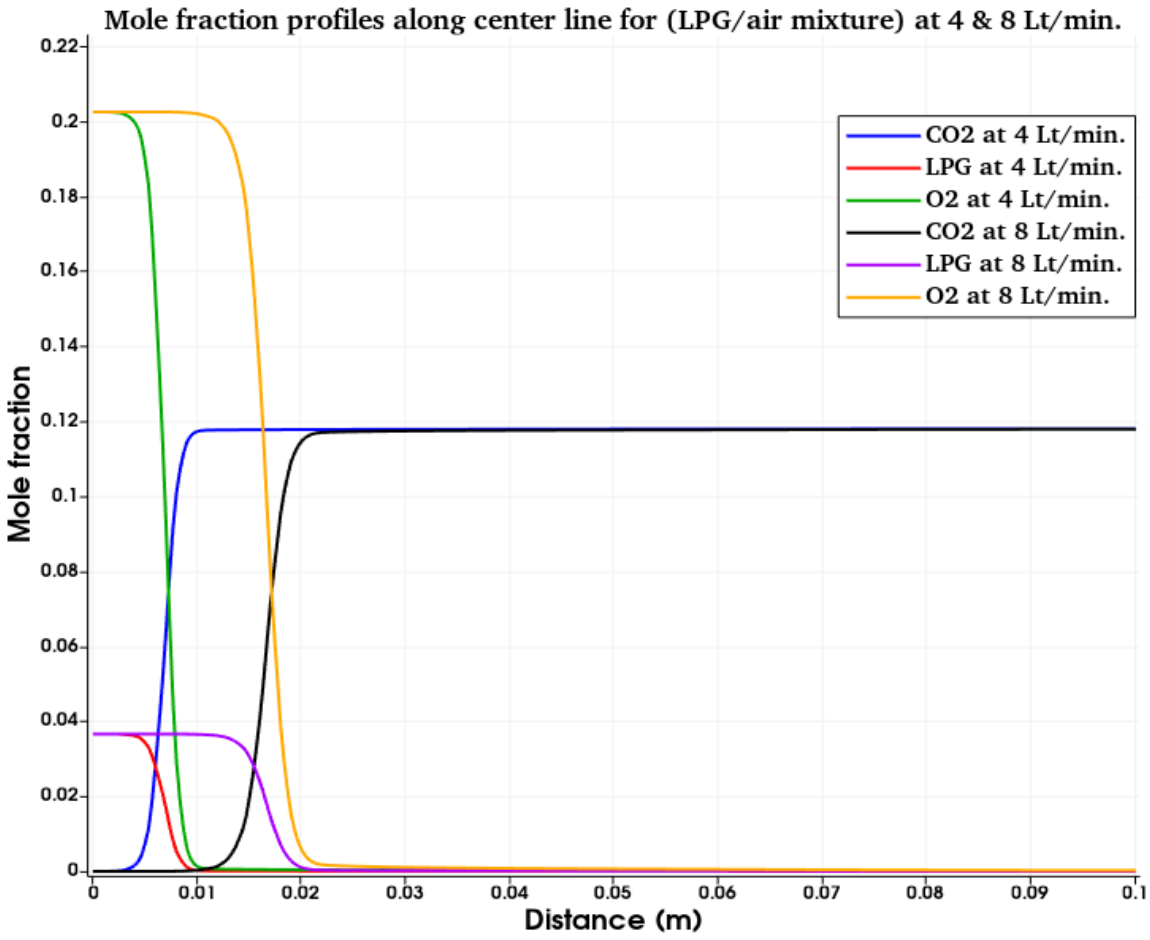

Fig. (5. 52) comparison of species mole fractions distribution along the center line for stoichiometric LPG/air mixture at different flow rates

5.3.4.3 Effect of Hydrogen Blending Ratio

The combustion of LPG-H_2/air mixture has been simulated for different hydrogen blending ratio at stoichiometric conditions to study the effect of blended H_2% on the species formation. The predicted mole fraction of the reactants (O_2 & LPG) and CO_2 along the center line are show in Fig. (5. 53). The abscissa shows the distance above the burner tip (in meters) and the ordinate shows the mole factions. This figure indicates the following details:

If hydrogen is blended to the LPG fuel, then the mole fraction of the oxidant decreases while it increases for the fuel (LPG-H_2). This finding is linked to the molar calculation of oxygen, fuel, and CO_2. The AFR of hydrogen is lower than that for LPG fuel. Thus, as H_2 is blended to the fuel it leads to

minimize the overall value for AFR of LPG-H_2 fuel as it compared with LPG fuel alone. Consequently, the number of air moles that required for one mole of LPG-H_2 decreases as H_2% increases. This means that the total moles of the reactants decrease which makes the of LPG-H_2 curves goes up, compare figures A & E for example. On a related note, blending H_2 reduces the CO_2 mole fraction. This is due to the decrease in the number of carbon and oxygen atoms in the fuel/ air mixture as the hydrogen is blended to the mixture instead of a part of LPG. Comparing the mole fraction of the combustion of LPG with that of LPG-H_2 50%, the oxygen and CO2 mole fractions decreases by about 3% and 9% respectively while the fuel mole fraction increases by about 78%.

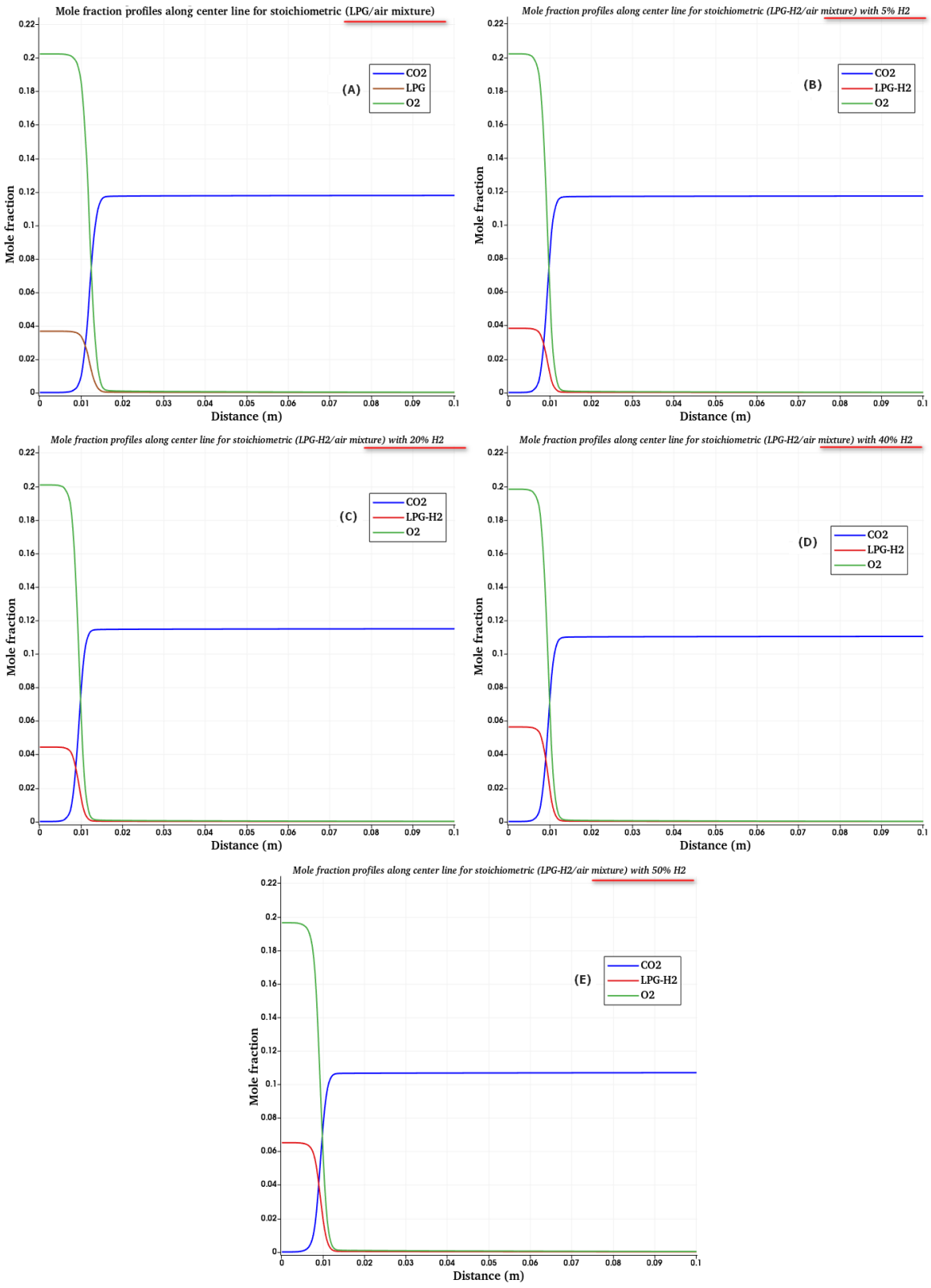

Fig. (5. 53) Species mole fraction profiles along the center line for stoichiometric LPG-H_2/air mixture at different hydrogen blending ratios

5.4 Comparison of the Results:

5.4.1 Comparison Presented Experimental & Numerical Results

5.4.1.1 Effect of Equivalence Ratio

Fig. (5. 54) shows a comparison of the experimental & numerical results for the effect of equivalence ratio for LPG/air mixture: **a)** flame photography & **b)** temperature contours. The temperature contour indicates flame inner zone only while the flame photography shows the full length of the visible flame. Both results show the same trend for the height and structure of the flame inner zone. The flame height increased both experimentally and numerically as the equivalence ratio increases. A high agreement between these results is obtained.

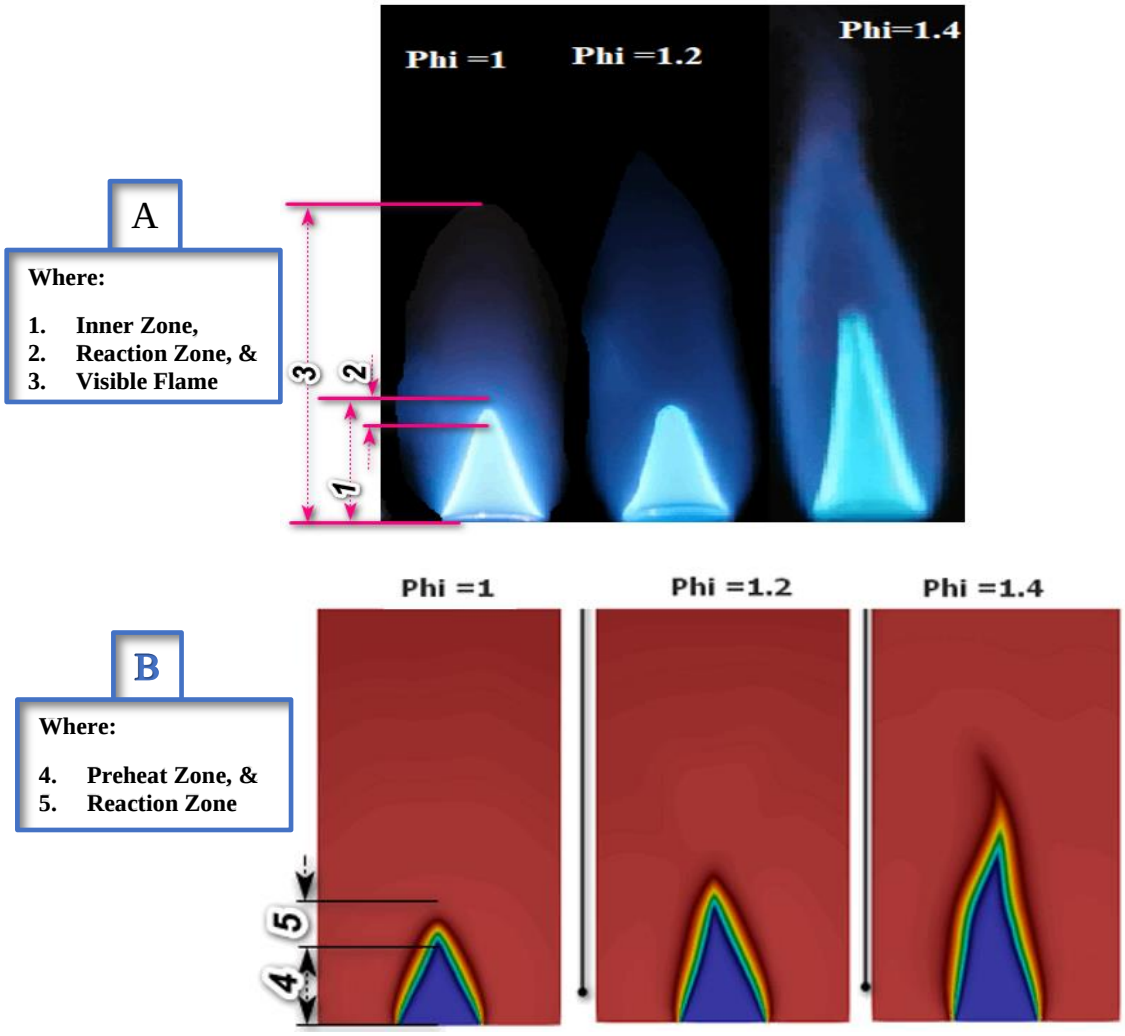

Fig. (5. 54) Comparison of the experimental & numerical results for the effect of equivalence ratio: a) flame photography & b) temperature contours

Fig. (5. 55) indicates the measured and predicted flame inner zone height for LPG/air mixture at different equivalence ratios at 6 Lt/min. It is noted that the flame height for both cases show close values to a high extent. The average difference in flame height is about 0.7 mm which represents 2.8%.

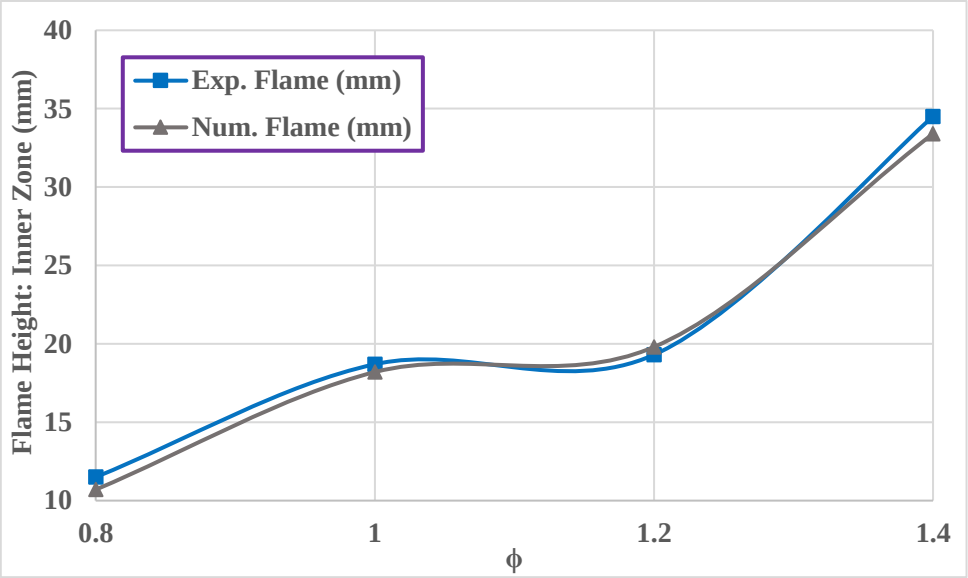

Fig. (5. 55) Comparison of the experimental & numerical results for flame height for different equivalence ratios

5.4.1.2 Effect of Flow Rate

Fig. (5. 56) shows a comparison of the experimental & numerical results for the stoichiometric LPG/air mixture for the effect of flow rate: a) flame photography & b) temperature contours. Both results show the same trend for the height and structure of the flame inner zone. The flame inner zone height increased as flow rate increases. A high agreement between these results is obtained.

Fig. (5. 57) indicates the measured and predicted flame inner zone height for stoichiometric LPG/air mixture at different flow rates. It is noted that the flame height for both cases show close values to a high extent. The average difference in flame height is about 0.6 mm which represents 3.7%.

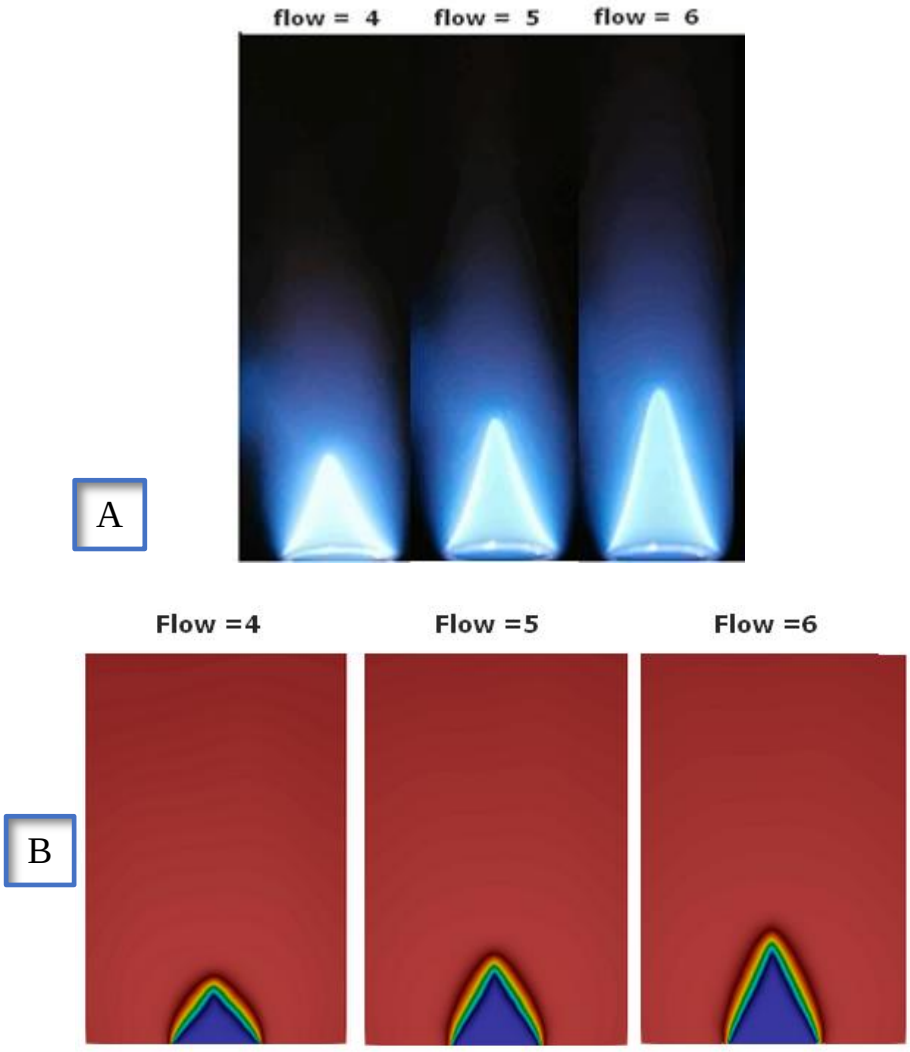

Fig. (5. 56) Comparison of the experimental & numerical results for the effect of flow rate: a) flame photography & b) temperature contours.

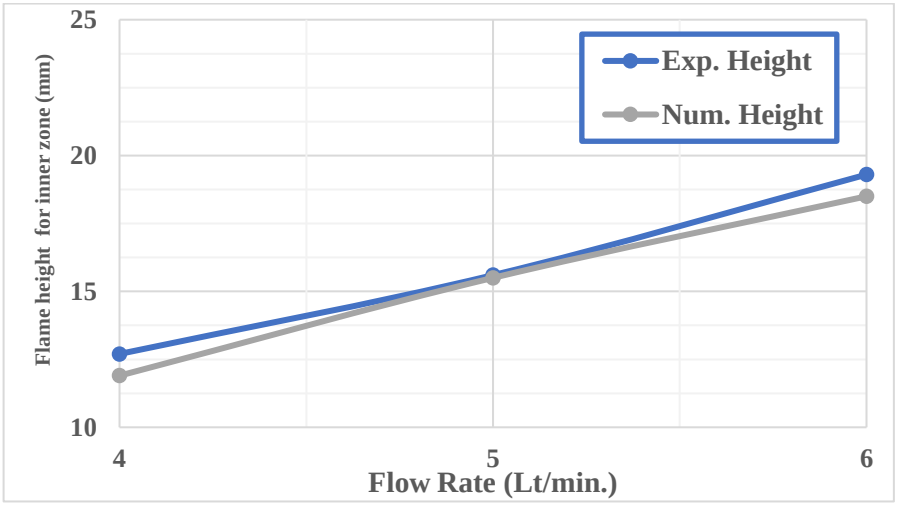

Fig. (5. 57) Comparison of the experimental & numerical results for flame height for different flow rates

5.4.1.3 Effect of Hydrogen Blending

Fig. (5. 58) shows a comparison of the experimental & numerical results for the effect of hydrogen blending ratio on the height and structure of the flame inner zone. Both results show the same trend for flame height and structure. The flame inner zone height decreases as flow rate increases. A high agreement between these results is obtained.

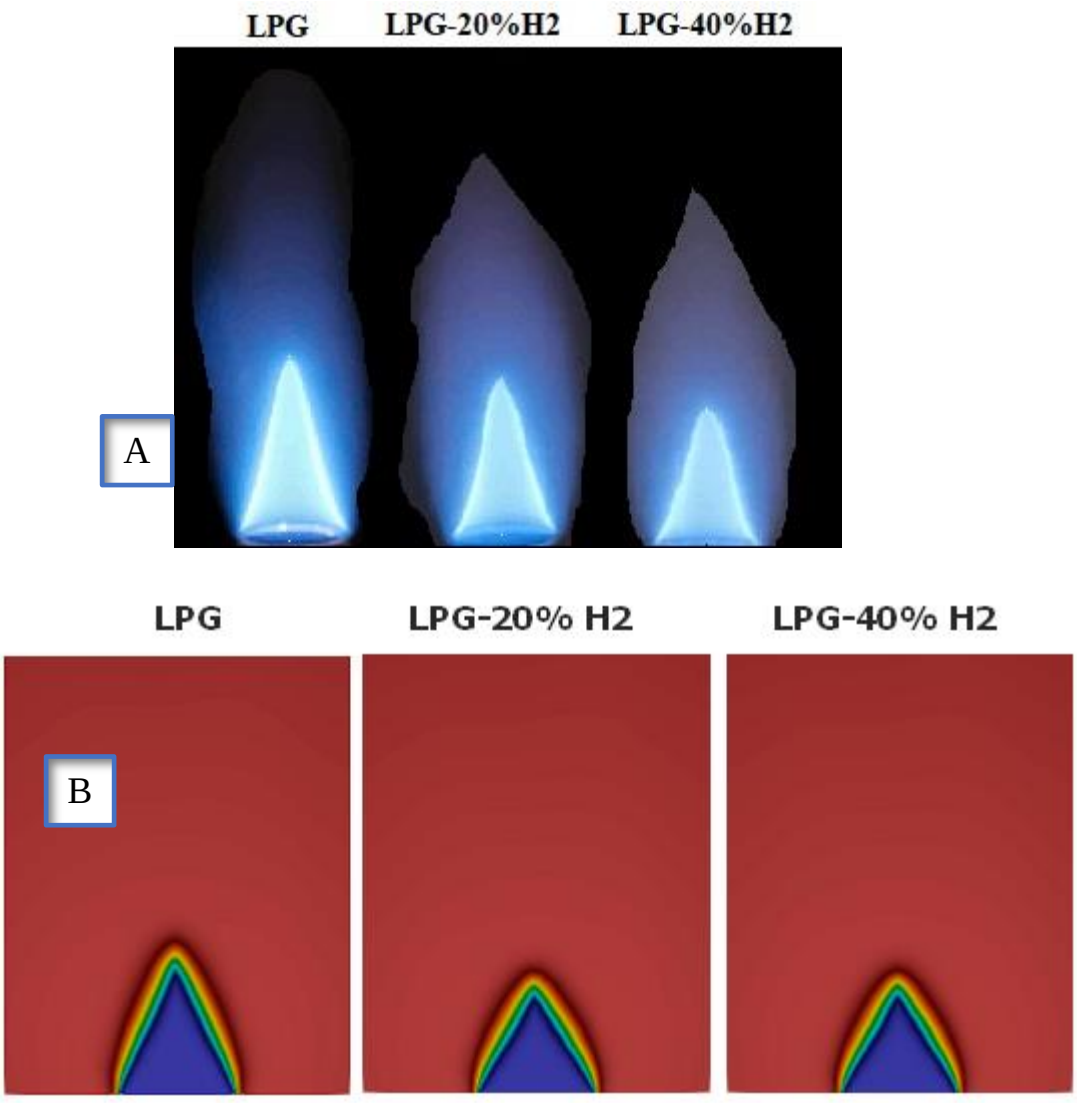

Fig. (5. 58) Comparison of the experimental & numerical results for the effect of H_2 % blending: a) flame photography & b) temperature contours.

Fig. (5. 59) indicates the measured and predicted flame height for stoichiometric LPG-H_2/air mixture at 6 Lt/min. for different hydrogen blending ratios. It is noted that the flame height for both cases show close values to a high extent and the flame height decreases with respect to hydrogen

blending. The average difference in flame height is about -0.8 mm which represents -1.8%.

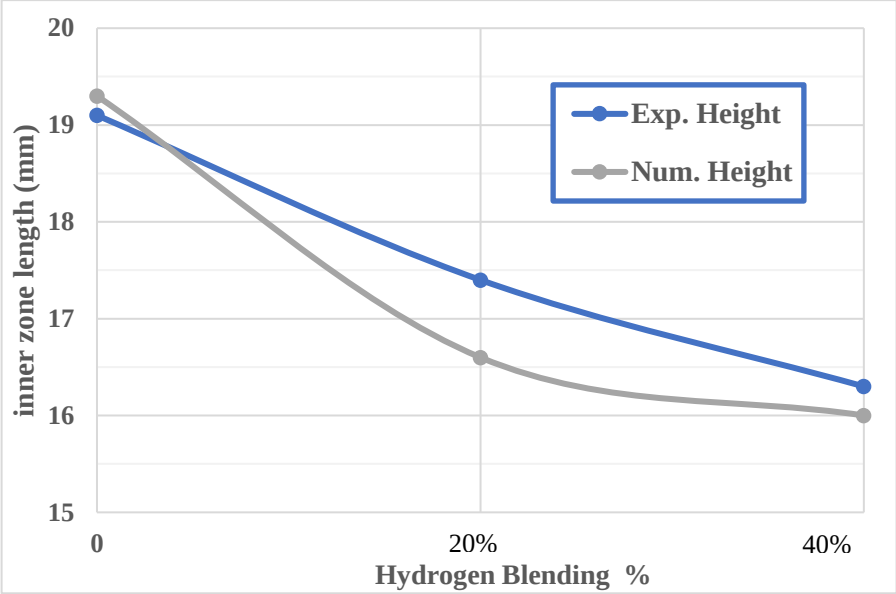

Fig. (5. 59) Comparison of the experimental & numerical results for flame height for different hydrogen blending ratios

5.4.2 Comparison the Present Results with Previous Works

Fig. (5. 60) shows a comparison for the flame photographs at 30° & 45° swirling burner for the present LPG with that presented by Patel & Shah 2018 [43] for the LPG-IDF flames. The general structure of flames in both studies is coincide. Each study indicates that the swirling burner with 45° produces a flame aspect ratio lower than that for 30°. Also, it is noticeable that the flame spinning in a counter-clockwise direction around its vertical axis in both results. It can also be noted that the flame in the two studies is narrow near the burner tip and then divided into parts and then the flame begins to expand transversely and its segments merge with each other when moving away from the edge of the burner tip. The difference in flames colours is normal. Pictures on the left column are for the present premixed flames while that on the right are for diffusion flames.

Fig. (5. 61) presents results of the effect of hydrogen blending on the length of flame inner zone for the experimental and numerical part of the current

study (on the left vertical axis) and comparing it with that presented by H.S. Zhen [102] (on the right vertical axis). All results show that the inner zone shortens due to hydrogen blending. The results of the current study coincide well with the trend of H. S. Zhen's results.

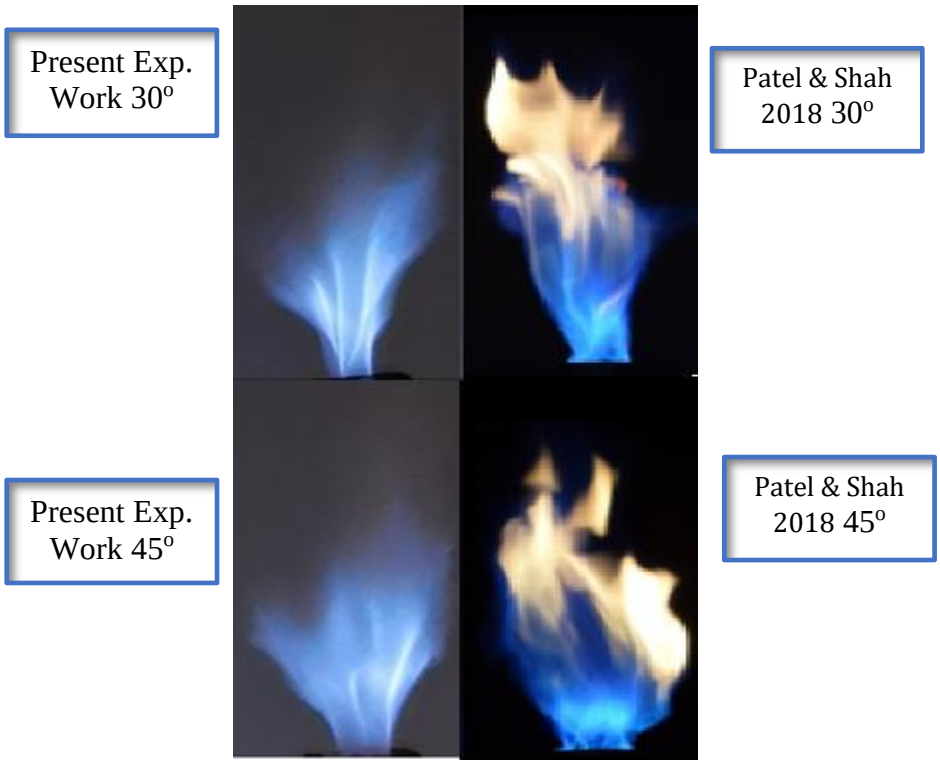

Fig. (5. 60) Comparison for flame photography of swirling burners for the present LPG and that presented by Patel & Shah 2018 [43].

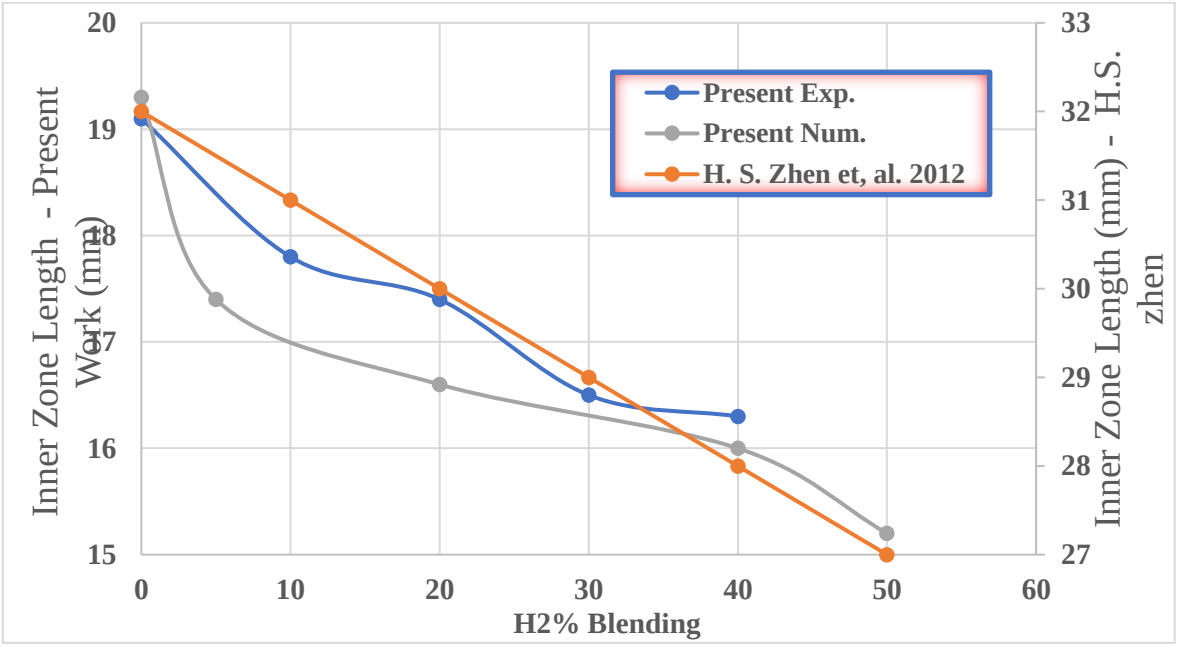

Fig. (5. 61) Comparison for the effect of hydrogen blending on the length of flame inner zone with that presented by H.S. Zhen [102]

The maximum flame temperature for LPG combustion predicted in this work is compared with the results of Mokhles Tawfeek 2020 [12] & Hamza M. Mjbel 2021[76] at 300K initial temperature and at atmospheric conditions. The comparison shows a high match for the present results with the results of Ref. [12] & [76] as shown in Fig. (5. 62). All results show that the maximum flame temperature drops for the more rich mixture due to the incomplete combustion of the fuel. The average difference in flame temperature of the present numerical simulation is about 17 K which represents 1.2% less.

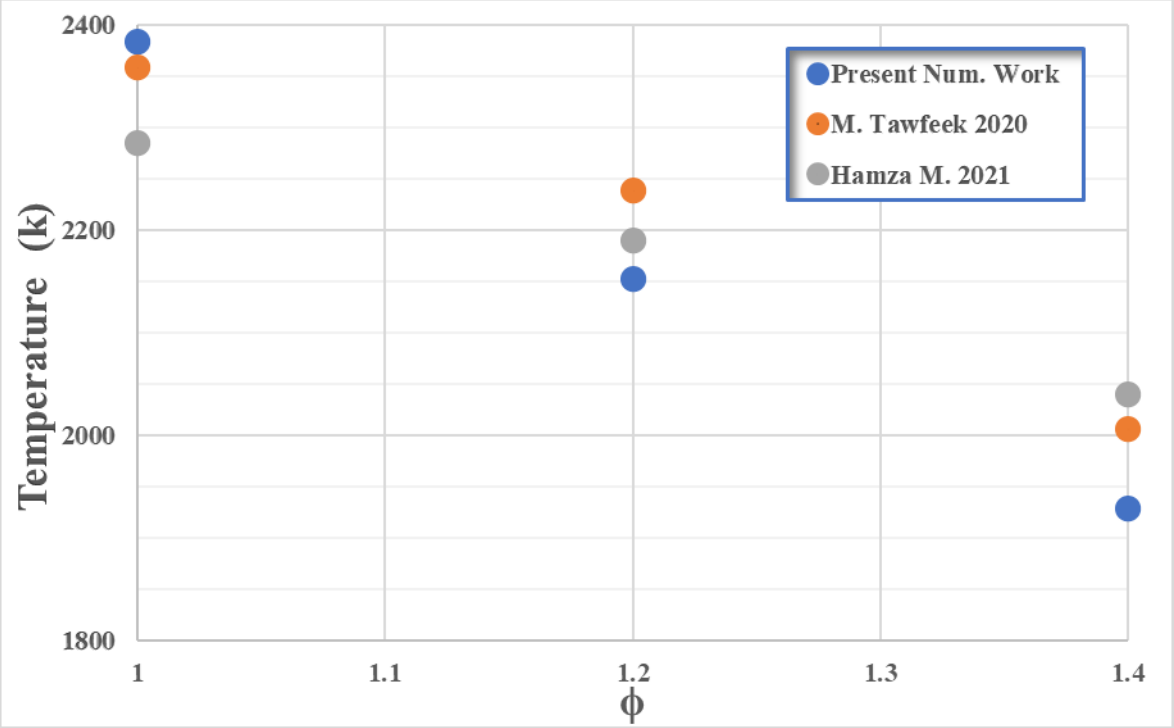

Fig. (5. 62) Comparison of the predicted flame temperature by OpenFOAM with other previous works for different equivalence ratios

Both results show that the temperature increases steadily in the first distance and the temperature increases clearly throughout the reaction zone and the temperature tends to decrease in the post flame region.

Fig. (5. 63) shows a comparison of present predicted species mole fraction for LPG with that obtained previously by Dakhil & Gabbar 2012 [103] for CH_4. It's clear that the present OpenFoam simulations predicted the same trend for species mole fraction with comparable values for O_2. The difference

in fuel and CO_2 values is due to lower carbon atoms in CH_4 as it compared with LPG.

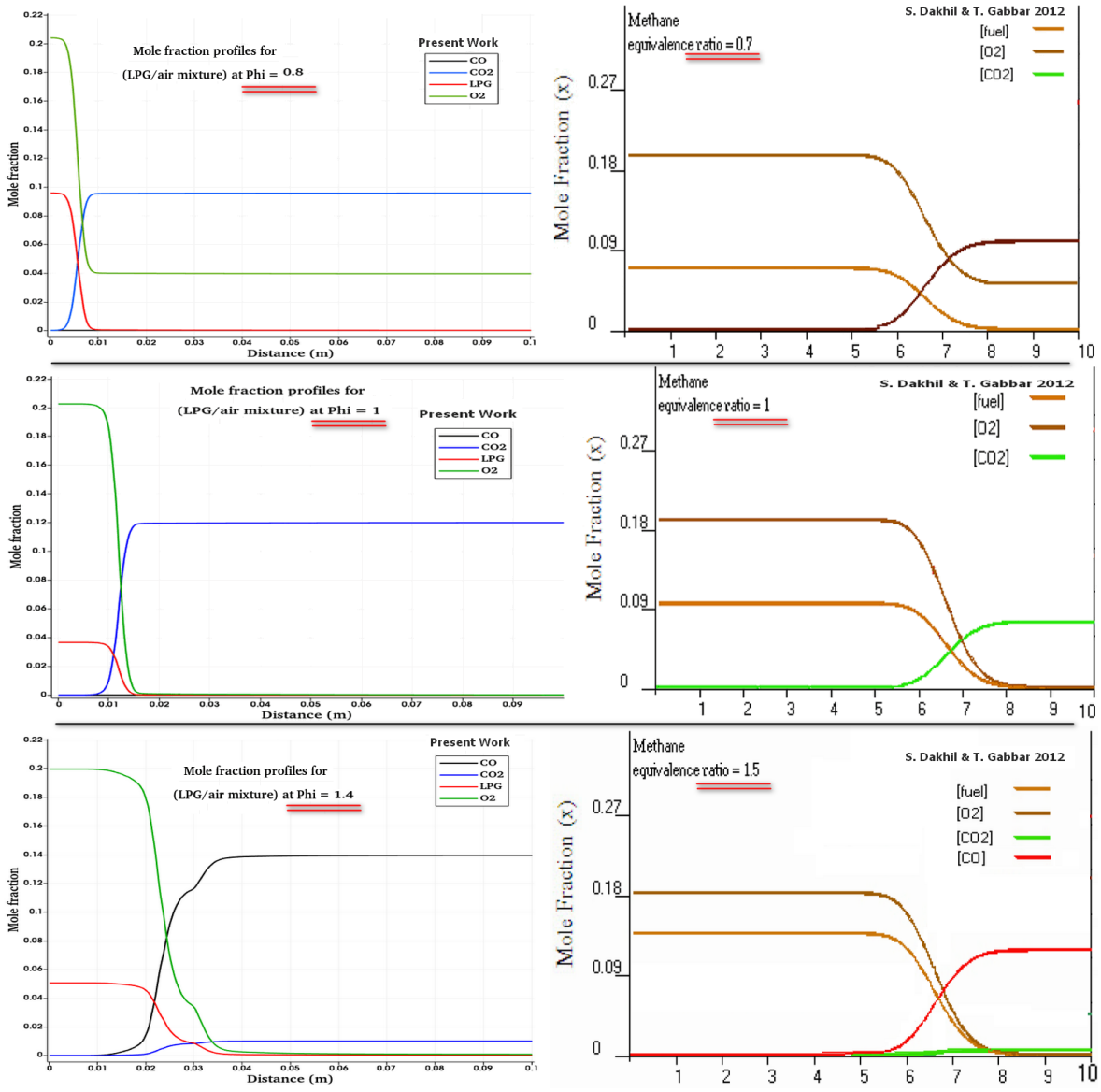

Fig. (5. 63)Comparison of present predicted species mole fraction with Dakhil & Gabbar 2012 [103]

CHAPTER SIX

CONCLUSIONS & SUGGESTIONS FOR FUTURE WORKS

Both experimental and numerical study has been carried out to investigate the effect of fuel type and composition on the height& characteristics of premixed flame for tube burner where LPG is considered as the primary fuel. The influencing of the following parameters has been studied which are: the equivalence ratio, mixture flow rate, H_2 blending ratio and/ or CO_2 dilution ratio, burner's aspect ratio, and the use of swirling/ non- swirling burner.

This chapter is devoted to presenting and summarizing the most prominent conclusions obtained (based on the observations throughout the results of current study) accompanied by the most important recommendations and suggestions for future research efforts that could become an extension for the current study.

6.1 Conclusions

The following conclusions represents a short answer to the most important inquiries about the current research:

1. The equivalence ratio dominants the flame height for all mixture types and composition at all operating conditions. Increasing the equivalence ratio maximizes all flame regions & producing a taller flame both experimentally and numerically. For example, the flame at ϕ = 1.4 has approximately twice the height at ϕ=1 for the inner zone and visible flame and for different mixtures.

2. Raising fuel/air mixture's flow rate leads to make the flame taller both experimentally and numerically for the different mixtures. A larger flow rate minimizes the flame temperature as it increasing the flame surface area leading to more heat lose.

3. When hydrogen is blended with LPG, the flame shortens but becomes wider. The higher the hydrogen blending ratio the higher flame temperature. Numerically if 50% H_2 is blended with stoichiometric LPG the temperature increases by about 12K. At the same time, increasing hydrogen blending ratio under the stoichiometric condition causes O_2 & CO_2 mole fraction to decrease.

4. If LPG fuel is diluted with CO_2 the flame lengthens but gets slim in the experimental findings. This result is in the inverse of the effect of hydrogen blending. The elongation in flame due to CO_2 dilution becomes more prominent with the increase of both parameters equivalence ratio or flow rate.

5. Concerning experiments of LPG-H_2-CO_2/air mixture, the flame extends with CO_2 dilution at a constant H_2 percent while it shrinks with H_2 blending at a constant CO_2 percent. The influence of CO_2 on prolonging the flame is substantially greater than the negative effect of H_2.

6. The burner aspect ratio effect on flame height is insignificant.

7. The use of swirling burner shortens the flame when ϕ = 1 & 1.2 while this reduction is not noticeably visible for a lean mixture, as the length of the flame is generally short. Besides, when increasing the number of swirler vanes a slight reduction in flame height has been concluded.

8. The swirling burner enhances the mixing process due to the wider surface area at flame inner core which is divided into segments equals to the number of swirl vanes with a flower shape flame at low flow rates. When

the level of flow is increased, the flame segments begin to merge with each other, as well as the inner zone merging with the outer zone.

9. Flame aspect ratio increases with respect to increasing ϕ, flow rate, and CO_2 dilution ratio while it decreases when H_2 is blended as well as when using a swirling burner.

10. Regarding to flame stability, it increases when ϕ increases and it enhances as a result of H_2 blending or CO_2 dilution. CO_2 enables the flame to overcome flashback while H_2 shifts flashback and blowout limits towards higher flow rates. The use of a swirling burner enhancing flame stability dramatically when ϕ = 1 & 1.2 while the inverse observed when ϕ = 0.8.

11. The numerical prediction results show that the temperature distribution along the flame center line slightly increased in the preheat zone, while it increases sharply & rapidly throughout the reaction zone. Later the temperature begins to decrease monotonically in the next downstream region.

12. The preheat zone's lowest temperature appears at the flame center line and rises toward the flame periphery. Moving downstream along the center line, the disparity becomes less. Outside of the flame, the temperature distribution has a parabolic form with a maximum at the center line and drops towards the flame periphery.

13. The progress variable provides a good indication about the chemical reaction progress. The flame height at unity progress variable is less than the maximum predicted Flame height.

14. Species mole fractions (reactant and/or products) change slightly through the first millimetres along flame center line (preheat zone). The higher rate of change in species mole fractions takes place throughout the next few millimeters (reaction zone). After this sharp change, the values of mole

fraction will approximately remain constant as the combustion being completed.

15. The thickness of the reaction zone extends when the equivalence ratio increased.

6.2 Suggestions for Future Works

The following suggestions are put forward for future works:

1. The experimental apparatus could be used for further works to study the flame characteristics and flame height for other fuels such as biofuels, syngas or landfill gas with different fuel additives.
2. Studying the effect of different design for the burner such as port array, slot burner including the effect of burner's material as well as testing the effect of turbulence generation.
3. Carrying out a similar investigation using other techniques for measuring flame height such as PLIF, Chemiluminescence, & Mach-Zehnder interferometry.
4. Studying the effect of higher initial temperatures and pressures on flame structure and pollutants formation and studying the heat release factor.
5. Studying the effect of the addition of different diluent gas instead of CO_2 such as inert gasses.
6. Take advantage of the available experimental apparatus to study the effect of flame height on the design of combustion systems including environmental and economic considerations.
7. Modifying and upgrading the present numerical code for studying different extended cases such as the swirling burner, different burner's design with different primary fuels, fuels blends, and fuel diluents.

REFERENCES

[1] M. A. Nemitallah, M. A. Haque, A. Abdelhafez, S. A. M. Said, and M. A. Habib, "Numerical analysis supported with experimental measurements of premixed oxy-propane flames in a fuel-flex gas turbine combustor," *Int. J. Energy Res.*, 2021.

[2] B. B. Samantaray and C. K. Mohanta, "Analysis of industrial flame characteristics and constancy study using image processing technique," *J. Mech. Eng. Sci.*, vol. 9, pp. 1604–1613, 2015.

[3] T. M. Dabade *et al.*, "CFD simulation of confined non-premixed flames," in *Heat Transfer Summer Conference*, vol. 44786, pp. 235–242, 2012.

[4] J. L. Consalvi, Y. Pizzo, B. Porterie, and J. L. Torero, "On the flame height definition for upward flame spread," *Fire Saf. J.*, vol. 42, no. 5, pp. 384–392, 2007.

[5] S. McAllister, J.-Y. Chen, and A. C. Fernandez-Pello, *Fundamentals of combustion processes*, vol. 302. Springer, 2011.

[6] K. K. Kuo and R. Acharya, *Fundamentals of turbulent and multiphase combustion*. John Wiley & Sons, 2012.

[7] S. Wang, Z. Yuan, and A. Fan, "Experimental investigation on non-premixed CH_4/air combustion in a novel miniature swiss-roll combustor," *Chem. Eng. Process. Intensif.*, vol. 139, pp. 44–50, 2019.

[8] J. Zhang, X. Li, H. Yang, L. Jiang, X. Wang, and D. Zhao, "Study on the combustion characteristics of non-premixed hydrogen micro-jet flame and the thermal interaction with solid micro tube," *Int. J. Hydrogen Energy*, vol. 42, no. 6, pp. 3853–3862, 2017.

[9] E. K. H. Salem, "numerical simulations of premixed flames of multi component fuels/air mixtures and their applications," 2018, doi:

https://doi.org/10.13023/etd.2019.113.

[10] S. S. Rashwan, A. H. Ibrahim, T. W. Abou-Arab, M. A. Nemitallah, and M. A. Habib, "Experimental study of atmospheric partially premixed oxy-combustion flames anchored over a perforated plate burner," *Energy*, vol. 122, pp. 159–167, 2017.

[11] R. T. Stephen, "An introduction to combustion: concepts and applications," *McGrw-Hill Companies, Inc*, 2000.

[12] H. A. K. Shahad and A. S. Yasiry, "An experimental study of the effect of hydrogen blending on laminar flame speed for iraqi LPG," *Iraqi J. Mech. Mater. Eng.*, vol. 17, no. 4, 2017.

[13] L. G. Zheng, M. G. Yu, S. J. Yu, and C. Lu, "Measurement of flame height by image processing method," in *Advanced Materials Research*, 2011, vol. 301, pp. 983–988.

[14] J. S. Newman and C. J. Wieczorek, "Chemical flame heights," *Fire Saf. J.*, vol. 39, no. 5, pp. 375–382, 2004.

[15] W. R. Hawthorne, D. S. Weddell, and H. C. Hottel, "Mixing and combustion in turbulent gas jets," in *Symposium on Combustion and Flame, and Explosion Phenomena*, 1948, vol. 3, no. 1, pp. 266–288.

[16] H. HC, "Fire modeling," in *International Symposium on the Use of Fire Models*, 1961, pp. 32–47.

[17] R. W. Wade and J. P. Gore, "Visible and chemical flame lengths of acetylene/air jet diffusion. In 1996, NISTR 5904: 41-42," in *NIST Annual Conference on Fire Research*, 1996.

[18] Charles S.Mcenally, Lisa D.Pfefferl, Andrew M.Schaffer, Marshall B.Long, Rahima K.Mohammed, Mitchell D.Smooke, and Meredith B.Colkei, "Characterization of a coflowing methane/air non-premixed flame with computer modeling, rayleigh-raman imaging, and on-line

mass spectrometry," *Proc. Combust. Inst.*, vol. 28, no. 2, pp. 2063–2070, 2000.

[19] L. Ying and J. Ahmad, "Investigation of Bunsen-type premixed flame response to acoustic excitation: temperature and flame profile," *J. Emerg. Investig.*, pp. 1–6, 2017.

[20] M. A. Mikofski, T. C. Williams, C. R. Shaddix, and L. G. Blevins, "Flame height measurement of laminar inverse diffusion flames," *Combust. Flame*, vol. 146, no. 1–2, pp. 63–72, 2006.

[21] H. S. Zhen, J. Miao, C. W. Leung, C. S. Cheung, and Z. H. Huang, "A study on the effects of air preheat on the combustion and heat transfer characteristics of Bunsen flames," *Fuel*, vol. 184, pp. 50–58, 2016.

[22] P. Kumar and D. P. Mishra, "Experimental investigation of laminar LPG–H_2 jet diffusion flame," *Int. J. Hydrogen Energy*, vol. 33, no. 1, pp. 225–231, 2008.

[23] P. Kumar and D. P. Mishra, "Effects of bluff-body shape on LPG–H_2 jet diffusion flame," *Int. J. Hydrogen Energy*, vol. 33, no. 10, pp. 2578–2585, 2008.

[24] D. P. Mishra and P. Kumar, "Experimental investigation of laminar LPG–H_2 jet diffusion flame with preheated reactants," *Fuel*, vol. 87, no. 13–14, pp. 3091–3095, 2008.

[25] M. T. AbdulAmeer, "Experimental investigation of flame flashback in premixed (liquefied petroleum gas-hydrogen/air) combustion system." Ms.C. Thesis, Mechanical Engineering, Babylon University, Babylon, Iraq, 2020.

[26] S. R. Turns, "An introduction to combustion: concepts and applications," *System*, vol. 499. p. 411, 2000, doi: 10.1016/j.ijhydene.2008.07.121.

[27] J. Miao, C. W. Leung, C. S. Cheung, and R. C. K. Leung, "Flame stability

and structure of liquefied petroleum gas-fired inverse diffusion flame with hydrogen enrichment," *Int. J. Mech. Mechatronics Eng.*, vol. 7, no. 1, pp. 70–75, 2013.

[28] F. G. Roper, C. Smith, and A. C. Cunningham, "The prediction of laminar jet diffusion flame sizes: Part II. Experimental verification," *Combust. Flame*, vol. 29, no. C, pp. 227–234, 1977, doi: 10.1016/0010-2180(77)90113-4.

[29] U. S. P. Shet, P. S. Krishnan, P. S. Kumar, and T. Sundararajan, "Flame structure analysis of partially premixed lpg-air flames by digital image processing," no. January, pp. 1–7, 2009, doi: 10.13140/2.1.3544.6726.

[30] S. Mahesh and D. P. Mishra, "Flame structure of LPG-air inverse diffusion flame in a backstep burner," *Fuel*, vol. 89, no. 8, pp. 2145–2148, 2010.

[31] L. L. Dong, C. S. Cheung, and C. W. Leung, "Combustion optimization of a port-array inverse diffusion flame jet," *Energy*, vol. 36, no. 5, pp. 2834–2846, 2011.

[32] L. Hu, Q. Wang, M. Delichatsios, F. Tang, X. Zhang, and S. Lu, "Flame height and lift-off of turbulent buoyant jet diffusion flames in a reduced pressure atmosphere," *Fuel*, vol. 109, pp. 234–240, 2013.

[33] T. Trindade, A. Ferreira, and E. Fernandes, "Characterization of combustion chemiluminescence: an image processing approach," *Procedia Technol.*, vol. 17, pp. 194–201, 2014.

[34] P. Tamadonfar and Ö. L. Gülder, "Flame brush characteristics and burning velocities of premixed turbulent methane/air Bunsen flames," *Combust. Flame*, vol. 161, no. 12, pp. 3154–3165, 2014.

[35] G. Hu, S. Zhang, Q. F. Li, X. B. Pan, S. Y. Liao, H. Q. Wang, C. Yang, and S. Wei, "Experimental investigation on the effects of hydrogen

addition on thermal characteristics of methane/air premixed flames," *Fuel*, vol. 115, pp. 232–240, 2014.

[36] B. Aravind, V. Ratna Kishore, and A. Mohammad, "Combustion characteristics of the effect of hydrogen addition on LPG-air mixtures," *Int. J. Hydrogen Energy*, vol. 40, no. 46, pp. 16605–16617, 2015, doi: 10.1016/j.ijhydene.2015.09.099.

[37] C. L. Tang, Z. H. Huang, and C. K. Law, "Determination, correlation, and mechanistic interpretation of effects of hydrogen addition on laminar flame speeds of hydrocarbon–air mixtures," *Proc. Combust. Inst.*, vol. 33, no. 1, pp. 921–928, 2011.

[38] A. Z. Najafian and M. Ashjaee, "Experimental study of a laminar premixed LFG/air flame in a slot burner using Mach-Zehnder interferometry," *Therm. Sci.*, vol. 20, no. 5, pp. 1649–1660, 2016.

[39] K. Zheng, M. Yu, L. Zheng, X. Wen, T. Chu, and L. Wang, "Experimental study on premixed flame propagation of hydrogen/methane/air deflagration in closed ducts," *Int. J. Hydrogen Energy*, vol. 42, no. 8, pp. 5426–5438, 2017.

[40] C. Tao, Y. Qian, F. Tang, and Q. Wang, "Experimental investigations on temperature profile and air entrainment of buoyancy-controlled jet flame from inclined nozzle bounded the wall," *Appl. Therm. Eng.*, vol. 111, pp. 510–515, 2017.

[41] K. Wang, C. Tao, Q. Liu, Y. Qian, and P. He, "An experimental investigation of flame height and air entrainment rate of double jet fires," *Exp. Heat Transf.*, vol. 31, no. 1, pp. 22–31, 2018.

[42] S. M. Kumaran, O. S. Karve, and Y. B. Kadam, "Experimental study of LPG flames in different configurations," *ISME J. thermofluids*, vol. 4, no. 1, pp. 36–48, 2018.

[43] V. Patel and R. Shah, "Experimental investigation on flame appearance and emission characteristics of LPG inverse diffusion flame with swirl," *Appl. Therm. Eng.*, vol. 137, pp. 377–385, 2018.

[44] A. Verdier, J. M. Santiago, A. Vandel, G. Godard, G. Cabot, and B. Renou, "Local extinction mechanisms analysis of spray jet flame using high speed diagnostics," *Combust. Flame*, vol. 193, pp. 440–452, 2018.

[45] C. Tao, Y. Liu, F. Tang, and Q. Wang, "An experimental investigation of the flame height and air entrainment of ring pool fire," *Fuel*, vol. 216, pp. 734–737, 2018.

[46] J. Al-Naffakh, M. Al-fahham, and Q. A. Abed, "The blowoff limits and flashback limits for different diameter to length ratio burner," MECSJ, 24, pp. 1-11, 2019.

[47] J. Al-Naffakh, K. S. Hasan,M. Al-fahham, and M. R. Al-Qasab, "Improve and reduce the economic cost and and pollutants of a swirl burner", IOP Conf. Series: Materials Science and Engineering 928 (2020) doi:10.1088/1757-899X/928/2/022013.

[48] Jameel Tawfiq Al-Naffakh, "Experimental investgation of the effect of burner geometrey on flame stability" Ms.C. Thesis, Mechanical Engineering Techniques, AL-Furat AL-Awsat Technical University, Najaf, Iraq, 2019.

[49] J. Al-Naffakh, M. Al-fahham, and Q. A. Abed, "Experimental investigate the effect of burner geometry on the operation window of the burner," Energy Research Journal, 2019, DOI: 10.3844/erjsp.2019.

[50] J. Al-Naffakh, M. Al-fahham, and Q. A. Abed, "Burner rim geometry effect on flame stability," 3rd International Conference on Engineering Sciences (ICES.ME52), Nov. 2019.

[51] M. Zhang, J. Wang, M. Chang, and Z. Huang, "Turbulent flame topology

and the wrinkled structure characteristics of high pressure syngas flames up to 1.0 MPa," *Int. J. Hydrogen Energy*, vol. 44, no. 30, pp. 15973–15984, 2019.

[52] Y. Nie, J. Wang, W. Zhang, M. Chang, M. Zhang, and Z. Huang, "Flame brush thickness of lean turbulent premixed Bunsen flame and the memory effect on its development," *Fuel*, vol. 242, pp. 607–616, 2019.

[53] eixiang He, Peng Wang, Kai Wang, Xiaoping Liu, Chunmei Wang, Changfa Tao, and Yongqiang Liu, "The evolution of flame height and air flow for double rectangular pool fires," *Fuel*, vol. 237, pp. 486–493, 2019.

[54] V. Patel and R. Shah, "Effect of hydrogen enrichment on combustion characteristics of methane swirling and non-swirling inverse diffusion flame," *Int. J. Hydrogen Energy*, vol. 44, no. 52, pp. 28316–28329, 2019.

[55] C. Tao, B. Liu, Y. Dou, Y. Qian, Y. Zhang, and S. Meng, "The experimental study of flame height and lift-off height of propane diffusion flames diluted by carbon dioxide," *Fuel*, vol. 290, p. 119958, 2021.

[56] F. G. Roper, "The prediction of laminar jet diffusion flame sizes: Part I. Theoretical model," *Combust. Flame*, vol. 29, pp. 219–226, 1977.

[57] T. Plessing, P. Terhoeven, N. Peters, and M. S. Mansour, "An experimental and numerical study of a laminar triple flame," *Combust. Flame*, vol. 115, no. 3, pp. 335–353, 1998.

[58] E. S. Oran, J. W. Weber Jr, E. I. Stefaniw, M. H. Lefebvre, and J. D. Anderson Jr, "A numerical study of a two-dimensional H_2-O_2-Ar detonation using a detailed chemical reaction model," *Combust. Flame*, vol. 113, no. 1–2, pp. 147–163, 1998.

[59] R. Cabra, J.-Y. Chen, R. W. Dibble, A. N. Karpetis, and R. S. Barlow,

"Lifted methane–air jet flames in a vitiated coflow," *Combust. Flame*, vol. 143, no. 4, pp. 491–506, 2005.

[60] B. E. Knudsen, O. Kurenkov, S. Kim, M. Oberlack, and H. Pitsch, "Modeling flame brush thickness in premixed turbulent combustion," *Cent. Turbul. Res.*, pp. 299–310, 2006.

[61] P. S. Cumber and M. Spearpoint, "A computational flame length methodology for propane jet fires," *Fire Saf. J.*, vol. 41, no. 3, pp. 215–228, 2006.

[62] J. D. Smith, A. Suo-ahttila, S. Smith, and J. Modi, "Evaluation of the air-demand , flame height , and radiation from low-profile flare tips using ISIS-3D," *Am. – Japanese Flame Res. Committees Int. Symp.*, 2007.

[63] S. Li, "Modeling of pressure effects on flame structure and soot formation of n-heptane/air co-flow laminar flames by skeletal reaction mechanism," *Appl. Therm. Eng.*, vol. 106, pp. 1458–1465, 2016.

[64] Y. Xie, Y. Tu, H. Jin, C. Luan, Z. Wang, and H. Liu, "Numerical study on a novel burner designed to improve MILD combustion behaviors at the oxygen enriched condition," *Appl. Therm. Eng.*, vol. 152, pp. 686–696, 2019.

[65] S. Zhong, F. Zhang, M. Jangi, X.-S. Bai, M. Yao, and Z. Peng, "Structure and propagation of n-heptane/air premixed flame in low temperature ignition regime," *Appl. Energy*, vol. 275, p. 115320, 2020.

[66] S. H. Won, B. Windom, B. Jiang, and Y. Ju, "The role of low temperature fuel chemistry on turbulent flame propagation," *Combust. Flame*, vol. 161, no. 2, pp. 475–483, 2014.

[67] H. Kutkan and J. Guerrero, "Turbulent premixed flame modeling using the algebraic flame surface wrinkling model:A comparative study between openFOAM and ansys fluent," *Fluids*, vol. 6, no. 12, 2021, doi:

10.3390/fluids6120462.

[68] J. Zarvandi, M. Baigmohammadi, and S. Tabejamaat, "A numerical study on the effects of the geometry and location of an inserted wire on methane–air flames in a micro–burner," *Energies*, vol. 15, no. 1, p. 93, 2022.

[69] P. R. Resende, L. C. Morais, C. Pinho, and A. M. Afonso, "Combustion characteristics of premixed hydrogen/air in an undulate microchannel," *Energies*, vol. 15, no. 2, p. 626, 2022.

[70] H. Xu, F. Liu, S. Sun, Y. Zhao, S. Meng, and W. Tang, "Effects of H_2O and CO_2 diluted oxidizer on the structure and shape of laminar coflow syngas diffusion flames," *Combust. Flame*, vol. 177, pp. 67–78, 2017.

[71] G. Rao,Y. Zhang, W. Cao, M. Zhao, W. Gao, H. Liang, and Y. Tan, "Experimental and numerical studies of premixed methane-hydrogen/air mixtures flame propagation in closed duct," *Can. J. Chem. Eng.*, vol. 96, no. 12, pp. 2684–2689, 2018.

[72] T. B. Maynard and J. W. Butta, "A physical model for flame height intermittency," *Fire Technol.*, vol. 54, no. 1, pp. 135–161, 2018.

[73] D. la Cruz-Ávila, D. León-Ruiz, I. Carvajal-Mariscal, G. Polupan, and L. D. G. Sigalotti, "Luminous flame height correlation based on fuel mass flow for a laminar to transition-to-turbulent regime diffusion flame," *arXiv2008.12209*, 2020.

[74] M. T. AbdulAmeer, H. A. K. Shahad, and S. M. AbdulHaleem, "Experimental investigation of iraqi liquefied petroleum gas (ILPG)/H_2/air premixed flame stability zone," 2020.

[75] M. T. AbdulAmeer, H. A. K. Shahad, and S. M. AbdulHaleem, "Investigation of flame flashback phenomena in LPG-H_2/air premixed combustion using boundary layer and peclet number," International

scientific Conference of the University of Babylon, ISCUB, Babylon, Iraq, Dec. 2019 .

[76] H. M. Mjbel, S. M. Abdulhaleem, and H. A. K. Shahad, "A numerical and experimental analysis of laminar flame speed for pre-mixed iraqi LPG/air mixture in a horizontal cylindrical combustion chamber," *J. Mech. Eng. Res. Dev.*, vol. 44, no. 1, pp. 176–189, 2021.

[77] G. D. Wight, *Fundamentals of air sampling, 1st Edition*. CRC press ISBN9780203755372 https://doi.org/10.1201/9780203755372, 1994.

[78] R. K. Rajput, *Fluid Mechanics and Hydraulic Machines*, 6th ed. India: S. Chand Publishing, 2015.

[79] "Bahnhofstraße 27 · 53577 Neustadt/ Wide, Germany, [Online], Available: info@ibeda.de ." .

[80] A. Mousemi, S. Mosadegh, A. Khademi, and G. Sorrentino, "Design and analytical evaluation of a swirler-injector system," *J. Fluid Flow, Heat Mass Transf.*, vol. 8, no. 1, pp. 166–177, 2021.

[81] Y. Z. Li, C. Huang, J. Anderson, and R. Svensson, "Verification , validation and evaluation of FireFOAM as a tool for performance design." p. 84, 2017.

[82] J. Paulasalo, "CFD modelling of industrial scale gas flame with OpenFOAM software," 2018.

[83] M. Povilaitis and J. Jaseliūnaitė, "Simulation of hydrogen-air-diluents mixture combustion in an acceleration tube with flamefoam solver," *Energies*, vol. 14, no. 17, p. 5504, 2021.

[84] R. . F. Courant K.; Lewy, H., "On the partial difference equations of mathematical physics," *IBM J. Res. Dev.*, vol. 11, no. 2, pp. 215–234, 1967.

[85] S. V. Avhad, "Study on dependence of cavitation number on super cavitation phenomenon using transient multiphase analysis," *Int. J. Sci. Dev. Res.*, vol. 5, no. 7, pp. 709–715, 2020.

[86] J. Paulasalo, "CFD modelling of industrial scale gas flame with OpenFOAM software," 2019.

[87] J. E. D. L.-R. M. De la Cruz-Ávila I. Carvajal-Mariscal, G. Polupan and L. Di G. Sigalotti, "Luminous flame height correlation based on fuel mass flow for a laminar to transition-to-turbulent regime diffusion flame," *arXiv2008.12209,* 2020.

[88] C. J. Greenshields, "OpenFOAM–The OpenFOAM foundation–user guide." 2018.

[89] C. J. Greenshields, "OpenFOAM–The OpenFOAM foundation–user guide." 2020.

[90] E. Yasari, J. Runsten, and J. Andric, "Tutorial XiFoam," *Sweeden,* 2010.

[91] D. B. Spalding, "Mixing and chemical reaction in steady confined turbulent flames," in *Symposium (International) on combustion*, 1971, vol. 13, no. 1, pp. 649–657.

[92] B. F. Magnussen and B. H. Hjertager, "On mathematical modeling of turbulent combustion with special emphasis on soot formation and combustion," in *Symposium (international) on Combustion*, 1977, vol. 16, no. 1, pp. 719–729.

[93] G. Zhang, G. Wang, Y. Huang, Y. Wang, and X. Liu, "Reconstruction and simulation of temperature and CO_2 concentration in an axisymmetric flame based on TDLAS," *Optik (Stuttg).*, vol. 170, pp. 166–177, 2018.

[94] P. Siewert, "Flame front characteristics of turbulent lean premixed methane/air flames at high-pressure." ETH Zurich, 2006.

[95] W. Guo, G. Zhu, B. Yao, F. Chen, and X. Xu, "Study on the fire extinguishing mechanism of small size wood crib based on small sand-throwing equipment," *Case Stud. Therm. Eng.*, vol. 25, p. 100942, 2021.

[96] F. Dionisius, S. Firdaus, M. E. Maulana, C. Carudi, B. Badruzzaman, and S. Suliono, "Characteristic of flame length on spuyer diameter in conventional LPG stove," in *IOP Conference Series: Materials Science and Engineering*, 2020, vol. 732, no. 1, p. 12088.

[97] J. Lozano, W. Tachajapong, D. R. Weise, S. Mahalingam, and M. Princevac, "Fluid dynamic structures in a fire environment observed in laboratory-scale experiments," *Combust. Sci. Technol.*, vol. 182, no. 7, pp. 858–878, 2010.

[98] S. Karaminejad, M. H. Askari, and M. Ashjaee, "Temperature field investigation of hydrogen/air and syngas/air axisymmetric laminar flames using Mach–Zehnder interferometry," *Appl. Opt.*, vol. 57, no. 18, pp. 5057–5067, 2018.

[99] H. S. Zhen, Y. S. Choy, C. W. Leung, and C. S. Cheung, "Effects of nozzle length on flame and emission behaviors of multi-fuel-jet inverse diffusion flame burner," *Appl. Energy*, vol. 88, no. 9, pp. 2917–2924, 2011.

[100] H. S. Zhen, C. W. Leung, C. S. Cheung, and Z. H. Huang, "Characterization of biogas-hydrogen premixed flames using Bunsen burner," *Int. J. Hydrogen Energy*, vol. 39, no. 25, pp. 13292–13299, 2014.

[101] J. Min, F. Baillot, H. Guo, E. Domingues, M. Talbaut, and B. Patte-Rouland, "Impact of CO_2, N_2 or Ar diluted in air on the length and lifting behavior of a laminar diffusion flame," *Proc. Combust. Inst.*, vol. 33, no. 1, pp. 1071–1078, 2011.

[102] H. S. Zhen, C. S. Cheung, C. W. Leung, and Y. S. Choy, "Effects of hydrogen concentration on the emission and heat transfer of a premixed LPG-hydrogen flame," *Int. J. Hydrogen Energy*, vol. 37, no. 7, pp. 6097–6105, 2012.

[103] S. F. Dakhil and T. A. Gabbar, "Study the effect of initial temperature and equivalence ratio on the pre–mixed flame propagation," *Basrah J. Eng. Sci*, vol. 12, no. 2, pp. 88–101, 2012.

[104] U. ATMACA, "Effects of mass flow rate and equivalence ratio on laminar premixed methane air flame," *Erzincan Univ. J. Sci. Technol.*, vol. 14, no. 1, pp. 195–203, 2021.

Appendices

APPENDIX A : PUBLICATIONS

APPENDIX A-1:

1st Manuscript: Published

Neuro Quantology | Jul 2022 | Volume 20 | Issue 7 | Page 2946-2968 | doi: 10.14704/nq.2022.20.7.NQ33373
Mohammed A. Al-Tayyar/A Review on Flame Height and Structure and Pollutants Formation

A Review on Flame Height and Structure and Pollutants Formation

Mohammed A. Al-Tayyar [1, a], D. AlKhafaji [2, b], Haroun A. K. Shahad [2, c]

[1] PhD student at Mechanical Eng. Dept, University of Babylon & Lecturer at University of Alkafeel / Iraq.

[2] Professors at Mechanical Engineering Department, University of Babylon, Iraq.
Corresponding Author: [a] Mohammed.altayyar@alkafeel.edu.iq, & mahtir85@gmail.com

[b] hakshahad@yahoo.com, [c] d.alkhafagiy@yahoo.com

Abstract. The combustion examination in every combustion system is a critical and complex problem. In general, this study aims to achieve a stable combustion appearing in industrial furnaces, combustors of gas turbines, diesel engines, spark ignition of engines and boiler furnaces etc. The study of characterizing and featuring different kinds of flame has become more important than ever in order to increase combustion efficiency and decrease particulate emissions. In this study, the most prominent experimental and theoretical techniques related to the measurement of the height and structure of flame as well as the formation of pollutants will be reviewed. The measurements of flame heights are defined in different ways. The flame length is determined by four primary factors such as the relative significance of early jet momentum fluxes and buoyant forces, stoichiometry, ratio of nozzle fluid to ambient gas density, initial jet diameter. In addition, the height of the flame is influenced by some factors such as fuel type and blending ratio and types of blending, laminar or turbulent, supply velocity, nozzle configuration, and burner and combustion chamber design.

Keywords: *Flame Height, Flame Structure, Pollutants, Premixed Flame, LPG, Hydrogen Blending, Swirl Burner.*

Number: 10.14704/nq.2022.20.7.NQ33373 **Neuro Quantology 2022; 20(7):2946-2968**

1 Introduction

The increase in the demand of energy has helped fossil-fuel combustion attract a great attention because of the rise in fuel consumptions and greenhouse gas emissions. Most of gas turbines, for example, burn fossil fuel air mixtures, which results in the emission of harmful GHG gases including CO_2, CO, NO_x, SO_x, etc. The available techniques for exhaust gases capturing are still too complicated and costly if utilized in all gas-turbine industry [1].

Laminar premixed flames, mostly combined with diffusion flames, are utilized in many residential, commercial, and industrial applications. These flames are by themselves significant; yet, possibly more significantly, understanding them is a necessary prerequisite for examining turbulent flames . Flame height affects the design of combustion chamber and furnaces and the flame height is affected by the fuel type. The fuel type also affects the pollutants formation. In industry, flame height measurements are utilized for the validation of the models of flame structures and computing the residence time of the soot particle. The flame length is particularly significant since the flame should not strike the combustion chamber walls for safety and system integrity considerations. The spread of a flame over the surface of a combustible material is of importance to fire safety research because it has an effect on the early growth of the fire and the heat release rates[2].

The investigation of combustion in every combustion system is a very significant and complex problem. Characterizing and displaying various types of flames has become more important than ever before in order to improve combustion efficiency and reduce particulate emissions, especially since flames require more attention in industrial furnaces, combustors of gas turbine, and furnaces of boilers etc. Because of the low achievable level of NO_X emissions by limiting the peak combustion temperature by the quantity of excess air, the gas turbine industry, for

APPENDIX A-2

2nd Manuscript: Accepted

19th International conference on Advanced Nanomaterials
11th International conference on Advanced Graphene Materials
11th International conference on Hydrogen Energy
9th International conference on Advanced Energy Materials
7th International conference on Advanced Magnetic and Spintronics Materials
6th International conference on Advanced Polymer Materials and Nanocomposites
6th International conference on Solar Energy Materials
4th International conference on Organic Light Emitting Diodes (OLED)

ANM 2022

27-29 July 2022
University of Aveiro, Aveiro- Portugal

CERTIFICATE OF PARTICIPATION

This is to certify that

Mohammed Al-Tayyar (University of Babylon, Al-Kafeel))

has participated in ANM2022 conference and has presented the work

An investigation on the effect of hydrogen blending on the height and structure of LPG/air premixed flame

in the session of HE- Hydrogen Energy

Dr. Elby Titus (Conference Chair), 29 July 2022

APPENDIX A-3

3rd Manuscript: Accepted

Acceptance Letter

Author : Mohammed A. Al-Tayyar
Affiliation : Ph.D. student - Mechanical Eng. Dept, University of Babylon & Lec. - University of Alkafeel / Iraq
Email : Mohammed.altayyar@alkafeel.edu.iq

Dear (author) We are pleased to inform you that your manuscript,
An Investigation into Burner Configuration Effects on Premixed Flame Characteristics for LPG Diluted with CO2
after being peer- reviewed , has been accepted for participating in the

4th INTERNATIONAL SCIENTIFIC CONFERENCE OF ALKAFEEL UNIVERSITY , ISCKU 2022

in Al-Najaf Al-Ashraf, Iraq ,December 20th -21st , 2022 . Given that your manuscript will be published after passing the conference Scopus-indexed journals requirements.

With Best Regards

N. ALDAHA

Prof. Dr. N. Al-Dahan
Rector of Alkafeel University

AIP Publishing Scientific.Net Scopus

APPENDIX B

APPENDIX B-1:
LPG Component Analysis

Oil Ministry
Gas Filling Company (General Company)
Babylon Branch
Gfc_mde535@yahoo.com
branch.furat@gfc.oil.gov.iq

وزارة النفط
شركة تعبئة الغاز (شركة عامة)
فرع بابل

إلى / جامعة بابل / كلية الدراسات العليا

وزارة النفط
شركة تعبئة الغاز فرع بابل
شعبة المعامل
العدد ١٨٦٨
التاريخ ٢٠١٩/٢/٦

العدد ١١٤٧
٢/٢

م / نتائج فحص الغاز السائل

اشارة الى كتابكم المرقم بالعدد ٢٤١ في ٢٠١٩/١/١٥ .
نود اعلامكم ان نتائج فحص مكونات الغاز السائل (LPG) ليوم ٢٠١٩/١/٢٣ كما في الجدول ادناه

للتفضل بالعلم .... مع التقدير

Material	Analysis by volume	Molecular weight (Kg/kmol)
C2H6	0.7%	30
C3H8	55.8%	40
C4H10	41.5%	58
C5H12	2%	72

احمد تركي مهجهج
مدير الفرع
م. علي حمزة علوان
وكيل مدير الفرع

احمد جواد كاظم
م .التدريب والتطوير

نسخة منه إلى :.

APPENDIX C:

CALIBRATION & CORRECTION FACTOR

Appendix C-1: Correction of measured flow rate of fuel/air mixture

The following procedur has been used for the correction of the values of fuel/air mixture flow rate measured by the rotameters.

$$Q_{adjusted} = Q_{scale} * Correction\ Factor\ (CF) \quad \text{(C.1)}$$

$$Correction\ Factor\ (CF) = \sqrt{\left(\frac{SG_{scale}}{SG_{new}}\right) * \left(\frac{P_{new}}{P_{scale}}\right) * \left(\frac{T_{scale}}{T_{new}}\right)} \quad \text{(C.2)}$$

Where:

$Q_{adjusted}$=Flow at new conditions (units are corrected volumetric flow)

Q_{scale} =Flow as indicated on flowmeter scale (same units as above)

SG_{scale}=Specific gravity of gas on flowmeter scale

SG_{new}= Specific gravity of new gas

P_{new}=New operation pressure (bar)

P_{scale}= pressure on flowmeter scale (bar)

T_{scale}=Temperature on flowmeter (K)

T_{new}= New operation temperature (K)

The standard pressure and temperature for designing the flowmeters are (1 bar) and (298 K). All the experimental tests have been conducted under the same pressure and temperature for the design conditions of the flowmeters. Thus eq. C. 2 could be reduce to be:

$$(CF) = \sqrt{\left(\frac{SG_{air}}{SG_{mixture}}\right)} = \sqrt{\left(\frac{\text{Molecular weight of air}}{\text{Molecular weight of fuel mixture}}\right)} \quad \text{(C.3)}$$

where: Molecular weight of fuel mixture$= \sum x_i MW_i$

Table C.1 shows the values of the correction factors for readjustment of the flow rate measured by the flowmeters.

Table C.1 : Correlation factor (CF) for readjustment measured flow rate

	H2 Blending (k)	LPG (1-k)	∅	MW air	MW mixture	CF
1	0	1	0.6	28.85	29.32758	0.991824
2	0.1	0.9	0.6	28.85	29.25611	0.993035
3	0.2	0.8	0.6	28.85	29.16919	0.994514
4	0.3	0.7	0.6	28.85	29.06117	0.99636
5	0.4	0.6	0.6	28.85	28.92335	0.998731
6	0	1	0.8	28.85	29.48207	0.989222
7	0.1	0.9	0.8	28.85	29.3871	0.990819
8	0.2	0.8	0.8	28.85	29.27177	0.99277
9	0.3	0.7	0.8	28.85	29.12874	0.995204
10	0.4	0.6	0.8	28.85	28.94668	0.998329
11	0	1	1	28.85	29.63431	0.986678
12	0.1	0.9	1	28.85	29.51599	0.988654
13	0.2	0.8	1	28.85	29.37252	0.991065
14	0.3	0.7	1	28.85	29.19497	0.994074
15	0.4	0.6	1	28.85	28.96948	0.997936
16	0	1	1.2	28.85	29.78432	0.98419
17	0.1	0.9	1.2	28.85	29.64282	0.986537
18	0.2	0.8	1.2	28.85	29.47151	0.9894
19	0.3	0.7	1.2	28.85	29.25988	0.992971
20	0.4	0.6	1.2	28.85	28.99177	0.997552
21	0	1	1.4	28.85	29.93218	0.981756
22	0.1	0.9	1.4	28.85	29.93316	0.98174
23	0.2	0.8	1.4	28.85	29.93436	0.981721
24	0.3	0.7	1.4	28.85	29.93586	0.981696
25	0.4	0.6	1.4	28.85	27.26235	1.028706
				Average CF = 0.9922		

Appendix C-2

Calibration of Rotameters

The orifice meter is used to calibrate the flowmeter. It consists of a circular plate as shown in Fig. (C.1) having circular sharp edged hole (called orifice) concentric with the pipe. The diameter of the orifice may vary from 0.4 to 0.8 times the diameter of the pipe but its value is generally chosen as 0.5. A differential manometer is connected at section (1) which is a distance of 1.5 to 2 times the pipe diameter upstream from the orifice plate and at section (2) which is at a distance of about the distance from the orifice plate on the downstream side [80].

All Parts of orifice are conducted in the Mechanical Engineering Department Laboratories at the University of Babylon as shown in fig. (C. 2). It consists of a straight length pipe of 50 cm; inside it a central orifice of 25 mm inlet diameter and 50.8 mm diameter of the pipe. The reading in both the limps (h_1 *and* h_2) of the differential manometer are used in equation (C.4) to calculate the air flowrate and this flowrate is compared with the flowrate reading:

$$Q_{calculated} = C_d \frac{A_1 A_0 \sqrt{2gh}}{\sqrt{(A_1^2 - A_0^2)}} \qquad \text{(C.4)}$$

Where:

A_1= Area of pipe at section (1).

A_0= Area of the orifice.

$h = h_1 - h_2$ = Readings in both the limbs ($h_1$and h_2) of the manometer.

$C_d = Q_{actual} / Q_{th.}$ = coefficient of discharge of orifice varies from 0.96 to 0.98.

Eq. (C.4) is used to calculated the air flow rate by measuring the level rise (h) in manometer for several different flow rate changing the rotameter valve

slightly. Many flow readings, as given in table (C.2) are taken to obtain a calibration curve. Figure (C.3) indicates that the accuracy of the air flowmeters compared with the standard orifice meter is acceptable where the error ranging between 3% & 4%.

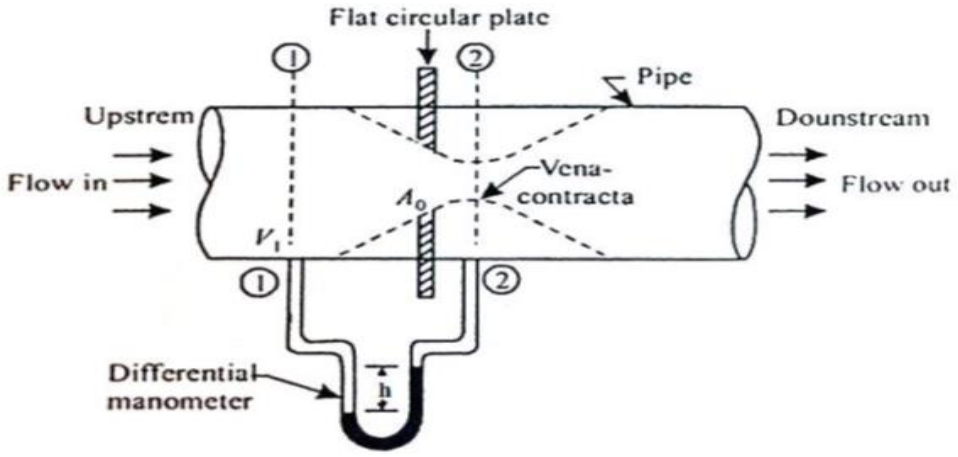

Fig. (C.1) Schematic of orifice meter [80]

Fig. (C.2) Calibration setup of the air flowmeter.

Table C.2 : Measuring and calculated results of air flowmeters

Flow rate of flowmeter 0.5-6 (L /min)	Measured	**1**	**1.50**	**2**	**2.50**	**3**	**3.5**	**4**
	Calculated	**1.125**	**1.625**	**2.25**	**2.625**	**2.75**	**3.625**	**4.04**
Flow rate of flowmeter 6-50 (L /min)	Measured	**6.5**	**7**	**8**	**8.5**	**9**	**9.5**	**10**
	Calculated	**6.75**	**7.4**	**8.923**	**8.95**	**8.753**	**9.623**	**10.8**

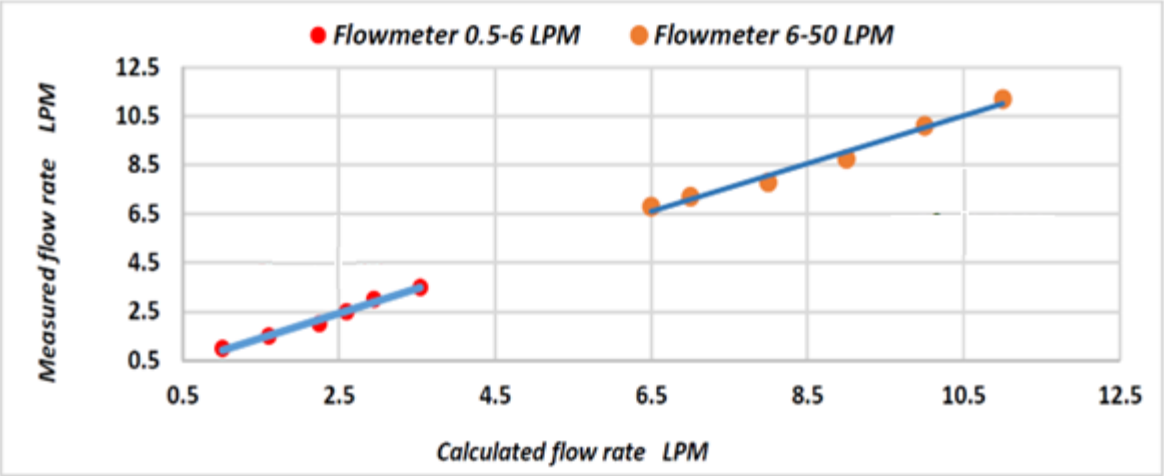

Fig. (C.3) Calibration results of air flowmeters.

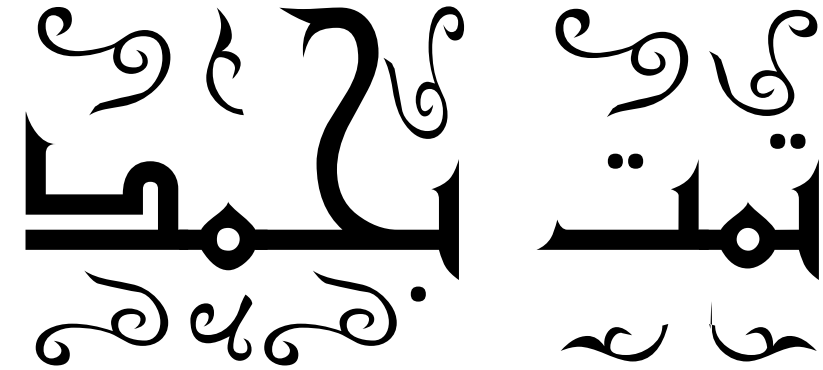
تمت بحمد

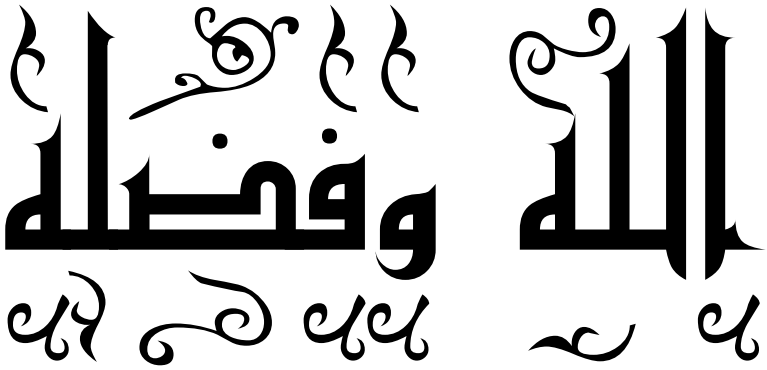
الله وفضله

الـــخـــلاصـــة

تتضمن الدراسة الحالية التقصي العملي والعددي لتأثير نوع الوقود المستخدم وتركيبته على كل من إرتفاع اللهب وخصائصه فضلاً عن دراسة الملوثات الناتجة وذلك للإحتراق المسبق الخلط لغاز البترول المسال LPG ضمن أنبوب مدور المقطع. وقد تم تجربة مزج غاز LPG مع وقود الهيدروجين إلى جانب تجربة تخفيف الخليط من خلال إضافة غاز ثاني اوكسيد الكاربون مع ملاحظة تأثير كل من نسبة تكافؤ الوقود مع الهواء، معدل الجريان للخليط، نسبة عرض الموقد إلى إرتفاعه، وكذلك دراسة نوعين من الموقد الدوامي وغير الدوامي. إن لدراسة إرتفاع اللهب آثار بارزة من خلال تأثيره على تصميم نظام الإحتراق وعملية إنتقال الحرارة فضلاً عن العديد من الإعتبارات البيئية والإقتصادية.

فيما يتعلق بالجانب العملي من الدراسة، فقد تم بناء وتجميع منظومة لتناسب إجراء تفاصيل التجارب العملية المطلوبة لتحقيق الإحتراق مسبق الخلط. تم إستخدام كاميرا ذات دقة عالية تدعم تقنية التصوير السريع لتصوير اللهب وتسجيل التكون اللحظي له. أجري تحليل صور اللهب بطريقتين: بتقنيات تحليل الصور الرقمية لبرنامج الماتلاب وكذلك بطريقة معايرة القياسات للأبعاد الهندسية للصورة ببرنامج الأوتوكاد. تضمنت التجارب العملية تجربة خمس نسب تكافؤ للوقود والهواء (٠,٦، ٠,٨، ١، ١,٢، و ١,٤)، خمس نسب لمزج الهيدروجين بالوقود (٠٪، ١٠٪، ٢٠٪، ٣٠٪، و ٤٠٪)، أربع نسب لغاز ثاني أوكسيد الكاربون (٠٪، ٥٪، ٧,٥٪، و ١٠٪)، خمس قياسات لتناسب العرض والطول للمحرق غير الدوامي (٢، ٤، ٦، ٨، و ١٠) وجميعها أجريت بتغيير معدل الجريان ما بين مدى إرتجاع اللهب وإنفصال اللهب. زيادة على ما تقدم، فقد تم إختبار قياسين للمحرق الدوامي أحدهما ذي خمسة والآخر ذي ٩ ريشات.

تضمنت الدراسة العددية إجراء محاكاة ثنائية الأبعاد لنموذج الإحتراق من خلال إستخدام برنامج (CFD OpenFOAM) ونموذج الحل (XiFOAM) للتنبؤ بإرتفاع المنطقة الداخلية للهب وتوزيع درجات الحرارة طوليًا وعرضيًا ، وتقدم التفاعل الكيميائي. علاوة على ذلك ، تتنبأ الدراسة العددية من حيث النوعية والكمية بتكوين نواتج الاحتراق. تمت محاكاة إحتراق خليط غاز البترول المسال / الهواء لنسب التكافؤ (١ ، ١,٢ ، ١,٤ ، و ١,٦) عند معدل جريان ٦ لتر / دقيقة. وكذلك محاكاة تأثير الجريان لـمعدلات (٤ ، ٥ ، ٦ ، ٧ ، و ٨ لتر / دقيقة) وضمن ظروف متكافئة. إلى جانب ذلك ، تم إجراء محاكاة لتأثير مزج الهيدروجين لنسب (٠٪ ، ٥٪ ، ٢٠٪ ، ٤٠٪ ، و ٥٠٪).

لوحظ أن نسبة التكافؤ هي المسيطر الأكبر على إرتفاع اللهب ولجميع أنواع الخلائط والتركيبات وفي جميع ظروف التشغيل. أيضًا لوحظ بأنه يتسع سمك منطقة التفاعل عندما تزداد نسبة التكافؤ. يزداد الطول المقاس عملياً للمنطقة الداخلية للهب واللهب المرئي لغاز LPG من ١٨,٧ مم إلى ٣٤,٤ مم ومن ٣٥,٨ مم إلى ٥٦,٥ مم على التوالي عند زيادة نسبة التكافؤ من ١ إلى ١,٤. يكون تأثير معدل تدفق خليط الوقود / الهواء على إرتفاع اللهب ونسبة أبعاد اللهب تأثيراً إيجابياً.

يقلل مزج الهيدروجين من نسبة أبعاد اللهب بينما يؤدي التخفيف بثاني أكسيد الكربون إلى زيادتها. تؤدي زيادة نسبة التكافؤ أو معدل التدفق إلى إطالة اللهب بشكل كبير عند التخفيف بثاني أكسيد الكربون نظراً لوجود عوامل متعددة متصاحبة في تأثيرها في إتجاه واحد. فيما يتعلق بخليط LPG- H_2-CO_2 / الهواء ، لوحظ أن الإستطالة الحاصلة في اللهب نتيجة ثاني أكسيد الكربون تتفوق على قصر اللهب الناتج عن مزج الوقود بالهيدروجين H_2. يولد مزيج (LPG-5%CO_2-10%H_2) ومزيج (LPG-10%CO_2-30%H_2) في ظروف الخلط المتكافئ لهباً أطول بنسبة ٣٪ و ٢٠٪ على التوالي مقارنةً باللهب الناتج عن غاز البترول المسال. تزداد نسب الإستطالة هذه إلى ١٢٪و ٣٠٪ عندما تكون نسبة التكافؤ ١,٢ ولنفس الخلائط المبينة آنفاً.

تؤثر نسبة أبعاد الموقد على ارتفاع اللهب بشكل ضئيل. يقصُرُ اللهب بشكلٍ واضحٍ عند استخدام الموقد الدوامي للمخاليط المتكافئة والغنية بالوقود في حين لا يكون هناك تغيير ملحوظ في حالة المزيج قليل الوقود. علاوة على ذلك ، عند زيادة العدد الدوامي سيزاد ارتفاع اللهب قليلاً. أيضًا ، يعمل الموقد الدوامي على تقسيم منطقة اللهب الداخلي إلى أجزاء مساوية لعدد الريش منتجة لهب بشكل يشبه الزهرة عندما تكون معدلات التدفق منخفضة.

فيما يتعلق بمدى إستقرارية اللهب ، فإنها تزداد بزيادة نسبة التكافؤ وكذلك فهي تتحسن نتيجة مزج الهيدروجين أو التخفيف بثاني أكسيد الكربون. يساعد ثاني أكسيد الكربون على تمكين اللهب من التغلب على ظاهرة إرتجاع اللهب، بينما يؤدي المزج بالهيدروجين إلى رفع حدود إرتجاع وانفصال اللهب نحو معدلات تدفق أعلى. إن استخدام الموقد الدوامي يعزز من إستقرارية اللهب بشكل كبير عندما تكون نسبة التكافؤ تساوي ١ أو ١,٢ بينما يلاحظ العكس عندما تساوي ٠,٨.

تنخفض درجة الحرارة القصوى المتوقعة للهب من ٢٣٨٣ كلفن إلى ١٨٤٠ كلفن ثم إلى ١٦٠٨ كلفن ولنسب التكافؤ ١ و ١,٤ و ١,٦ على التوالي لغاز البترول المسال. تتسبب زيادة معدل التدفق في إنخفاض طفيف في درجة حرارة اللهب بسبب زيادة الحرارة المتحررة من اللهب نظراً لزيادة المساحة السطحية. لوحظ ظهور زيادة متواضعة في درجة حرارة اللهب عند مزج الهيدروجين حيث تزداد بمقدار ١٢ كلفن عند مزج ٥٠٪ من الهيدروجين مع غاز البترول المسال ولظروف التكافؤ القياسية. تزداد درجة الحرارة على طول المنتصف بشكل حاد ولحظي (حوالي ٢٠٠٠ كلفن لغاز البترول المسال ولظروف التكافؤ القياسية خلال منطقة التفاعل. بعد ذلك ، تبدأ درجة الحرارة في الإنخفاض بشكل رتيب (حوالي ١٩٥ كلفن). داخل منطقة التسخين المسبق تكون درجة الحرارة في أدنى معدلاتها عند المنتصف وتزداد بإتجاه محيط اللهب. خارج اللهب، يصبح الأمر معكوساً حيث تتوزع درجة الحرارة في شكل مكافئ وتكون شديدة عند المنتصف وتقل بإتجاه الأطراف.

تبين عمليات المحاكاة العددية إلى أن أكبر كمية من الوقود والأوكسجين تستنفد ضمن منطقة التفاعل حيث يكون معدل الزيادة هو الأكثر حدة في درجة الحرارة وعامل التقدم على طول خط منتصف

اللهب. في نفس الوقت ، فأن الزيادة الأكبر في الكسور الجزيئية لنواتج الإحتراق تظهر في هذه المنطقة الصغيرة. بعد هذا التغيير الحاد ، ستبقى قيم الكسور الجزيئية ثابتة تقريبًا بسبب إكتمال الإحتراق. فيما يتعلق بتكوين الملوثات ، تنخفض الكسور الجزيئية لثاني أكسيد الكربون في حين تزداد لأحادي أكسيد الكربون عند زيادة نسبة التكافؤ. تنتج زيادة معدل التدفق تغيراً طفيفاً في قيم الكسور الجزيئية للمواد المتفاعلة أو الناتجة. مزج الهيدروجين في ظروف متكافئة يقلل من الكسور الجزيئية للأوكسجين و ثنائي أكسيد الكربون. يقلل احتراق خليط (LPG-H2 50%) الكسور الجزيئية للأوكسجين وثنائي أكسيد الكربون بحوالي ٣٪ و٩٪ على التوالي بينما تزداد للوقود بحوالي ٧٨٪ مقارنة بوقود LPG.

تظهر مقارنة النتائج الحالية تطابقاً جيدًا بنسبة خطأ بحوالي ٢,٨٪ و١,٨٪ لإرتفاع منطقة اللهب الداخلية المقاسة والمتوقعة لخليط LPG و$LPG-H_2$ على التوالي. تمت مقارنة درجة الحرارة القصوى المتوقعة للهب غاز LPG مع بعض الأعمال السابقة وكان متوسط الفرق حوالي ١,٢٪. تُظهر النتائج العددية للكسور الجزيئية لمواد الإحتراق التي تمت دراستها عند مقارنتها مع عمل سابق نفس السلوك العام للمنحنيات.

جمهورية العراق
وزارة التعليم العالي والبحث العلمي
جامعة بابل/كلية الهندسة
قسم الهندسة الميكانيكية

تقصي عملي و عددي لتأثير نوع الوقود على إرتفاع اللهب

أطروحة

مقدمة الى جامعة بابل/كلية الهندسة– قسم الهندسة الميكانيكية كأحد متطلبات نيل درجة دكتوراه فلسفة في الهندسة / الهندسة الميكانيكية / (قدرة)

أعدت من قبل

مُحَمَد عَبْدُ الخَالِق هَاشِم عَبْدُ الرَسُول

بإشراف

الأستاذ الدكتور
ضرغام عبد الحسن الخفاجي

الأستاذ الدكتور
هارون عبد الكاظم شهد

٢٠٢٢ م

١٤٤٤ هـ